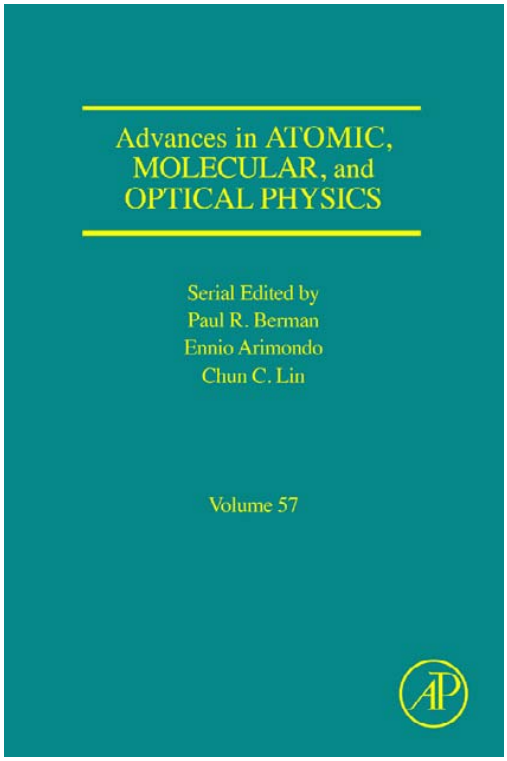




From: T. J. Gay, Physics and Technology of Polarized Electron Scattering from Atoms and Molecules. In E. Arimondo, P. R. Berman, & C. C. Lin, editors: Advances in Atomic, Molecular, and Optical Physics, Vol. 57,
Burlington: Academic Press, 2009, pp. 157-247.
ISBN: 978-0-12-374799-0

CHAPTER 4

# Physics and Technology of Polarized Electron Scattering from Atoms and Molecules[1]

**T. J. Gay**

*Behlen Laboratory of Physics, University of Nebraska, Lincoln, NE 68588-0111, USA*

Contents



[1]This chapter is dedicated to M. S. Lubell and the late V. W. Hughes, who introduced the author to polarized electron physics.

Advances in Atomic, Molecular, and Optical Physics, Volume 57 
ISSN 1049-250X, DOI: 10.1016/S1049-250X(09)57004-8 

Abstract

This monograph reviews developments in the general area of polarized electron scattering from atoms and molecules since 1991, the date of the last such review in this series of monographs [Kessler, J. (1991). *Advances in Atomic, Molecular and Optical Physics, 27*, 81]. The physics of spin dependence in electronic collisions with atomic and molecular targets is outlined, with emphasis on the qualitative effects that can be probed using polarized beams and/or targets as well as analysis of the residual target and the scattered electron polarizations. Using the categories of exchange scattering, spin–orbit coupling, and interference between the two, experiments which elucidate these interactions are discussed for atomic and molecular targets, respectively. Developments in polarized electron sources and electron polarimeters since 1991 are also reviewed, and promising new technologies discussed.

## 1. INTRODUCTION

Following the demonstration that free electrons could have spin (Schull et al., 1943), the study of polarized electrons was motivated by questions related to the electron's magnetic properties (Louisell et al., 1954) and, following the Fall of Parity, the polarization of beta radiations (see, e.g., Gay & Dunning, 1992). More recently, the study of polarized electrons has focused on their interactions with solids, individual atoms and molecules, and as probes of the spin structure of nucleons and nuclei and the electroweak interaction. Indeed, a major motivation for early atomic collisions and condensed matter studies involving polarized electrons was the development of reliable sources of polarized electrons for nuclear physics applications. The purpose of this review is to critically summarize developments in the field of polarized electron interactions with atoms and molecules since 1991, the date of the first review in this series involving polarized electrons by Prof. Kessler (1991). In the intervening years, many significant developments in polarized electron–molecule scattering and polarized electron technology have occurred. A second goal of this review is to acquaint students and workers in other areas of atomic, molecular, and optical physics with the field of polarized electrons, and the reasons why it is so important in the study of atomic and molecular collisions.

There exist a number of books and earlier reviews of these topics. Prof. Kessler's excellent book *Polarized Electrons* (1985) is the standard reference work in this area, but the reader is also directed to several more recent books on one or more topics covered in this review: Anderson and Bartschat (2001), Blum (1996), Burke and Joachain (1997), Campbell and Kleinpoppen (1996), Dunning and Hulet (1996), and Kleinpoppen and Newell (1995). The series of conference proceedings associated with the International Conference on Photonic, Electronic, and Atomic Collisions (ICPEAC; formerly the International Conference on the Physics of Electronic and Atomic Collisions) and its satellite meeting on Coherence, Correlation, and Polarization (and, more recently, $(e/2e)$ collisions) also serve as good overviews of the field. Review articles of special interest in this regard are those in this series by Blum and Thompson (1997) and Compton and Pagni (2002) on scattering from chiral molecules, general reviews of spin-dependent atomic collisions by Hanne (1983) and Andersen et al. (1997), and those on Mott scattering by Dunning (1994) and Gay and Dunning (1992). Developments in polarized electron technology are periodically reviewed in conference proceedings associated with the International Spin Physics Symposium and its associated workshop on polarized electron sources and polarimeters. While not directly connected with this review, the topic of polarized electrons in condensed matter physics has always been relevant to studies of magnetism, but has been of particular interest recently with the advent of spintronics (see, e.g., Žutić et al., 2004). Two older books of interest for this general topic are those on polarized electrons at surfaces by Kirschner (1985) and Feder (1985).

The plan of this chapter is as follows. In Section 2, we discuss the basic physics of atomic and molecular collisions that generally leads to spin-dependent interactions and that require for their study the use of polarized electrons and/or targets, or the analysis of scattered electron spin. In Section 3, we consider electron–atom scattering; in Section 4, molecular targets are discussed. Finally, in Section 5, we review recent developments in polarized electron technology and their applicability to atomic and molecular gas phase experiments.

## 2. SPIN-DEPENDENT INTERACTIONS

Coulombic forces do not act directly on the spins of electrons. Thus spin-dependent effects in collisions must be due to other interactions. These interactions are the magnetic coupling of electrons spins with the other angular momenta in the collision, and the ''Pauli force,'' that is, the requirement that wavefunctions of identical fermions be antisymmetrized. In addition, combinations of these two interactions lead to distinguishably different spin effects as well. Other manifestations of the

electron–target interaction, such as resonance formation and the emission of bremsstrahlung, can also be spin dependent.

## 2.1. Electron Exchange

Electrons, being identical fermions, cannot be distinguished unless their spin is known and is known not to change throughout the course of a given collision process. Such collisions, involving only two electrons, are shown schematically in Figure 1. They can be designated by quantum-mechanical amplitudes corresponding to whether the electrons switch places (an ''exchange'' process with amplitude g) or not (a ''direct'' process with amplitude $f$). If both electrons have the same initial spin, the amplitudes must be added (with a minus sign, because they are fermions) before their sum is squared to give a differential scattering cross section. Equivalently, the scattering process can be specified in terms of whether the electrons are in a singlet state or a triplet state. In this case the scattering amplitudes are written as singlet or triplet amplitudes:

$$a^1 = f + g, \tag{1a}$$

$$a^3 = f - g. \tag{1b}$$

To illustrate these ideas conceptually, consider the elastic scattering of a beam of completely spin-up electrons from a beam of hydrogen atoms whose electrons are completely spin-down. If we detect electrons that have been scattered by an angle $\theta$ to within a solid angle $d\Omega$, the scattered beam electron spin polarization is given by

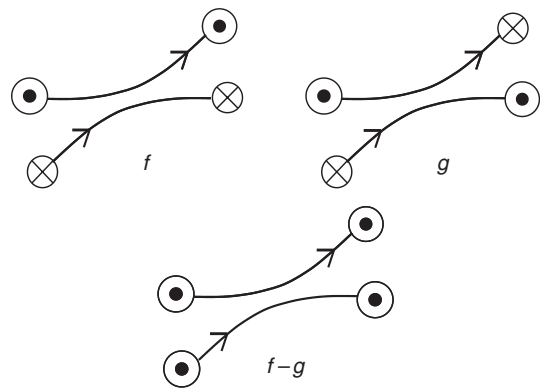


**FIGURE 1** Schematic of a collision process involving electrons (with relevant nuclei suppressed). The circles with crosses and concentric dots represent the electron spin directions

$$P_e \equiv \frac{N^{\uparrow} - N^{\downarrow}}{N^{\uparrow} + N^{\downarrow}} = \left(1 - \frac{2|g(\vartheta)|^2}{\frac{d\sigma_{av}(\vartheta)}{d\Omega}}\right), \tag{2}$$

where $N^{\uparrow(\downarrow)}$ is the number of electrons in the scattered beam with spin-up (down), and

$$\frac{d\sigma_{av}(\vartheta)}{d\Omega} \equiv \sigma_{av}^{tot} = \frac{1}{4}|f(\vartheta) + g(\vartheta)|^2 + \frac{3}{4}|f(\vartheta) - g(\vartheta)|^2 = \frac{1}{4}\sigma^1(\vartheta) + \frac{3}{4}\sigma^3(\vartheta) \tag{3}$$

is the spin-averaged differential scattering cross section, where $\sigma^1$ and $\sigma^3$ correspond to the individual singlet and triplet scattering cross sections. The first part of Equation (3) serves as the general definition for the polarization of any ensemble of electrons. If the exchange amplitude $g$ is negligible, the polarization of the scattered and incident beams is the same. If exchange dominates the differential cross section, the polarization of the scattered beam is flipped.

In the discussion above, it is assumed that the electrons involved in the scattering process do not flip their individual spins due to magnetic forces. Such processes are generically referred to as ''exchange scattering,'' (even if exchange does not occur!) to indicate that magnetic interactions do not occur.

## 2.2. Spin–Orbit Interactions

We now consider situations in which the complete Hamiltonian of the scattered electron–target system contains terms associated with magnetic as opposed to Coulombic forces, that is, has terms containing $\alpha$ and the inner product of two angular momenta. We will neglect spin–spin coupling terms, and consider only spin–orbit interactions in this discussion. These in turn can be associated with internal target fine-structure splitting (and possibly intermediate coupling) or the interaction of the continuum electron spin with its own orbit. The former splittings are generally small enough that they have little influence on dynamical scattering mechanisms. However, they can play an important role in production of spin-dependent asymmetries, as we will see in the next section. Continuum electron spin-dependent interactions lie at the heart of polarized electron physics, in that they were what Mott suggested as a mechanism whereby free electron spin could be detected (Mott, 1929). It is for this reason that we will often refer to a spin-dependent coupling to the continuum electron as ''Mott scattering.''

Mott scattering yields two kinds of scattering asymmetry, one spatial, the other related to spin polarization. If an incident unpolarized beam is scattered to an angle $\theta$, the scattered beam will have a spin polarization

$P_e \equiv S_p$ perpendicular to the scattering plane. Alternately, if spin-polarized electrons are scattered from the same target, they will exhibit a left–right scattering asymmetry

$$A \equiv \frac{I(+\vartheta) - I(-\vartheta)}{I(+\vartheta) + I(-\vartheta)} = S_A P_e, \tag{4}$$

where $I$ is the scattered intensity to a given angle and, again, the electron polarization is specified perpendicular to the scattering plane. When the elastic scattering occurs from spinless targets, $S_A = S_P = S$, the latter being referred to as the ''Sherman function'' after Noah Sherman, the first person to calculate extensive tables of $S$ as a function of scattering angle and incident (relativistic) electron energy (Hanne, 1983; Sherman, 1956).

One can understand in a simple way why such asymmetries arise considering such collisions in the target's rest frame (Figure 2). A boosted magnetic dipole appears in this frame to have an electric dipole component (Fisher, 1971)

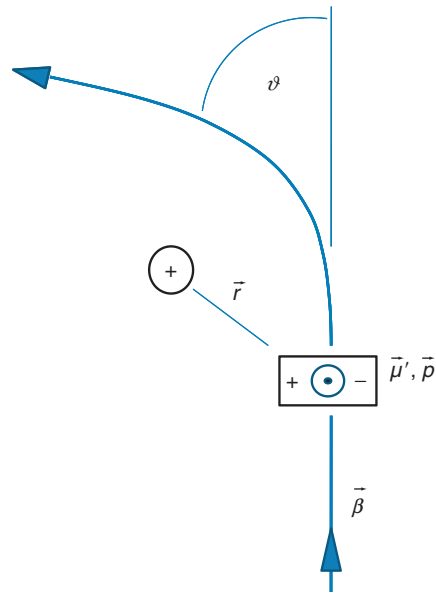


**FIGURE 2** Mott scattering as observed in the rest frame of the nuclear target. The continuum electron has a spin (magnetic moment) out of (into) the page, yielding an electric dipole in the rest frame that points to the left. Spin-flip reverses the direction of the electric-dipole moment

$$\vec{p} = \vec{\beta} \times \vec{\mu}\,', \tag{5}$$

where $\vec{\beta}$ is the electron's velocity vector divided by $c$ and $\vec{\mu}\,'$ is the proper magnetic dipole moment. Depending on whether the incident electron's spin is up or down, the rest frame electric dipole will point to the left or right. Thus, electrons with impact parameter equally to the left or right of the nucleus will feel attractive or repulsive forces due to this dipole interaction, in addition to the Coulomb force. This asymmetry yields in turn a spatial scattering asymmetry. Similar arguments can be used for the production of spin polarization at a given scattering angle.

Because of the way Mott framed his original arguments and the proportionality of the continuum spin–orbit coupling term to $\beta$, it was believed for years that only highly relativistic electrons could produce appreciable Mott asymmetries. However, by the 1960s, it had become apparent that large asymmetries could be observed even for incident electron energies well below 1 keV if heavy targets such as Hg were used (Kessler, 1969). This is because after penetrating the outer electronic structure of such targets, the continuum electron is accelerated to relativistic speeds by large, unscreened Coulomb forces. In all Mott scattering events, the spin direction of the incident electrons generally rotates as their lab-frame electric dipole moments rotate in the nuclear Coulomb field. Having picked an axis of quantization, this rotation corresponds to the spin-flips that do not occur in exchange scattering.

### 2.3. Combinations of Spin–Orbit and Exchange Effects

Let us now consider how combinations of exchange scattering and spin–orbit coupling can lead to different types of spin-dependent effects. Consider first, the collision shown schematically in Figure 3(a), elastic scattering from ground-state Column I atoms. We detect the number of electrons scattered to a specific angle. If Mott scattering is important (Fr, Cs, and possibly Rb), then one would expect to see an intensity change (asymmetry) with an unpolarized target when the incident electron spins are flipped. Similarly, in the case of H or Li targets, where only exchange scattering should occur, intensity asymmetries will result when the target is spin polarized, and the relative directions of the incident and target spins are reversed. Burke and Mitchell (1974) have shown that these two effects can interfere, producing a third asymmetry, in which unpolarized electrons will be scattered with different intensities if the target is spin polarized and this polarization direction is reversed. This effect can be envisioned as a situation in which exchange polarizes the incident electrons during the scattering process, and they subsequently produce a Mott asymmetry. In general, we can consider an experiment in which all three effects are important, and in which electrons with polarization $\vec{P}_e$

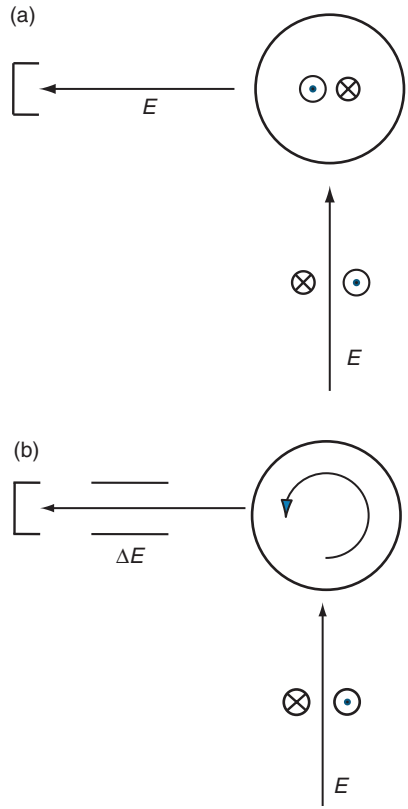


**FIGURE 3** Exchange, spin–orbit coupling, and combinations of the two (see text). (a) Elastic scattering from polarized and unpolarized targets. Electrons scattered to a specific angle are detected without spin analysis. (b) Polarized electrons scatter from an unpolarized target in which a fine-structure-resolved ($^2P_{3/2}$) state is excited by exchange. The scattering produces orbital angular momentum pointing out of the diagram. Fine-structure resolution is achieved by measuring the electron kinetic energy before and after scattering

scatter from atoms with electron spin polarization $\vec{P}_a$. The differential cross section can then be written as (Leuer et al., 1995)

$$\frac{\mathrm{d}\sigma(\vartheta)}{\mathrm{d}\Omega} = \frac{\mathrm{d}\sigma_{\mathrm{av}}(\vartheta)}{\mathrm{d}\Omega}[1 - A_{\mathrm{ex}}\vec{P}_e \cdot \vec{P}_a + A_{\mathrm{so}}\vec{P}_e \cdot \hat{n} + A_{\mathrm{int}}\vec{P}_a \cdot \hat{n}], \tag{6}$$

where $A_{\mathrm{ex}}$ is the pure exchange asymmetry, $A_{\mathrm{so}} = S_p$ is the pure Mott asymmetry, and $A_{\mathrm{int}}$ is the asymmetry due to the interference of the first two. Table 1 shows how various combinations of incident electron

**TABLE 1** Spin combinations to extract $A_{ex}$, $A_{so}$, and $A_{int}$

| Spin combinations | | |
|---|---|---|
| $I_1$ | $I_2$ | $\frac{I_1-I_2}{I_1+I_2}$ |
| $\downarrow\uparrow+\uparrow\downarrow$ | $\uparrow\uparrow+\downarrow\downarrow$ | $A_{ex}\vec{P}_e\cdot\vec{P}_a$ |
| $\uparrow\uparrow+\uparrow\downarrow$ | $\downarrow\uparrow+\downarrow\downarrow$ | $A_{so}\vec{P}_e\cdot\hat{n}$ |
| $\uparrow\uparrow+\downarrow\uparrow$ | $\downarrow\downarrow+\uparrow\downarrow$ | $A_{int}\vec{P}_a\cdot\hat{n}$ |

and atomic spins can be arranged to measure these quantities. In general, one would expect $A_{int}$ to be appreciable only of both Mott scattering and exchange are individually important.

Next, consider an inelastic collision with the same target, in which the fine structure of the excited state is resolved, for example, by precise measurement of both the incident and scattered electron energies (Figure 3(b)). Since we consider the general case in which the scattering angle is not zero, the incident and final electron $k$-vectors define an axial vector perpendicular to the plane of the diagram which we will take to define the axis of quantization. This means that in general the expectation value of $m_l$ will be nonzero, that is, the orbital angular momentum will be ''oriented,'' as indicated by the anticlockwise circulation of the target in the diagram. Let us now assume that the $J = 3/2$ state is known to have been excited, and that electron exchange is responsible for a significant fraction of the excitation cross section. This can only occur if the incident electrons are spin-up, allowing the $L$ and $S$ vectors in the excited target to add up to $J = 3/2$. We see that the scattering rate will thus depend on the incident electron spin direction, that is, $S_p$ will be nonzero, even in the absence of spin–orbit coupling to the continuum electron. This effect, first proposed by Hanne in the 1970s (Hanne, 1983), is generally referred to as the ''fine-structure effect'' and is due to the combination of internal target spin–orbit coupling and exchange scattering.

## 2.4. Relevant Scattering Amplitudes: Characterization of Excited States and the Scattered Electron

Complete characterization of a scattering event requires knowledge of all the target and continuum electron quantum-mechanical amplitudes immediately following the collision. An experiment that provides all of these details is said to be ''perfect.'' As the target becomes more complex, the number of required quantum-mechanical amplitudes increases. Ultimately, one must consider all of the spin components of the scattered electron and all of the $m_l$ and spin components of the target (before

spin–orbit coupling has time to scramble them) or, equivalently, the complete $m_j$ distribution. These requirements and the discussion thus far can be summarized by Figures 4 and 5. We will consider only atomic targets and neglect nuclear spin.

We consider as the simplest case elastic scattering by He (Figure 4). Since the target state is a singlet and spin–orbit forces on the continuum electron are negligible, only one amplitude, $a$, is required to give the differential scattering cross section. In elastic scattering from H, however, we must take into account electron exchange and the possible spin states of the two electrons, either singlet or triplet. (Equivalently, we could use $f$ and $g$; Equation (1).) These amplitudes have a physically meaningful

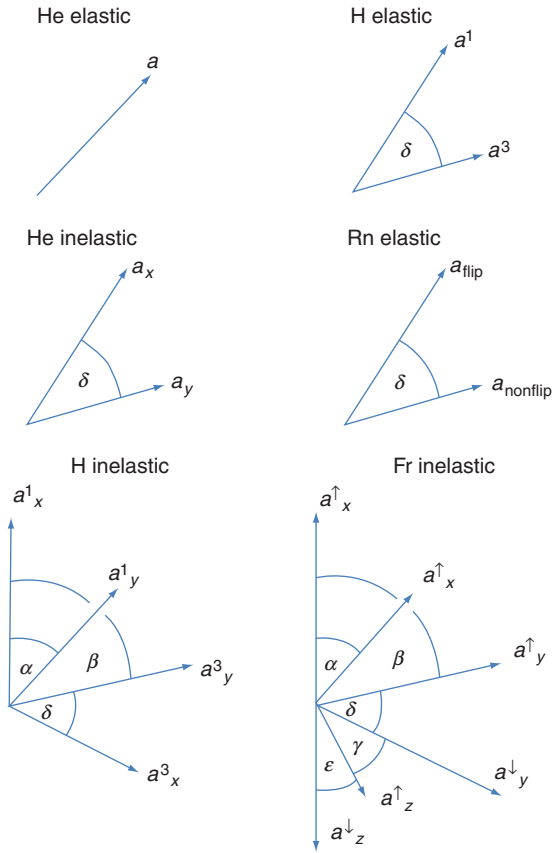


**FIGURE 4** Exchange and Mott scattering amplitudes for light and heavy closed-shell and open-shell targets in the complex plane (see text). Inelastic scattering amplitudes are for $S \rightarrow P$ excitation. Greek letters indicate relative phases between the various amplitudes

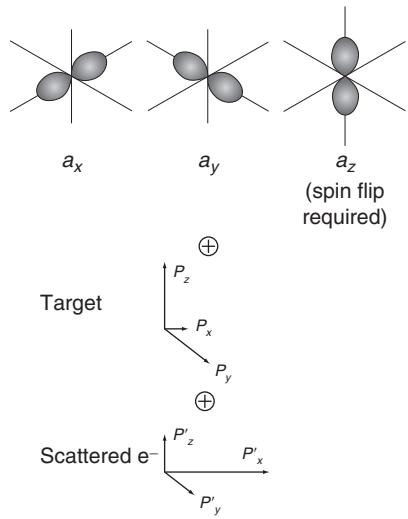


**FIGURE 5** Relevant Cartesian-basis geometric elements for atomic *P*-state excitation immediately after the collision (see text). Nuclear spin is ignored. The $p_z$ orbital can only be excited if spin–orbit coupling causes continuum electrons to flip their spin direction. Exchange scattering allows only electronic polarization along the *z*-axis

relative phase, so three parameters are needed to completely describe the scattering. In the case of elastic scattering from a closed-shell heavy target such as Rn, electron exchange does not affect polarization, but magnetic forces on the continuum electron can cause its spin to flip. Thus we must again consider three scattering parameters, $a_{\text{flip}}$ and $a_{\text{nonflip}}$ and their relative phase. In these last two cases, knowing the three scattering parameters is equivalent to knowing the target (in the case of H) and scattered electron polarizations for any given input target and electron polarization. For inelastic scattering from He, the overall spin state of the electrons still factors out, but we must now consider the excited atom, which, for simplicity, we will take to be in a *p*-state (Figure 5). Since no individual electron flips its spin in this case, reflection symmetry in the *x*–*y* scattering plane allows only excitation of the $p_x$ and $p_y$ Cartesian components (Andersen et al., 1997). Thus we need only specify the individual amplitudes for excitation of these two states, $a_x$ and $a_y$, and their relative phase.

Next, we consider H(2*p*) excitation. Again, we can only excite the $p_x$ and $p_y$ states, but can now do this via either the triplet or singlet channel. Thus four amplitudes and three relative phases are required. Geometrically, these give us the relative sizes of the $p_x$ and $p_y$ charge clouds and their relative phase, as well as the target and scattered electron polarizations. Equivalently, the aspect ratio (length to width) and orientation of the excited *p*-state in the *x*–*y* plane is established. Finally, we consider Fr(7*p*) excitation. Because of Mott scattering, the incident electron can flip

its spin, meaning that $p_z$ states can be excited; only the $a_z$ amplitude requires such spin-flips. The scattering amplitudes now also depend on the direction of spin of the incident electron, indicated by the arrow superscripts in Figure 4 (Anderson & Bartschat, 1994a,b). This yields six complex scattering amplitudes or eleven independent parameters. These can in turn be related to the spin polarization of the two active electrons along the $x$, $y$, and $z$-axes, as well as the absolute sizes of the three component p-orbitals and their relative phases.

Typically, experiments will give partial information about the geometric shapes of the excited-state charge cloud and the magnitude and direction of the target and continuum electron polarizations. Various sets of experimental observables such as the ''generalized Stokes parameters'' and ''generalized STU parameters'' (Anderson & Bartschat, 2001) as well as irreducible multipole moments of the excited-state density matrix (Blum, 1996) can be used to extract the scattering amplitudes or (perhaps more satisfyingly) geometric information on the excited states and electronic polarizations. Such observables are generally not independent of each other, and extracting the most fundamental scattering amplitudes or geometric information from them can be numerically arduous, or, worse, ambiguous.

Following the collision, typically on the time scale of nanoseconds, the $L$ and $S$ states will relax into $J$ states. When these are resolved experimentally, the shape of the charge cloud is modified irreversibly. When fine structure is not resolved, the cloud will oscillate reversibly. These spatial quantum beats are the result of coupling between the various angular momenta in the excited target. In the case of molecular targets, there can be as many as four such angular momenta to consider when nuclear spin is included. This situation is shown schematically in Figure 6, where the oscillatory amplitudes of spring-coupled pendula correspond to the various angular momenta in the system. Experimental observables are usually those associated with angular-momenta-coupled states, but one can often extract the excited-state parameters immediately following the collision by writing the steady-state excited-state density matrix in a decoupled basis (Al-Khateeb et al., 2000, 2005; Blum, 1996; Hayes et al. 1996). Such coupling makes possible optical electron polarimetry (Gay, Furst et al., 1996a,b; see below) and, in principle, allows one to measure the relative phase of two excitation amplitudes (e.g., for $p_x$ and $p_y$ states) if experimental observables can be measured on a time scale comparable to that of the quantum beat period.

## 2.5. Theory, Archiving, and Formalism

One key aspect of the study of collisions involving polarized electrons is the very close collaboration between experimentalists and theorists. This is apparent from the large numbers of papers cited here with both theorists and experimentalists as authors. We make here only a few brief

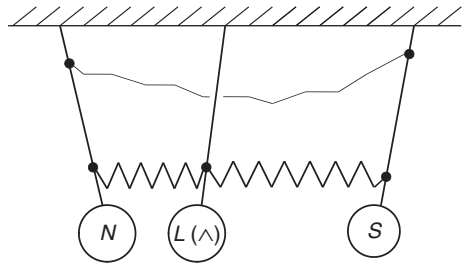


**FIGURE 6** Coupled pendula as an analog for spin–orbit, orbit rotational, and spin rotational coupling in atoms and molecules (see text). The case shown corresponds to a molecule with electronic orbital angular momentum L (with component Λ along the internuclear axis), electronic spin *S*, and rotational angular momentum *N*. Nuclear spin is ignored. The sagging spring indicates relatively weak coupling. The time required for amplitude oscillations of these pendula corresponds to the various eigenstate splittings of the target

comments about the state of theory. Close-coupling techniques—the so-called ''convergent close-coupling'' (CCC) method developed in Australia and the *R*-matrix methods developed originally in Belfast—have become increasingly sophisticated since the mid-1990s and have essentially solved all problems associated with light, one- and two-electron targets. They begin to run into trouble with the heavier noble gases and alkalis, even with the inclusion of relativistic and semirelativistic variations. Perturbative methods developed in York, Des Moines, and Rolla have had impressive success at higher energies, especially with (e,2e) problems. They are particularly useful in terms of closed-shell elastic processes. In both cases, all bets must be taken off the table for the ''great outback'' of the periodic table, that is, very heavy targets and lighter targets with partially filled shells. In this review, we will generally present only the most recent or sophisticated calculations when comparing experiment with theory. The reader should consult the relevant references for examples of earlier theory, and to see how the various physical assumptions incorporated in the theory cause changes in the predicted quantities.

It is important to remember the role played by computer engineering in the progress of theory. Problems that required prohibitively large amounts of computer time on mainframes in 1991 now run overnight with PCs, especially when the codes have been parallelized to run on numerous machines. Finally, the essential contribution of data reviewers and the development of formalism should be mentioned. The effort of compiling and organizing disparate data sets and the development of optimal mathematical frameworks for reporting and understanding these results is crucial for providing a road map for the future of the field.

The efforts of Profs. N. Anderson, K. Bartschat, and K. Blum are particularly noteworthy in this regard.

## 3. ATOMIC TARGETS

### 3.1. Exchange Scattering

#### 3.1.1. (e,e) and (e,2e) Processes

As examples of collisions in which only the exchange interaction is important, we first consider polarized electron scattering from light alkalis, Li and Na, which are also spin polarized. These collisions have been studied in detail in extensive experiments by the NIST (Na) and Bielefeld (Li) groups. Figure 7 shows the exchange asymmetry $A_{ex}$ (Equation (6)) as a function of scattering angle for Na with an incident electron energy of 4.1 eV (Lorentz et al., 1993). The asymmetry is measured by determining the counting rate for scattered electrons at a given angle as a function of the relative orientation of the incident and target electron spins. (Note, from Equation (6), that the overall orientation of the spins relative to the scattering plane is irrelevant.) In this experiment, the polarized incident

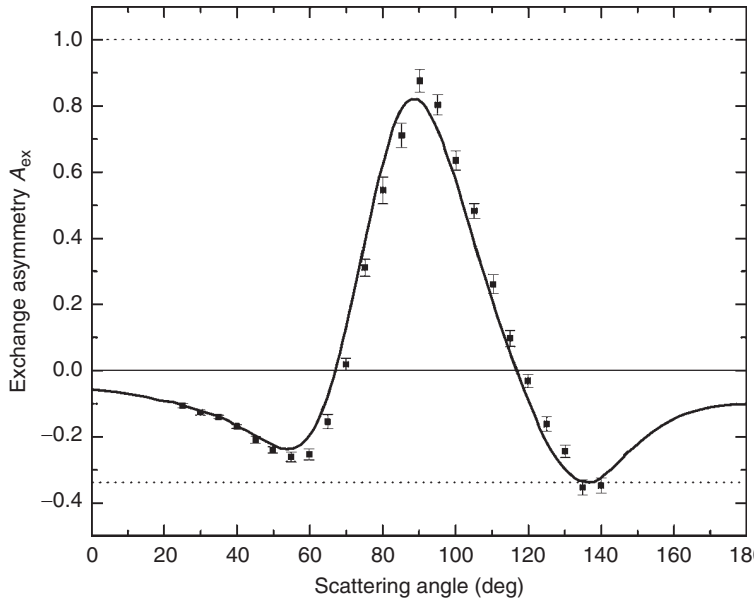


**FIGURE 7** Exchange asymmetry $A_{ex}$ for 4.1 eV electron-Na elastic scattering. Limits for pure singlet and pure triplet scattering are indicated by dashed lines (see text). Theory of Zhou et al. (1995) and Bray and McCarthy (1993) are essentially indistinguishable and are indicated by the solid line. Redrawn figure with permission from Zhou et al. (1995), *Physical Review A, 52*, 1152. Copyright (1995) by the American Physical Society

electrons were produced by laser photoemission from GaAs (Pierce et al., 1980; see Section 5.1.1 below). The spins of these electrons can be flipped by reversing the helicity of the laser. The Na was spin polarized to greater than 98% by optical pumping, allowing optical reversal of the target spin as well. The exchange asymmetry can be written in terms of the singlet and triplet cross sections (see Equation (3)):

$$A_{\mathrm{ex}} = \frac{|a^1|^2 - |a^3|^2}{|a^1|^2 + 3|a^3|^2} = \frac{\sigma^1 - \sigma^3}{\sigma^{\mathrm{tot}}_{\mathrm{av}}}. \tag{7}$$

Thus pure singlet scattering corresponds to $A_{\mathrm{ex}} = 1$ and pure triplet scattering implies $A_{\mathrm{ex}} = -1/3$. If $A_{\mathrm{ex}} = 0$, then exchange effects are unimportant in the collision. For light alkali atoms like Na, close-coupling (CC) theories involving a large number of excited states, which have become quite tractable in the last 15 years, do an excellent job of predicting these data (Bray & McCarthy, 1993; Zhou et al., 1995). The angular dependence of $A_{\mathrm{ex}}$ is due to the diffractive shape of the individual singlet and triplet cross sections (Zhou et al., 1995), but the reason why singlet scattering dominates at 90°, for example, has not been discussed in the literature.

The NIST group also investigated superelastic scattering from the first excited ($4^7P_4^o$) state of Cr (Hanne et al., 1993), and find results that are substantially similar to the equivalent quantities measured with Na (see, e.g., McClelland et al., 1989; Nickich et al., 1990). The Cr experiments were motivated by the high spin multiplicity of both the ground ($3d^54s$) and first excited state ($3d^54p$); both are spin septets. Apparently, however, the five spin-aligned d electrons essentially act as spectators to the continuum electron interaction with the 4p target electron. Interestingly, the spin-dependence of the angular momentum transfer to the target perpendicular to the scattering plane, $L_{\mathrm{perp}}$, is significant at both energies studied (6.8 and 13.6 eV), while the exchange asymmetry at 6.8 eV is essentially zero. Not surprisingly, a two-state CC calculation of these quantities does not predict them well (Bartschat, 1995).

More recently, the Münster group (Meintrup et al., 2000) has investigated spin exchange in elastic scattering from the ($3d^54s^2\ ^5S_{5/2}$) ground state of Mn by measuring the ratio of scattered electron polarization to that of the incident beam, $P'/P$. (Experiments of this type will be discussed in detail in Section 4.1.1.) In this situation, exchange must occur via a d-shell electron, of which there are five. It is instructive to consider the maximum value of the angular differential exchange cross section *per target electron in unfilled shells*, $g(\theta)$, normalized to the spin-averaged differential cross section. In Mn, at 20 eV and $\theta = 100°$, it reaches ~0.05. In the case of Na at 12.1 eV and 50° (Hegemann et al., 1993; see Section 4.1.1), it is three times larger. Thus most of the (direct) scattering from Mn is

occurring from the 4*s* electrons. A five-state *R*-matrix with pseudostates (RMPS) calculation by Bartschat (Meintrup et al., 2000) provides only fair agreement with the experimental $P'/P$ data.

The Bielefeld group of Profs. Baum and Raith has investigated scattering from Li and Cs. In this section, we consider only (e,2e) experiments with Li. The major apparatus used for this experiment (and also for studies of Cs—see below) is shown in Figure 8 (Streun et al., 1998). A polarized electron beam crosses a Li beam polarized by passage through a 6-pole magnet. The beam polarizations are monitored by a Mott polarimeter and another 6-pole magnet, respectively. Two rotatable hemispherical energy analyzers view the collision region. Figure 9 shows the data for $A_{ex}$ (Equation (7); constructed from the two-electron coincidence rates with opposite orientations of incident electron and target spin) with an incident energy of 54.4 eV obtained when both continuum electrons after the ionization have the same energy, 24.5 eV. One of the ionized electron detection angles is fixed at $\theta_A = 45°$ from the incident electron direction in the plane perpendicular to the polarization axis. These data indicate that singlet scattering dominates these processes and that its fraction of the total scattering cross section varies little with scattering angle between the two electrons. Note that when the 2e wavefunction is spatially symmetric about the incident beam direction, that is, at $\theta_B = 45°$, antisymmetrization of the total wavefunction demands that the electrons be in an antisymmetric, that is, singlet state. This requires $A_{ex} = 1$, which is consistent with the two data runs shown. Both the CCC and distorted-wave Born approximation (DWBA) calculations

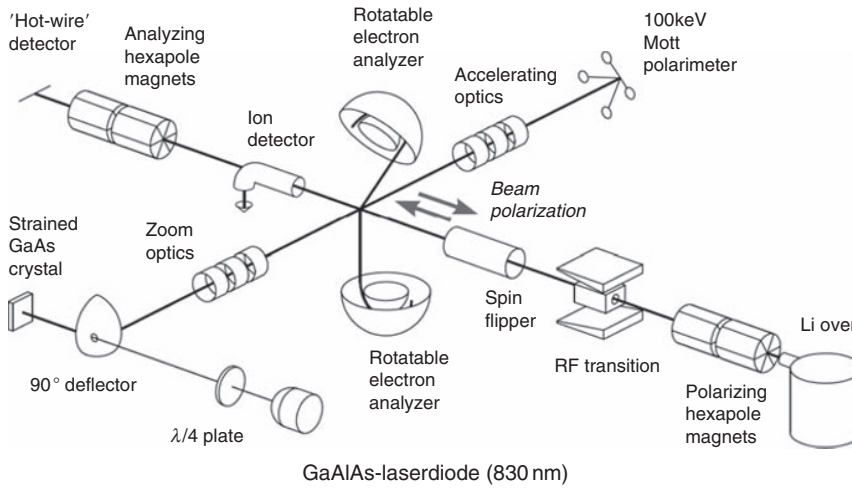


**FIGURE 8** Apparatus used by Streun et al. (1998) to investigate exchange effects in Li (e,2e) collisions

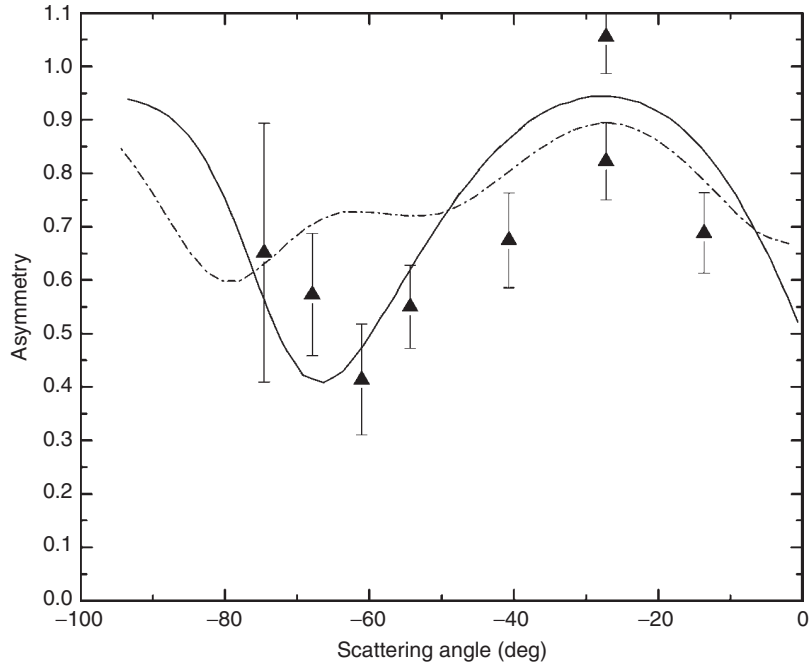


**FIGURE 9** Data of Streun et al. (1998) for $A_{ex}$ for 54.4 eV electrons ionizing Li as a function of the scattering angle $\theta_B$ of one of the ionized electrons. The second electron is detected at a fixed angle $\theta_A = 45^\circ$ relative to the incident beam axis. Theoretical predictions of a convergent close-coupling (CCC) calculation and a distorted-wave Born approximation (DWBA) calculation from Streun et al. (1998) convoluted with the experimental resolution, are also shown

of Streun et al. (1998) are qualitatively consistent with the data. More recent CCC calculations by Bray et al. (1999) do not change this picture significantly.

In this regard, we note that exchange effects in total ionization cross sections have been made for all of the Column I elements except Rb and Fr, as well as He*($2^3$S) metastable states (see Lubell (1993) and Baum et al. (1993), and references therein). In this case, $A_{ex}$ is measured by determining the positive ion yield integrated over all electron trajectories as a function of the relative spin directions of the incident and target electrons. At the ionization threshold, $A_{ex}$ is always positive, indicating the dominance of singlet scattering. With the possible exception of K, it also has a positive slope with increasing energy in the vicinity of threshold. Attempts to show that $A_{ex}$ for these systems is particularly sensitive to departures from the classical Wannier ionization threshold law, such as the

Temkin Coulomb-dipole picture, have proved controversial, and no clear evidence yet exists for this assertion (Lubell, 1993; Guo, & Lubell, 1993).

### 3.1.2. (e,$\gamma$e) and (e,$\gamma$2e) Processes

In the case of target excitation, fluorescence polarization can be a sensitive probe for study of the relative importance of direct and exchange processes. In a typical ''integrated Stokes parameter'' measurement (Furst et al., 1993), a beam of polarized electrons excites a target, and the polarization of the light emitted in the direction of the incident polarization axis is determined. The three relative Stokes parameters needed to completely characterize the polarization state of the fluorescence are

$$P_1 = \frac{I_0 - I_{90}}{I_0 + I_{90}}; \quad P_2 = \frac{I_{45} - I_{135}}{I_{45} + I_{135}}; \quad P_3 = \frac{I_{\mathrm{RHC}} - I_{\mathrm{LHC}}}{I_{\mathrm{RHC}} + I_{\mathrm{LHC}}}, \tag{8}$$

where the $I$s with numerical subscripts $\theta$ correspond to the intensities of linearly polarized light at an angle $\theta$ relative to a given axis of quantization, and $I_{\mathrm{RHC(LHC)}}$ are the intensities of right-handed (left-handed) circularly polarized light. In the most typical case of transverse polarization in which the axis of quantization is taken to be the electron beam direction, one can show that $P_1$ is independent of polarization, that $P_2$ will be nil unless spin–orbit forces act, and that $P_3$ is proportional to the exchange cross section (Anderson & Bartschat, 2001; Blum, 1996; Furst et al., 1992).

Extensive measurements of this type have been made recently by the Perth group of Prof. Williams and the Rolla and Nebraska groups of the author (see Al-Khateeb et al., 2005; Yu et al., 2001; and references therein). Figure 10 shows the polarization fraction $P_3$ as a function of incident electron energy for two transitions in Ne($2p^5 3p$) from the $3p[5/2]_3$ $^3D_3$ state (Figure 10(a) and (b)) and the $3p'[3/2]_2$ ''$^3P_2$'' states (Figure 10(c)). The spectroscopic notation for the latter state is in quotes because it is intermediately coupled—a mixture of 18% $^3D_2$, 53% $^3P_2$, and 29% $^1D_2$ Russell–Saunders states (Luke, 1986). The $^3D_3$ state is well $LS$ coupled, that is, it is a pure triplet state. As such, it can only be excited by exchange (Kessler, 1985). This means that its decay fluorescence is ideal for electron polarimetry (Gay, Furst et al., 1996a,b; see Section 4.2.2 below) as long as cascading does not influence the transition. This begins to occur 1.1 eV above the $^3D_3$ excitation threshold, and we see that $P_3$ is quite flat within this range (Figure 10(b)). As the incident electron energy increases, $P_3$ drops off due to cascading from unpolarized higher lying states that can be excited by direct transitions. This stands in contrast with the ''$^3P_2$'' state, which drops quickly from its maximal spin polarization as direct excitation of the main state becomes increasingly important. A combination of the diminishing importance of exchange and cascading drive $P_3$ to zero within 20 eV of

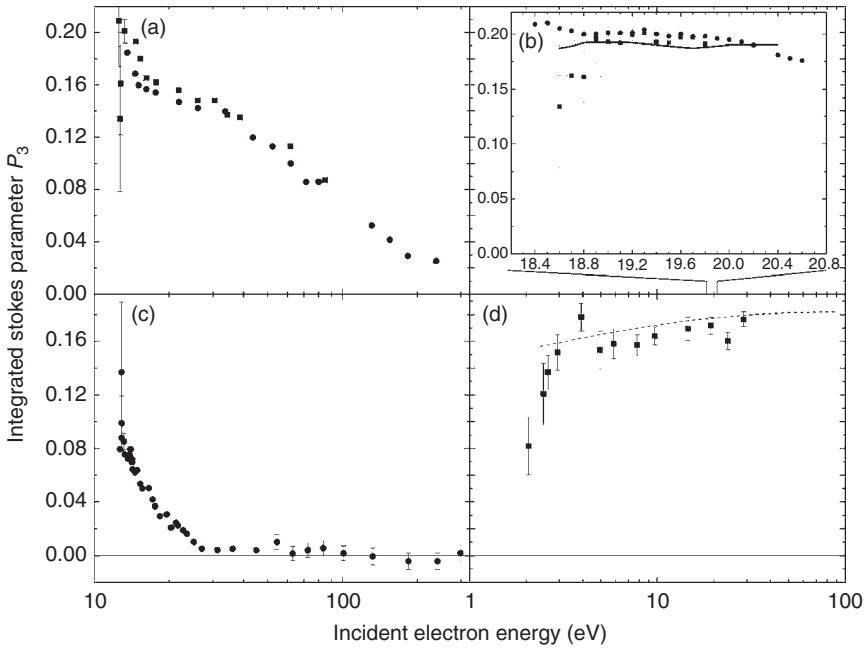


**FIGURE 10** (a) and (b) Relative Stokes parameter $P_3$ corresponding to circular polarization for the Ne $2p^5 3p[5/2]_3 \rightarrow 3s[3/2]_2$ 640.2 nm transition. Solid circles are the data of Hayes et al. (1996), solid squares are those of Furst et al. (1993). Solid line: semirelativistic *R*-matrix calculation of Bartschat and Zeman (Yu et al., 2000). (c) Data for the $3p'[3/2]_2 \rightarrow 3s[1/2]_1$ 667.8 nm Ne transition; data of Yu et al. (1997b). (d) Data from Bukhari et al. (1995) for the fine-structure-unresolved $3^2P \rightarrow 2^2S$ transition in spin-polarized Na excited by unpolarized electrons. Dashed line: theory of Kennedy et al. (1977)

threshold. *R*-matrix CC calculations have yielded quite good predictions of the integrated Stokes parameters in the case of the light noble gases such as Ne. Generally speaking, however, the reliability of these calculations diminishes as the target $Z$ increases (Yu et al., 2000).

An interesting variation on experiments of this type has been done by Bukhari et al. (1995), in which they excited Na and K atoms spin polarized in a 6-pole magnet with unpolarized electrons. In this case, the resonance fluorescence will exhibit nonzero $P_3$ only in the case of a direct excitation. In contrast with the spinless initial target states just discussed for the noble gases, $P_3$ in these experiments increases to an asymptotic value with no apparent effects due to cascading (Figure 10(d)).

This technique has also been used to investigate ionization/excitation collisions with noble gases (Al-Khateeb et al., 2000, 2005; Hayes et al., 1998) and Zn (Yu et al., 2001). The Nebraska group investigated production of the $Ar^{+*}[3p^4(^1D)4p]$ manifold of states. The collision process excites

and/or ionizes individual electrons over ~50 as. In this configuration, the core holes subsequently couple in ~1 fs to form a core orbital angular momentum $l_c = 2$, and a core spin $s_c = 0$ (see Figure 11). Within about 3 fs, $l_c$ and the outer orbital angular momentum $l_o = 1$ couple to form $L = 1, 2,$ or 3. Core-outer spin coupling occurs over ~10 fs, and $L$ and $S$ relax into the fine-structure $^2F_{7/2,5/2}$, $^2D_{5/2,3/2}$, and $^2P_{1/2,3/2}$ states over the course of hundreds of femtoseconds. By making integrated Stokes parameter measurements for at least three of these states, one can determine the electric quadrupole and hexadecapole of the core, corresponding to its rank 2 and rank 4 multipole moments, respectively (Blum, 1996), as well as the quadrupole moment and magnetic dipole moment of the outer $4p$ electron, the latter being proportional to its spin polarization.

This information allows one to study the collision on a timescale of femtoseconds, and to determine the multipole moments of individual excited-state shells. The data for the coupled-$L$ electric quadrupole moments and the outer-shell magnetic dipole moment are shown in Figure 12(a). The assumption that the individual shell multipole moments are formed during the collision, regardless of the final fine-structure states they ultimately couple to form, is confirmed by that fact that the final spin magnetic dipole is independent of the fine-structure state in which it is measured, and the fact that the two $F$ fine-structure states yield the same $L = 3$ quadrupole moment. The value of the magnetic dipole moment for the $4p$ electron would be 0.71 if the outer shell were excited exclusively by exchange. The measured value of ~0.25, thus, indicates a significant

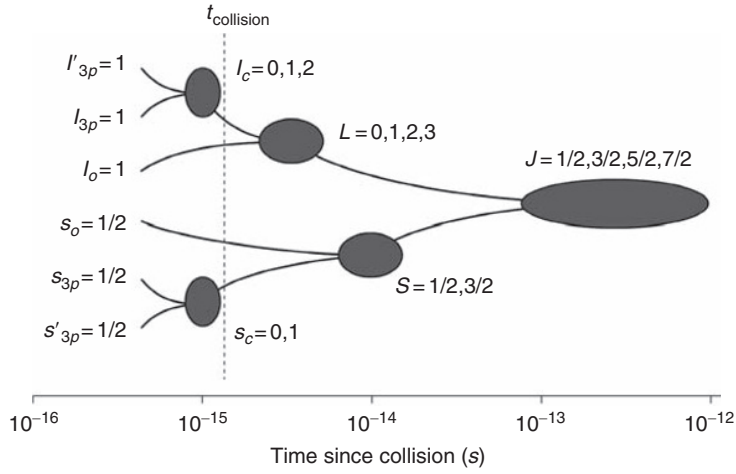


**FIGURE 11** Angular momentum coupling times of the $Ar^+$ ($3p^4 4p$) states. Vertical dotted line indicates the collision time. The horizontal widths of the ovals represent the range of coupling times for the entire configuration (from Al-Khateeb et al., 2005)

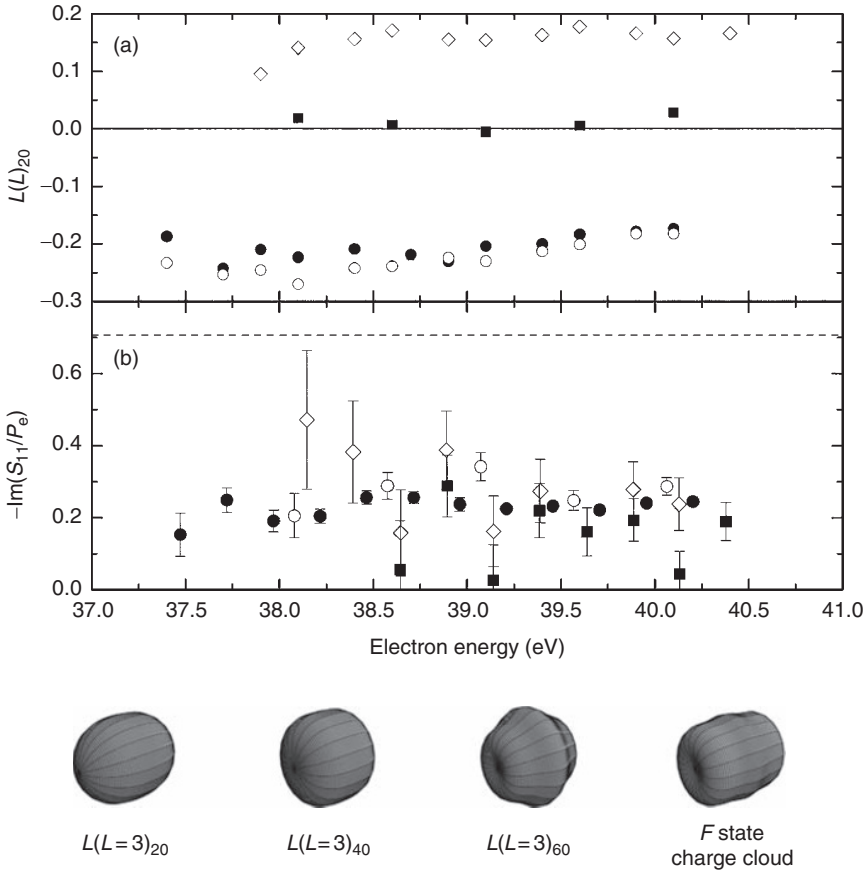


**FIGURE 12** (a) $Ar^+$ ($3p^4 4p$) derived $L$-state electric quadrupole moments and (b) $S$-state magnetic dipole moments (see text). Data are for the excited $^2F_{7/2}$ states (open circles), $^2F_{5/2}$ states (solid circles), $^2D_{5/2}$ states (diamonds), and $^2P_{3/2}$ states (squares). The dashed line corresponds to pure exchange excitation of the 4p subshell. At the bottom are shown contributions to the $L = 3$ charge cloud of the quadrupole (20), hexadecapole (40), and hexacontatetrapole (60) moments for an incident electron energy of 40.15 eV

direct-excitation amplitude. Parenthetically we note that this multistate measurement procedure allows one to determine the electric multipole moments for the $F$-state up to rank 6—the hexacontatetrapole moment. The $F$-state charge cloud spatial distribution, including this moment as well as the quadrupole and hexadecapole contributions, is shown at the bottom of Figure 12.

Similar experiments involving Kr have been done in Perth (Hayes et al., 1998), in which they investigated excited states with a $^3P$ core. Individual-shell multipole moments were not extracted in this work. Finally, we note an interesting integrated Stokes parameter experiment, also done at Perth, in which the $3d^9 4s^2\ ^2D_{3/2}$ ionic state was excited from the ground $3d^{10}4s^2\ ^1S_0$ state of Zn (Yu et al., 2001). In this case, the 3d core hole is spin polarized by exchange, albeit weakly; the magnetic dipole moment of the core decreases from a maximum value of 0.06 near the excitation/ionization threshold. No theory for any of the excitation-ionization experiments of this type has been published.

## 3.2. Mott Scattering

### 3.2.1. (e,e) Processes

In its simplest form, spin–orbit coupling of the scattered continuum electron to the target manifests itself as nonzero values of $S_A(\theta)$ or $S_P(\theta)$ (Section 2.2). In the case of elastic scattering from spinless targets, these two must be the same. Thus their equivalence can serve as a check on experimental accuracy. To resolve gross discrepancies between earlier experiments and theory, very careful cross measurements of $S_A$ and $S_P$ were performed by the Münster group with Xe targets (Müller & Kessler, 1994). Their results for 150 eV incident electron energy as a function of scattering angle are shown in Figure 13(a). The two data sets, based on completely different experiments with different systematics, are in quantitative agreement. The semirelativistic calculations of Bartschat, McEachran, and Stauffer (private communication with Münster) are in generally good agreement with the experiment, but have difficulty in the regions of the differential cross section diffractive minima, where $S$ is the largest. The experimental angular resolution may also contribute to the disagreement.

The presence of Mott scattering can also lead to breakdown in the kinematic relationships associated with the fine-structure effect (see the following section). In the case of inelastic scattering from a target, $S_A$ need no longer equal $S_P$. However, one can show that if spin–orbit coupling is negligible in the case of $^1S \rightarrow {}^3P$ exchange excitation where fine structure is resolved, one must have $S_A(^3P_0) = -2S_A(^3P_2)$ (Hanne, 1983). Such measurements, made with essentially the same apparatus as those just discussed, are shown in Figure 13(b) (Dümmler et al., 1995). While the kinematic relation appears to hold for low scattering angles, large deviation, indicating the presence of spin–orbit effects, occur at angles greater than 60°. Similar experiments and theory have recently been carried out for a variety of other targets, including Kr (Went et al., 2002), Rb (Guinea

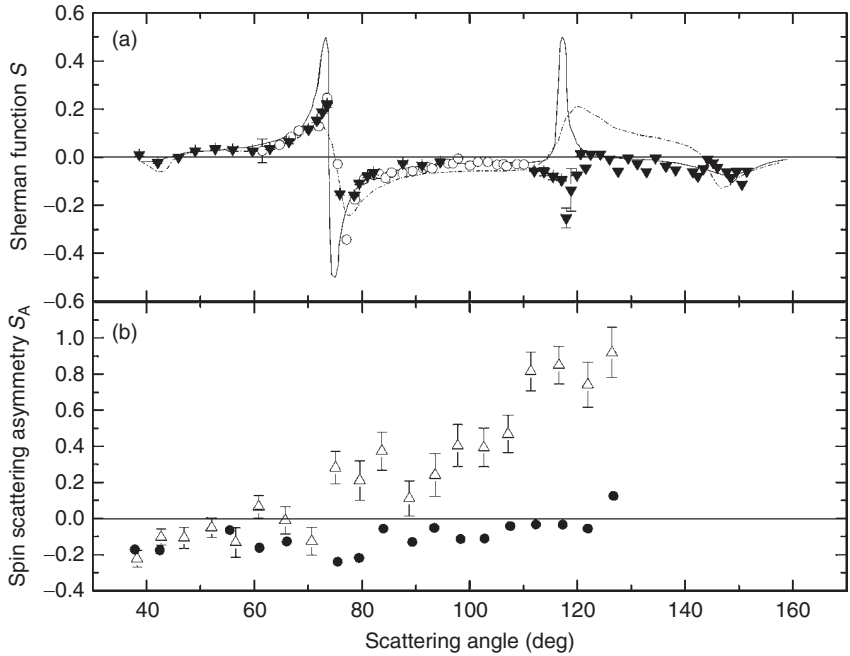


**FIGURE 13** (a) Sherman function for 150 eV elastic scattering from Xe as a function of scattering angle. Solid triangles are values of $S_A$; open circles are the $S_P$ data (see text). Solid line represents the semirelativistic calculations of Stauffer; the dashed line those of Bartschat (see Müller & Kessler, 1994, for details). (b) Comparison of $S_A(^3P_0)$ (solid circles) and $-2S_A(^3P_3)$ (open triangles), which should be the same in the absence of Mott scattering (Dümmler et al., 1995)

et al., 2005; Payne et al., 2005), Hg, Tl, and Pb (Dümmler et al., 1992), Zn, Cd, and In (Bartsch et al., 1992), and Ca, Sr, Ba, and Yb (Yuan, 1995).

Mott scattering in Cs, the heaviest practicable alkali target, has been studied extensively by the Bielefeld group for both elastic and inelastic scattering (Baum et al., 1999, 2002, 2004; Leuer et al., 1995) in close collaboration with a broad effort in theory (Ait-Tahar et al., 1997; Anderson & Bartschat, 2002; Bartschat, 1993; Bartschat & Bray, 1996; Thumm et al., 1993; Zeman et al., 1994, 1995). Figure 14 shows the experimental and theoretical data for elastic scattering at 3 eV. This is an energy that the Bielefeld group and their theoretical collaborators chose to optimize the chances for agreement, based on experimental systematic issues and count rates, and the better applicability of CC approaches at low energies. The exchange asymmetry, $A_{ex}$, the spin–orbit asymmetry, $A_{so} = S$, and the interference asymmetry $A_{int}$ (to be discussed in the next section) contained in Equation (6) were measured, as well as the differential cross section. While the state-of-the-art calculations (except for the

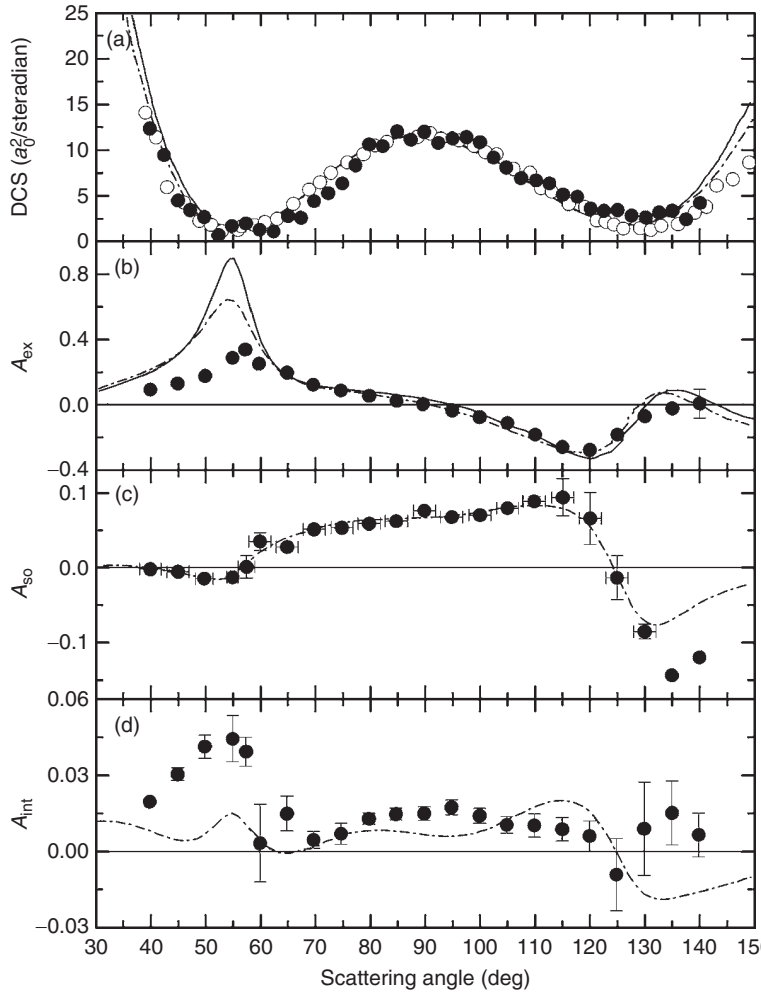


**FIGURE 14** Elastic scattering of 3 eV electrons from Cs. Data for (a) the differential cross section (DCS); (b) $A_{ex}$; (c) $A_{so}$; (d) $A_{int}$. Solid circles, data of Baum et al. (1999); open circles, data of Gehenn and Reichert (1977). Theory: dashed line (––), semirelativistic Breit–Pauli 8-state calculation; solid line (–), nonrelativistic CCC calculation (see Baum et al., 1999). For the DCS, the CCC calculation was multiplied by 0.82; it is identically zero for $A_{so}$ and $A_{int}$. Experimental angular resolution has been taken into account for the theory curves. Redrawn figure with permission from Baum et al. (1999), *Physical Review Letters, 82*, 1128. Copyright (1999) by the American Physical Society

fully relativistic one!) quantitatively predict the spin-averaged differential cross section, only the semirelativistic Breit–Pauli theory matches $S$ ($A_{so}$), and even its predictions break down at the highest scattering angles. The exchange asymmetry is poorly described at the lowest scattering

angles, presumably due to the failure of the theories to account for the target core polarization. At this low energy, the exchange effects are generally larger than the Mott scattering effects.

#### 3.2.2. (e,e$\gamma$) and (e,2e) Processes

We now increase the incident electron energy by five orders of magnitude (with an increase in $\gamma$ from 1.0000059 to 1.59) and consider the scattering of 300 keV electrons from high-$Z$ targets in manifestly relativistic collisions. The Tübingen group of Prof. Nakel has studied spin asymmetries in differential bremsstrahlung production, as well as in (e,2e) processes (Besch et al., 1998; Mergl et al., 1992; Prinz et al., 1995; Sauter et al., 1998). The former process is shown schematically in Figure 15(a). The angular distribution of bremsstrahlung will depend sensitively on the trajectory of an electron near the heavy nucleus from which it scatters. This trajectory will, in turn, depend on the electron's spin. Hence, one would expect a spin dependence of the bremsstrahlung fluence at a given emission angle. This asymmetry is shown for a Au target in Figure 16(a) for a scattered electron energy loss of 100 keV. The early calculations of Haug (Mergl et al., 1992) are in good agreement with the measurements, although later, more sophisticated relativistic partial-wave calculations of Tseng (2002) are in poorer agreement.

Similar effects are seen in (e,2e) experiments from Au (Sauter et al., 1998). Collisions of this type are shown schematically in Figure 15(b). In this case, the scattered electron angular distribution is dominated by the binary peak, corresponding to electron ejection following a direct electron–electron collision. The broader recoil maximum comprises electrons that, following the initial electron–electron interaction, swing by the nucleus before emerging from the collision volume. Because binary peak electrons are produced directly without significant interaction with the nucleus, spin–orbit coupling, and hence spin dependence, should be small. The recoil peak, however, is expected to exhibit large asymmetries. This expectation is realized in the data (Figure 16(b)), where the binary peak asymmetry is consistent with zero, while the recoil asymmetries are as large as 20%. A relativistic distorted-wave Born approximation (rDWBA; Keller et al., 1999) is in quantitative agreement with these results.

### 3.3. Combinations of Spin–Orbit Coupling and Exchange Effects

#### 3.3.1. The Fine-Structure Effect and its Variants

**3.3.1.1. (e,2e) Experiments** The ''fine-structure'' effect (see Section 2.3) was studied extensively in the 1970s and 1980s for excitation (and de-excitation) of a variety of targets, most prominently Na and Hg

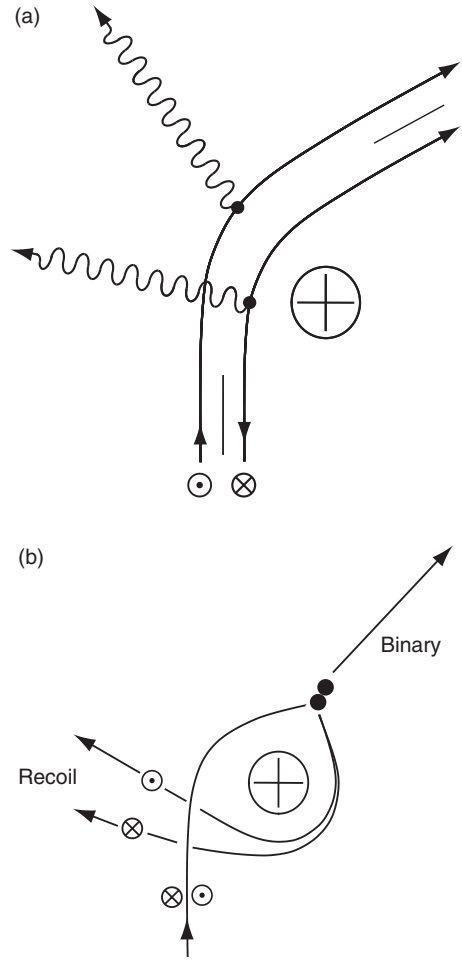


**FIGURE 15** Schematic representations of (a) bremsstrahlung production and (b) ionization in the vicinity of a heavy (+) nucleus (see text)

(see Hanne, 1983; Anderson & Bartschat, 2001; and references therein). In effect, it results from an interference between exchange processes and the target's internal spin–orbit interaction. It results in, for example, a dependence on the incident electron spin of the differential scattering cross section for excitation of an unpolarized target, even if spin–orbit forces acting on the continuum electron are negligible. In this way, it mimics Mott scattering, but requires that the fine-structure state of the excited

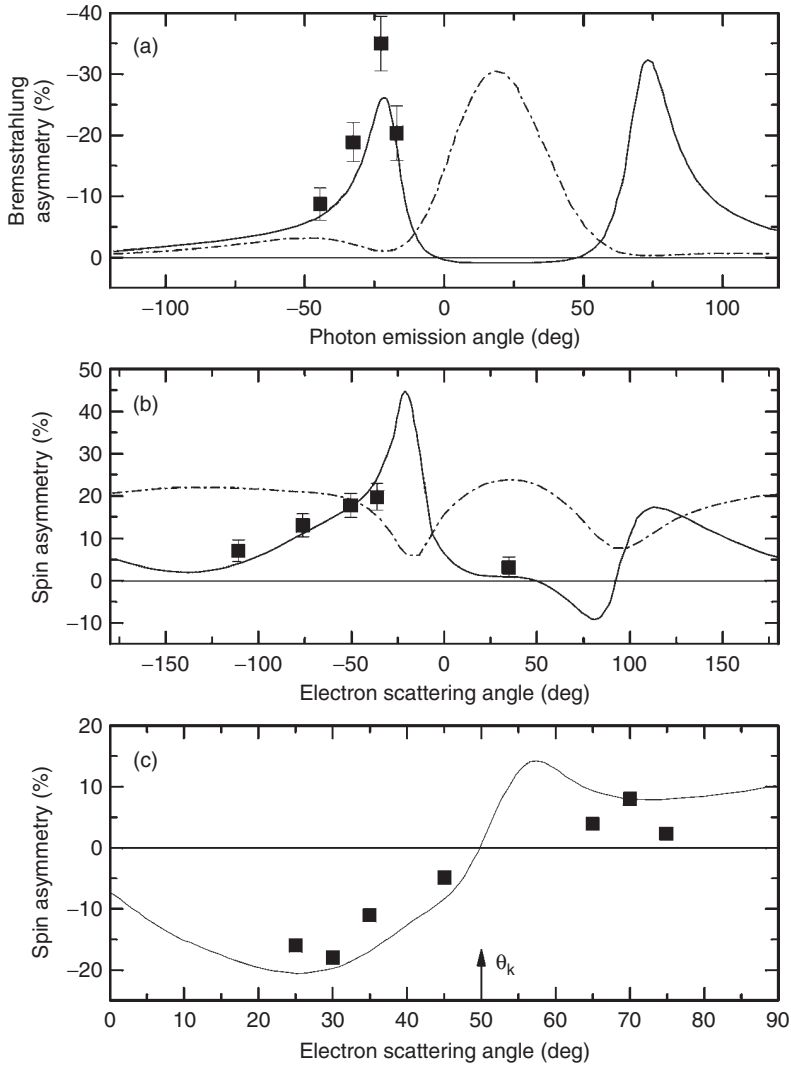


**FIGURE 16** Relativistic collisions of 300 keV electrons with Au and U. (a) Spin asymmetry of bremsstrahlung production versus emission angle for electron scattering from Au at 45° with 100 keV energy loss. Data of Mergl et al. (1992). Solid line—fully relativistic DWBA (rDWBA) calculations of spin asymmetry by Haug (see Mergl et al., 1992); dashed curve—theoretical photon emission cross section for unpolarized incident electrons. Redrawn figure with permission from Mergl et al. (1992), *Physical Review Letters, 69*, 901. Copyright (1992) by the American Physical Society. (b) Spin asymmetry as a function of the fast (148 keV) electron scattering angle for ionization of Au target K-shells. The slow scattered electron was measured at −9° with 71 keV energy. Data of Sauter et al. (1998); solid line—rDWBA calculation of Keller et al. (1999) for the spin asymmetry; dashed line—DCS for unpolarized electrons indicating the binary and recoil maxima. (c) Spin asymmetry for ionization of the L-shell $2p_{3/2}$ level of U versus outgoing slow (72.8 keV) electron scattering angle. Fast electron

target be resolved. Following a suggestion by Hanne in the early 1990s, it was realized that similar spin-dependent effects could exist in (e,2e) processes, specifically with regard to noble gas targets.

Consider a process in which an incident (spin-up) electron ionizes a 5p Xe electron (Jones et al., 1994). For simplicity, we consider an asymmetric scattering energy and geometry for the two electrons, but assume that the incident electron spin is perpendicular to the scattering plane containing them. By measuring the energies of the two scattered electrons, we determine that the residual ion is in, for example, the $5p^5\,{}^2P_{3/2}$ state. Moreover, this valence-hole state will in general have been given orbital angular momentum perpendicular to the scattering plane—we will take it to be ''up'' in this case. There will thus be a propensity for the ionized electron to be spin-''down.'' If, for these kinematics, we take the triplet scattering amplitude to exceed the singlet amplitude, then the differential (e,2e) cross section for this case will be bigger for incident spin-down electrons than for those with spin-up.

The first observation of this type of spin asymmetry was made by Guo et al. (1996). More recent data from the ANU group (Dorn et al., 1997) are shown in Figure 17. The asymmetries for the two residual ion fine-structure states are large, and in good agreement with semirelativistic and nonrelativistic DWBA calculations. (However, the agreement with theory is significantly worse for other kinematic variables that were investigated.) If continuum spin–orbit effects are negligible, then $A({}^2P_{1/2})$ should equal $-2A({}^2P_{3/2})$. This is very nearly the case, as is seen from Figure 17(c). (Compare with the data for Xe $({}^3P_{2,0})$ excitation in Figure 13(b).) Interestingly, however, relativistic effects do manifest themselves in the fine-structure cross section branching ratios. If dynamics were not important, one would expect the statistical ratio of 2 for $\sigma({}^2P_{3/2})/\sigma({}^2P_{1/2})$. Instead, it ranges from $\sim$2.4 to 3.2 over the angular range of the experiment. However, given that the ionic fine-structure splitting in Xe is 1.3 eV, while the incident electron energy in this experiment was 147 eV, the deviation from the statistical ratio is somewhat surprising. Both fine-structure asymmetries have zeros on the ''Bethe ridge,'' the kinematic point where there is no momentum transfer to the residual ion. This symmetry forbids the ion from having orbital angular momentum perpendicular to the scattering plane, and hence no fine-structure spin-propensity can arise.

The fine-structure effect in the ionization of Xe has been studied extensively, primarily because it is relatively easy to separate the ionic valence-

energy loss is 90 keV with a scattering angle of $-24.8°$. Redrawn figure with permission from Besch et al. (1998), *Physical Review A, 58*, R2638. Copyright (1998) by the American Physical Society. The momentum transfer direction, $\theta_K$, is indicated (see text); the angular range of the graph corresponds to the binary peak. Data of Besch et al. (1998); solid line—rDWBA calculation of Keller et al. (1999)

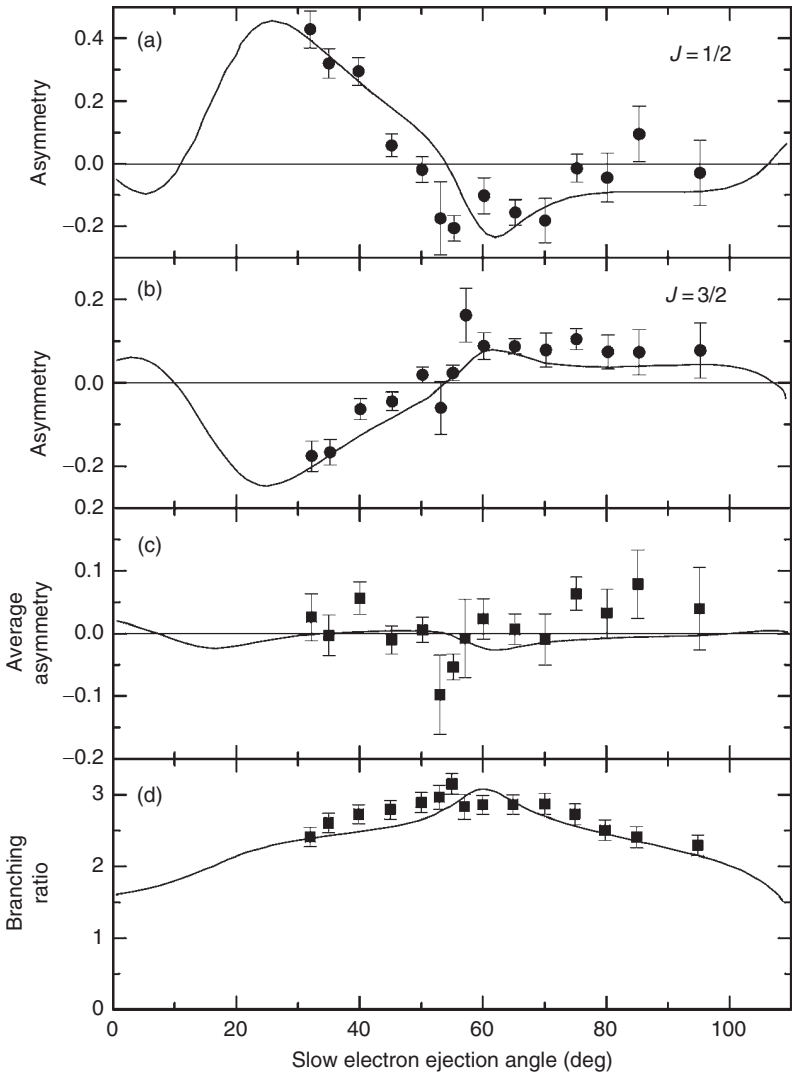


**FIGURE 17** Fine-structure spin asymmetries for 147 eV ionization of Xe as a function of the slow scattered electron angle. Fast electron energy is 100 eV and its scattering angle is 28°. Solid line represents the predictions of a semirelativistic DWBA calculation; both data and theory are from Dorn et al. (1997). (a) Asymmetry $A_{1/2}$ for residual $5p^5\ ^2P_{1/2}$ ionic states. (b) Asymmetry $A_{3/2}$ for residual $5p^5\ ^2P_{3/2}$ ionic states. (c) Average asymmetry $= (A_{1/2} + 2A_{3/2})/3$ corresponding to the fine-structure-unresolved case. (d) Branching ratio for the $J = 3/2$ to $J = 1/2$ cross sections (see text)

hole fine structure (Bellm et al., 2008b; Madison et al., 1998; Mette et al., 1998; Panajotovic et al., 2006; Prideaux & Madison, 2004). One experimental investigation of Kr has been carried out (Bellm et al., 2008a). While

state-of-the-art DWBA calculations are in excellent agreement with the Kr data, Xe experimental asymmetries are generally only in qualitative agreement with these calculations.

In this context, we return to the Tübingen (e,2e) data (Figure 16(c)). Besch et al. (1998) studied emission from U foils and considered only ionized electrons from the L-shell $2p_{3/2}$ state. By looking at the binary peak, where spin–orbit forces on the continuum electrons are expected to be small (see Figure 16(b)), any spin asymmetry would be due to a pure fine-structure effect. The observed asymmetries are significant, with a flip in their sign at the Bethe ridge. This provides strong circumstantial evidence that these asymmetries are, in fact, caused by the fine-structure effect.

3.3.1.2. (e,e$\gamma$) Experiments Fluorescence polarization is often strongly dependent on the combination of exchange excitation and internal target spin–orbit coupling. The measurement of integrated Stokes parameters, while having the disadvantage that dynamics specific to the scattering angle of the electron are averaged over, has the benefit of relatively high count rates. Moreover, the increased axial symmetry of the collision means that some dynamical effects can be seen unambiguously. Bartschat and Blum (1982) were the first to point out that in an integrated Stokes parameter measurement with transversely polarized incident electrons and observation along the polarization axis, $P_2$ would be identically zero in the absence of spin–orbit forces, either due to Mott scattering or internal target coupling, that cause the total spin wavefunction to not be factorable from the overall wavefunction. Thus, measurement of this Stokes parameter acts as a sensitive test of such interactions; in an electron–photon coincidence measurement, $P_2$ can result from purely Coulombic interactions.

We consider in this section the case of relatively low-$Z$ targets such as Ne, Ar, and Kr (meaning that Mott scattering can be neglected) that have intermediately coupled excited states. We consider the $np^5(n+1)p$ states of these atoms. In the intermediate coupling scheme, the $J, M$ states can be written as (Blum, 1996)

$$|J,M\rangle = \sum_i a_i \sum_{M_{L_i},M_{S_i}} |L_i S_i M_{L_i}, M_{S_i}\rangle \langle L_i S_i M_{L_i}, M_{S_i}|JM\rangle, \tag{9}$$

where the $a_i$ are the intermediate coupling coefficients and the summed ket states are well $LS$ coupled. In this case, the excited state density matrix multipole moments can be written as (Hayes et al., 1996)

$$\langle T(J)^{+}_{KQ}\rangle = \sum_{i,j} a_i a_j \sum_{K_1 Q_1} \sqrt{2k+1}\sqrt{2K+1}(2J+1)(K_1 Q_1 kq|KQ) \times \begin{Bmatrix} K_1 & k & K \\ L_j & S_j & J \\ L_i & S_i & J \end{Bmatrix} \langle T(L_i L_j)^{+}_{K_1 Q_1}\rangle \langle T(S_i S_j)^{+}_{kq}\rangle, \tag{10}$$

where $\langle T(L_i L_j)^{+}_{K_1 Q_1}\rangle$ and $\langle T(S_i S_j)^{+}_{kq}\rangle$ are the multipole moments of the coupled spin and orbital angular momentum of the excited state. Referring to Equation (8), we note that

$$P_1 \propto \langle T(J)^{+}_{20}\rangle; \quad P_2 \propto \langle T(J)^{+}_{21}\rangle; \quad P_3 \propto \langle T(J)^{+}_{10}\rangle, \tag{11}$$

for the geometry under consideration. The linear polarization fraction $P_1$ is independent of the electron polarization and is sensitive only to the Coulombic interaction with the target. The circular polarization $P_3$ is proportional to the exchange cross section. For the linear polarization $P_2$ to be nonzero requires both exchange and that more than one $a_i$ coefficient be nonzero in the expansion (9).

In the absence of Mott scattering $\langle T(L_i L_j)^{+}_{21}\rangle$ is identically zero, so the only $L$ and $S$ multipole moments that can be produced in the collision are $\langle T(L_i L_j)^{+}_{00}\rangle$, $\langle T(S_i S_j)^{+}_{00}\rangle$, $\langle T(L_i L_j)^{+}_{20}\rangle$, and $\langle T(S_i S_j)^{+}_{10}\rangle$. The first two correspond to the total excitation cross section, while the latter two are the excited state's nascent alignment along the beam axis and spin polarization perpendicular to it. As the atom relaxes into its fine-structure components, the $\langle T(J)^{+}_{KQ}\rangle$ are established. Using Equation (10), it can be shown (Birdsey, 2003) that under these conditions, $\langle T(J)^{+}_{21}\rangle$ and, thus, $P_2$, is identically zero, even for the case of intermediate coupling, unless some multipole moments with $L_i \neq L_j$ and $S_i \neq S_j$ are nonzero. Such ''rectangular'' multipole moments correspond to coherence between the different values of $L$ and $S$ present in the intermediate coupling expansion (Equation (9)). Only integrated measurements of $P_2$ are sensitive to these coherences.

An example of such a measurement with a Kr target is shown in Figure 18 (Furst et al., 1993). This canted linear polarization fraction indicates that the charge cloud of the excited atom has rotated is a direction corresponding to the direction of spin of the exchanged, polarized electron now in the target. This is allowed by symmetry: the axial vector of electron spin has become a spatial axial vector defined by the beam axis and the new axis of symmetry of the excited atom. This conversion occurs as a result of the breakdown of spin and orbital angular momentum as good quantum numbers in the target. The coherence between the different values of $L$ and $S$ determine the final angle through which the charge cloud is rotated. Integrated measurements of $P_2$ for a

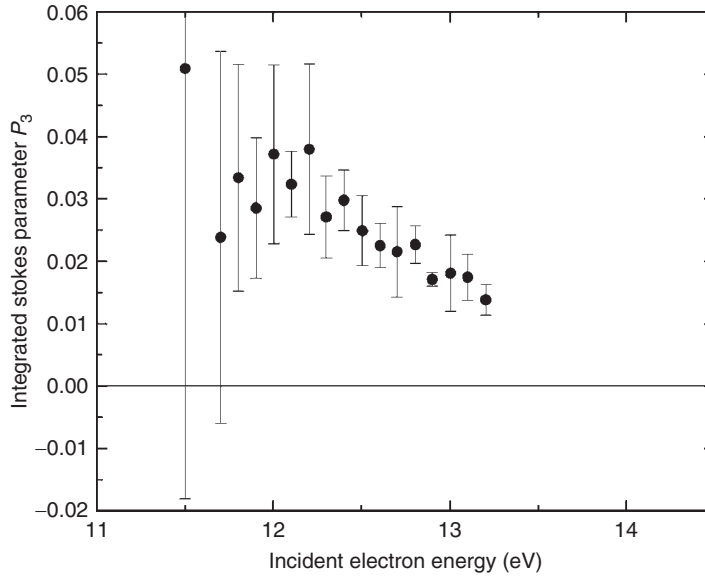


**FIGURE 18** Integrated Stokes parameter $P_2$ for the $4p^5 5p[5/2]_2 \rightarrow 4p^5 5s[3/2]_1$ 877.7 nm transition in Kr. Threshold for the excitation of the upper intermediately-coupled state is at 11.44 eV. Data of Furst et al. (1993)

variety of targets and extensive theoretical work have been carried out (Ne, Kr, Xe—Yu et al., 2000; Ne, Kr—Zeman et al., 1997; Ar, Xe—Srivastava et al., 1996; Ar, Kr, Xe—Srivastava et al., 1995; Xe—Uhrig et al., 1994). Except for the heaviest targets, specifically Xe, agreement between experiment and the best theory is generally quite good. Nonzero values of $P_2$ may also have been seen in excitation/ionization collisions with Zn targets yielding open-shell excited states (Pravica et al., 2007c).

### 3.3.2. Combinations of Exchange with Mott Scattering

**3.3.2.1. (e,e) and (e,2e) Experiments** The elastic scattering experiments of the Bielefeld group on Cs discussed above also succeeded is measuring an interference between Mott scattering from the heavy target and exchange (see Section 2.3, Equation (6), and Table 1.) Such an interference is manifest in the asymmetry parameter $A_{\text{int}}$; these data are shown in Figure 14(d). We note that even with a heavy target like Cs, the interference is small and, surprisingly, is at a minimum (near 125°) when the Sherman function is at a maximum. None of the sophisticated calculations brought to bear on this problem are adequate over the entire angular range.

An interesting (e,2e) experiment carried out by the ANU group (Lower et al., 2001a,b) with an optically pumped Na target is similar in certain respects to the Bielefeld experiment, but differs in two crucial ways (in addition to measuring ionization as opposed to elastic scattering): the target is much lighter, and the (reversible) spin polarization of the target is always coupled in a $3p$ $m_F = \pm 3$ state to orbital orientation in the same direction. Classically speaking, the spin-polarized target electron is always circulating around the nucleus in the direction of its spin. For equal energy sharing of the outgoing electrons and for a fixed direction of one electron detector, the ANU experiment measured spin asymmetries as a function of the second electron's scattering angle. These asymmetries, of which there are three, are analogous to the asymmetries of Table 1, except that the second spin is coupled to an orbital orientation. Thus, $A_{\mathrm{ex}}$ is still an exchange asymmetry, but now the singlet scattering occurs in the context of a counter-rotating target, while the triplet scattering occurs with a corotating one. (Lower et al., 2001a,b refer to this asymmetry as $A_{m,o}$.) The asymmetry referred to as $A_{\mathrm{orb}}$ is equivalent to our $A_{\mathrm{int}}$, except that when an unpolarized electron becomes polarized by exchange and begins to Mott scatter, it is ''aided'' by a circulating current with the same sense of rotation as the newly polarized electron. Finally, their $A_{\mathrm{mag}}$ is completely equivalent to $A_{\mathrm{so}} = S_A$, except that now the target is aligned, being oblate with respect to the spin axis and having no net angular momentum perpendicular to the scattering plane. Given the low $Z$ of Na, one would thus expect this latter asymmetry to be quite small.

The data for an incident energy of 83 eV and one fixed angle of 37° are shown in Figure 19. The asymmetry $A_{m,o}$ (analogous to $A_{\mathrm{ex}}$) is consistent with unity at all scattering angles, corresponding to pure singlet scattering. The ''aligned Sherman function'' $A_{\mathrm{mag}}$ is consistent with zero (as would be expected physically) except at 50°, where it is ~0.70(15). Later $A_{\mathrm{mag}}$ data taken by the ANU group are all consistent with zero, in opposition to the dynamically screened three-body Coulomb wave calculations of Berakdar, except for incident electron energies of 151 eV (Lower et al., 2001b). Analogous to $A_{\mathrm{int}}$, the values of $A_{\mathrm{orb}}$ are as large as $-0.5$. Given the fairly small values of $A_{\mathrm{int}}$ in the Cs data (albeit for a different physical process), these large values are also surprising.

3.3.2.2. (e,e$\gamma$) Experiments Electron scattering from Hg is a collision of the type characterized schematically in Figure 4(f). Everything that can possibly happen to confuse the situation does: Hg is intermediately coupled and is heavy enough that Mott scattering is certain to occur. In principle, eleven parameters are needed to describe the excited target and scattered electron (see Section 2.4 and Figures 4 and 5). Fortunately, this complicated system has been investigated in great detail by the Münster group (Außendorf et al., 2006a,b; Herting et al., 2002, 2003; Raeker et al., 1993; Sohn & Hanne, 1992, and references therein).

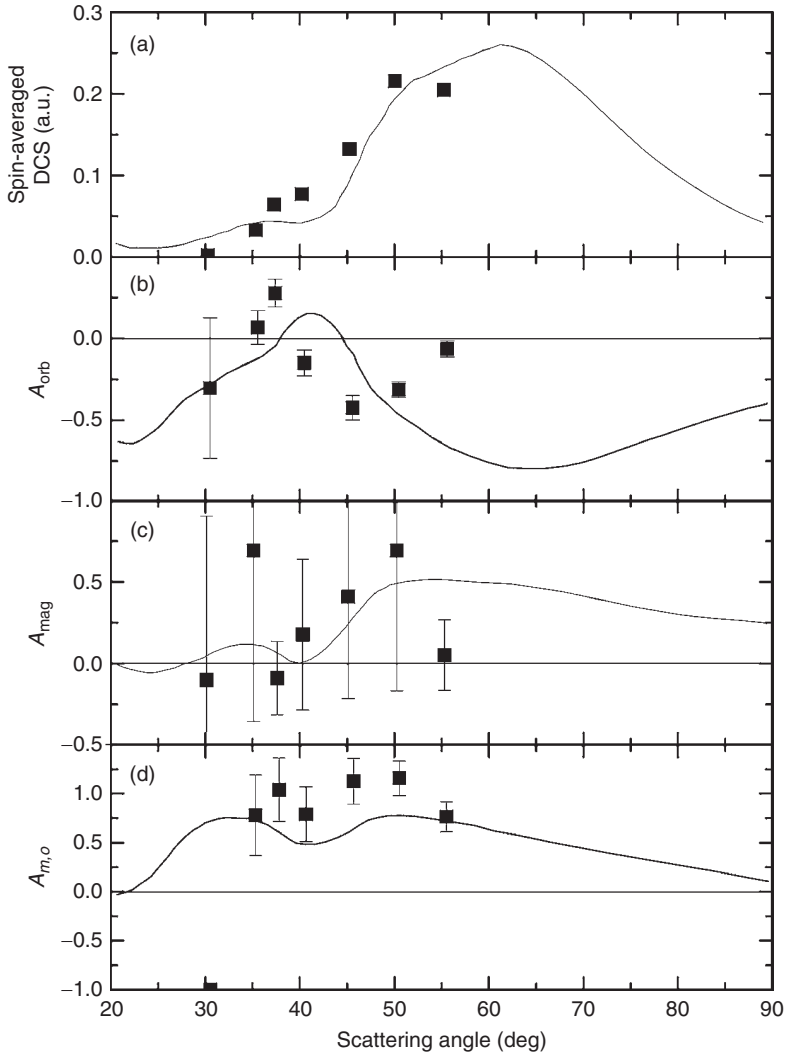


**FIGURE 19** Measurements of (e,2e) spin-dependent processes with optically pumped Na targets, incident electron energy = 83 eV, and equal energy sharing of the two scattered electrons with one detected at $\theta = 37^{\circ}$ (Lower et al., 2001a). (a) Spin-averaged DCS for 3p $^2P_{3/2}$ target states with $m_F = \pm 3$. (b) $A_{orb}$, comparable to $A_{int}$ (see text). (c) $A_{mag}$, comparable to $A_{so}$. (d) $A_{m,o}$, comparable to $A_{ex}$. Solid line—dynamically screened three-body Coulomb wave calculation of Lower et al. (2001b). Redrawn figure with permission from Lower et al. (2001a), *Physical Review Letters, 86*, 624. Copyright (2001) by the American Physical Society

As discussed above, Hg's intermediate coupling means that the charge cloud will tilt about the polarization axis of the incident electron. However, electron polarization in the scattering plane is not equivalent to plane-perpendicular polarization because Mott scattering can affect the latter case. This means that a complete investigation requires the use of three polarization axes for the incident electron and that the scattered electron be detected. The Münster group has investigated these collisions in electron–photon coincidence experiments, in which the scattered electron is detected but not polarization analyzed. Instead, ''generalized Stokes parameters'' (Anderson & Bartschat, 1994a,b) were used to extract information about the geometry of the final excited-state Hg target (Sohn & Hanne, 1992). Representing what is perhaps the pinnacle of complexity in electron–photon coincidence experiments, the apparatus of Sohn and Hanne is shown in Figure 20. In their experiment the $(6s^2)^1S_0 \rightarrow (6s6p)^3P_1$ excitation was studied at 8 and 15 eV, and the 254 nm fluorescence from transitions to the ground state was monitored. By measuring the various Stokes parameters in combination with different incident electron spin directions, shapes and orientation angles of the excited-state charge cloud could be determined. An example is shown in Figure 21, in combination with Breit–Pauli $R$-matrix calculations from the Belfast group (Bartschat private communication with Münster). More recent calculations by the Drake, York, and Murdoch groups for various observables show improved general agreement and an increasing understanding of the requirements

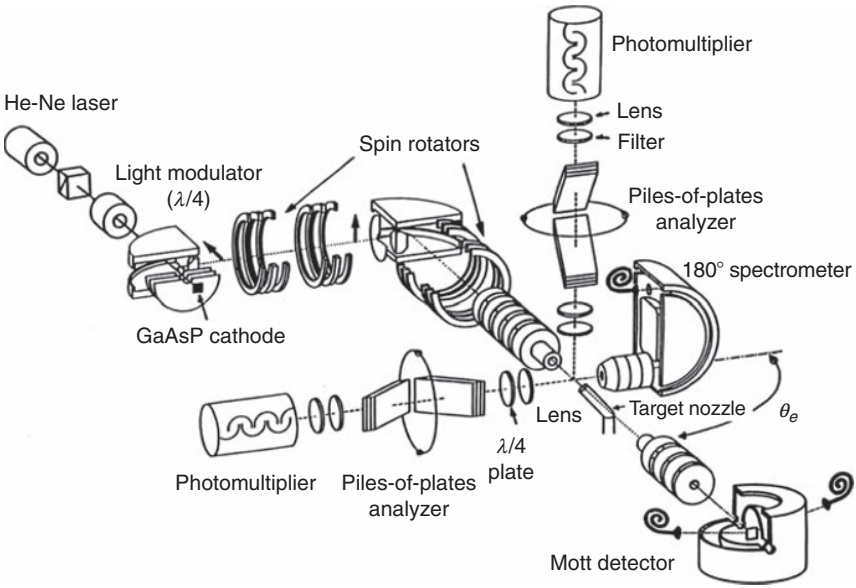


**FIGURE 20** Electron–photon coincidence apparatus of Sohn & Hanne (1992)

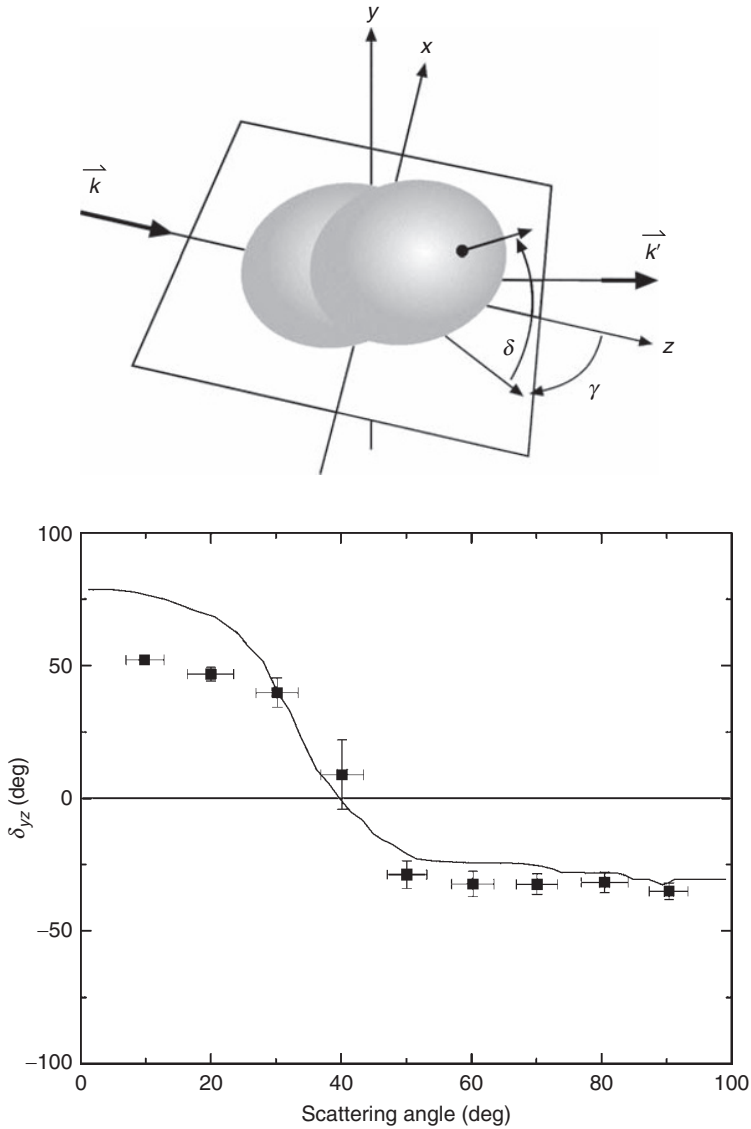


**FIGURE 21** Tilted Hg (6*s*6*p*) $^3P_1$ charge cloud showing the angle of tilt, $\delta_{yz}$ above the *x*–*z* plane. Data for $\delta_{yz}$ of Sohn & Hanne (1992). Solid line—Breit–Pauli *R*-matrix calculation of Bartschat

for an accurate theoretical understanding of this complex scattering system (Außendorf et al., 2006a,b; Herting et al., 2002, 2003).

The discussion associated with Equations (9), (10), and (11) implies that if one excites a well-*LS*-coupled state (i.e., one with only one coefficient $a_i$),

$P_2$ in an integrated Stokes parameter measurement should be identically zero unless Mott scattering is significant. In this case, transversely polarized electrons would scatter preferentially to one side of the plane containing the target atom and the incident spin-polarization axis, producing a nonzero value of $\langle T(L_iL_j)^+_{21}\rangle$, with $L_i = L_j$. The $^3D_3$ states of an excited $np^5(n+1)p$ configuration of the heavy noble gases are well *LS* coupled, so a measurement of $P_2$ in the fluorescence from such states would provide an unambiguous signature of Mott scattering. Dümmler et al. (1995) found that in, for example, Xe, $S_A$ values for excitation of the $np^5(n+1)s$ states are comparable to and generally larger than $S$ values for elastic scattering. The number of electrons that scatter to the ''left'' versus those that scatter to the ''right'' is determined by the integral over the polar scattering angle of spin asymmetry ($S$ or $S_A$) weighted by the appropriate differential scattering angle:

$$A_{\text{left-right}} = \int_0^{\pi} S(\theta)\frac{d\sigma}{d\theta}(\theta)d\theta. \tag{12}$$

This asymmetry is ~0.03 for elastic scattering from Xe at 10 eV (Müller & Kessler, 1994), and one can assume comparable or larger values for inelastic scattering given the results of Dümmler et al. (1995) To the extent that $A_{\text{left-right}}$ can be associated with $\langle T(L=3)^+_{21}\rangle$, one might thus expect to measure a nonzero $P_2$. Indeed, calculations of $P_2$ for emission from $^3D_3$ states using a Breit–Pauli *R*-matrix technique (Birdsey et al., 1999), which is expected to be the most accurate theory near threshold where the experimental results would not be affected by cascading (Furst et al., 1993; Srivastava et al., 1995), indicates that $P_2$ should be ~0.02–0.03 for the best case of Kr. However, all measurement of $P_2$ below the cascading threshold have been consistent with zero, with statistical precision as good as 0.0011 (absolute) for Ne (Birdsey et al; 1999, Furst et al., 1992, 1993; Gay, Furst et al., 1996a,b).

### 3.3.3. Resonant Effects

Both the Perth and Nebraska groups have studied resonance effects using integrated Stokes parameter measurements and found it to be a powerful tool for understanding the angular momentum dynamics of these features. Yu et al. (1997) found a strong resonance at threshold in the cross section and all three Stokes parameters for excitation of the Ne $2p^53p[1/2]_1$ state. The configuration of this resonance is $2p^53p^2$, with a $J = 3/2$ core. The two outer $p$ electrons of the resonance can only comprise $^1S$ or $^1D$ levels, since $^3P$ resonances have excitation energy below that of the $2p^53p$

manifold. Moreover, one can assume that only the lowest orbital angular momentum channels contribute to the resonance excitation, since it is so close to threshold. Yu et al. (1997b) were thus able to show that the $^1S$ and $^1D$ $J = 3/2$ resonances will yield $P_3 = 0.33$, whereas the remaining $^1D$ $J = 1/2$ resonance gives $P_3 = 0.17$. Since $P_3$ is observed to be ~0.32 at the resonance energy, the $J = 1/2$ resonance can be ruled out.

Maseberg and Gay (2006) investigated the excitation of the He $2s^22p$ and $2s2p^2$ resonances, but found no clear evidence in either $P_2$ or $P_3$ for the action of spin–orbit coupling over the ~10 fs resonant lifetime. However, Pravica et al. (2007a,b,c) and Zn targets, have found evidence for several resonant effects in $P_2$ and $P_3$. In the excitation/ionization production of the $3d^{10}5d$ closed-shell state (Pravica et al., 2007c), a resonance or combination of resonances about 0.8 eV above threshold is apparent, but, interestingly, only unambiguously in the $P_3$ channel. This implies that changes in the exchange cross section, as opposed to magnetic effects, are important at the resonant energy.

In excitation of the $Zn^{*-}$ ($3d^94s^24p^2$) configuration, two resonances were observed in the region between 10.5 and 12 eV. By measuring the Stokes parameters for the fluorescence from the ($3d^{10}4s4d$ $^1D_2$) state following its population from the decay of the resonance, Pravica et al. (2007a,b) were able to see variations in $P_2$ and $P_3$ of the order of 1%. This required remarkable precision (~ 0.0006); these data are shown in Figure 22. While magnetic effects are apparent in the low-energy resonance by virtue of the variation of $P_2$, the higher energy resonance is not obviously affected in this way. As before, variations in $P_3$ could be due to a variation in the exchange cross section, which is clearly the case for the higher energy resonance, or a combination of magnetic and exchange effects.

## 4. MOLECULAR TARGETS

We now consider molecular targets. To date, the only experiments in which molecules have been bombarded by spin-polarized electrons involved either diatomics or relatively complicated chiral targets, which must comprise at least four atoms. In the former case, the interesting new physics is related to complications arising from molecular rotation and the dissociation channel, while the latter case is of interest because of the unique stereochemical structure from which the electron is scattering. Three review papers in this series have discussed the problem of chiral molecules (Blum & Thompson, 1997; Compton & Pagni, 2002; Kessler, 1991), and Hanne (1997, 1998) has discussed diatomic as well as chiral targets. For the sake of brevity, we will not discuss early experiments by Kessler's group (Hilgner & Kessler, 1969; Hilgner et al., 1969; Kessler

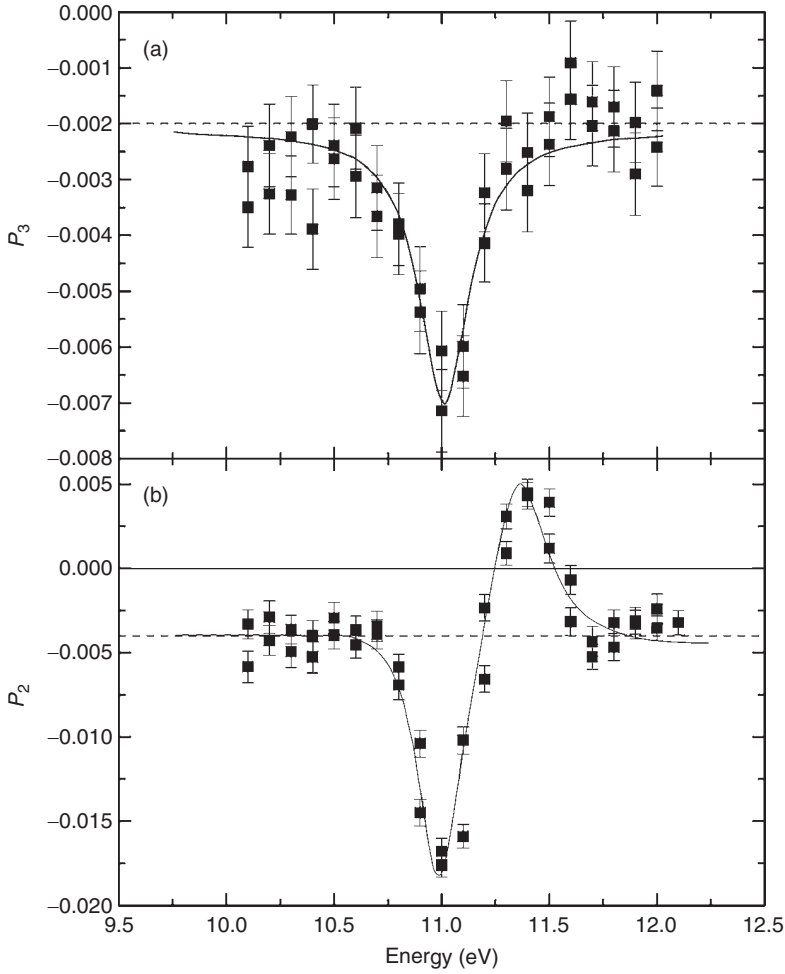


**FIGURE 22** Integrated Stokes parameters $P_2$ and $P_3$ for the decay of the Zn $(3d^{10}4s4d)\ ^1D_2$ state following its population by $Zn^-{}^*(3d^9 4s^2 4p^2)$ resonances. Solid line represents a fit to Beutler–Fano profiles (Pravica et al., 2007a); dashed lines correspond to fits to the background polarization. Redrawn figure with permission from Pravica et al. (2007a), *Physical Review A, 75*, 030701. Copyright (2007) by the American Physical Society

et al., 1971; and references therein) in which the development of spin polarization due to Mott scattering of unpolarized electrons from molecules with at least one heavy atom (e.g., $I_2$, $C_2H_5I$, $Bi(C_6H_5)_3$) was studied. These experiments, done at energies of the order of 1 keV, showed that the molecules could be treated, to a very good approximation, with the independent atom model (Kessler, *et al.*, 1969).

## 4.1. Simple Diatomic Molecules

### 4.1.1. The Exchange Interaction in Elastic Scattering

The first experiment involving the scattering of polarized electrons by gas-phase diatomic molecules was reported by the Rice group (Ratliff et al., 1989). Using targets of $O_2$ and NO, they studied spin-exchange rate constants ($k$) at thermal electron energies. The targets $O_2$ and NO were chosen because they have open (unsaturated) valence shells which, unlike targets in singlet spin states, permit spin-flip to occur even in the $LS$ coupling approximation. The rate constants are proportional to the velocity and scattering-angle-averaged spin-exchange cross sections, which are in turn proportional to the averaged values of $|g|^2$. The Rice apparatus consisted of a flowing-afterglow source of polarized electrons, in which metastable He($2^3S$) atoms in a microwave discharge afterglow were optically pumped by $(2^3S) \leftrightarrow (2^3P)$ 1.08 μm resonance radiation, making them spin polarized. Subsequent chemi-ionization by $CO_2$ produced polarized electrons which diffused through a mixture of the flowing He, the $CO_2$, and a target gas. Downstream from the $CO_2$ and target gas injection points, the free electrons were extracted from the flowing volume electrostatically, and their polarization analyzed with a Mott polarimeter. (The free electron spins are not depolarized in collisions with the $CO_2$ or the He because both have spin-singlet ground states.) By measuring the extracted electron polarization as a function of the target gas pressure-length product, the value of $k$ can be determined.

Surprisingly, the values of $k$ for the open-shelled molecular targets were found to be dramatically lower than those expected for open-shelled atomic targets: roughly $9 \times 10^{-11}$ $cm^3s^{-1}$ versus $4 \times 10^{-9}$ $cm^3s^{-1}$ calculated for H (Smith, 1966). Equivalently, these rate constants correspond to averaged spin-exchange cross sections of $\sim 10^{-17}$ $cm^2$, compared with alkali-metal cross sections in the same energy regime that are $\sim 2 \times 10^{-14}$ $cm^2$. Naively, one might expect spin-exchange processes to occur with similar probability in both atomic and molecular targets that do not have saturated spins in the ground state. However, a simple explanation for these low values may lie in the total spin-averaged cross sections; $O_2$ and NO have values that are comparable to most other diatomic molecules for thermal electrons—about $5–10 \times 10^{-16}$ $cm^2$, as opposed to those for H and the alkali metals which approach $500 \times 10^{-16}$ $cm^2$. Since the spin-flip cross section must be less than the total scattering cross section, this would explain the low rate of spin degradation observed: basically, the thermal scattering from the target molecules is negligible, so the spin degradation is too.

Simple explanations of this type, however, fail when differential spin-exchange elastic cross sections are measured. The Münster group in the early 1990s made the first detailed measurements of this type, again with

$O_2$ and NO (Hegemann et al., 1991, 1993). Moreover, they compared their results directly with those for an alkali target, Na. In the Münster experiment, polarized electrons with energies between 2.5 and 15 eV from a GaAsP photocathode were directed onto an effusive target. Electrons scattered between 0° and 110° in a plane perpendicular to the incident electron polarization direction were energy analyzed and subsequently accelerated to 100 keV for analysis by a Mott polarimeter. The ratio of the scattered-to-incident electron polarization, $P'/P$ (measured perpendicular to the scattering plane) was thus determined. Under the assumption that continuum spin–orbit forces do not cause a rotation of the electron polarization vector, that is, that $S$ and $M_S$ of the total electron wave function are good quantum numbers, it can be shown that for elastic scattering (Hegemann et al., 1993)

$$\frac{P'}{P} = 1 - \frac{(8/3)|g|^2}{\sigma_{\text{av}}^{\text{tot}}}. \tag{13}$$

The factor of 8/3 pertains to scattering from spin-triplet targets ($O_2$) and is reduced to unity for spin-doublet targets (NO, Na). (In the case of the Rice experiment, the squared modulus of the exchange amplitude must be taken as an average over electron scattering angle and energy.)

We now focus on the elastic scattering results of the Münster experiment at 4 eV (Na) and 5 eV ($O_2$, NO), which are shown in Figure 23, in conjunction with theoretical calculations of Bray and McCarthy (1993), da Paixão et al. (1996), and Tashiro (2008). Again, we find the counterintuitive result that open-shelled atoms (or, at least Na) are much more effective at scattering depolarization than are open-shelled molecules. Unlike the Rice result, however, invocation of a relatively small spin-averaged cross section will not explain these results, because it is the *ratio* of the exchange-to-total cross section (Equation (13)) that determines the polarization reduction factor. The detection of an electron at some nonzero angle means that it has already been scattered, so the only remaining question is its origin—the beam or the target? Still the molecular depolarization is very small.

Early attempts to explain this result hinged on the idea that the necessary averaging over molecular target orientation in the Münster gas-phase experiment resulted in a ''washing out'' of depolarizing effects. Using a Schwinger multichannel calculation (SMC), da Paixão et al. (1992) were able to qualitatively reproduce the Münster $O_2$ data, but were also able to show that for various angles of molecular orientation, results qualitatively similar to the Na data of Figure 23 could be obtained. They thus concluded that an orientational average was the chief mechanism for the lack of depolarization with molecular targets. This explanation is

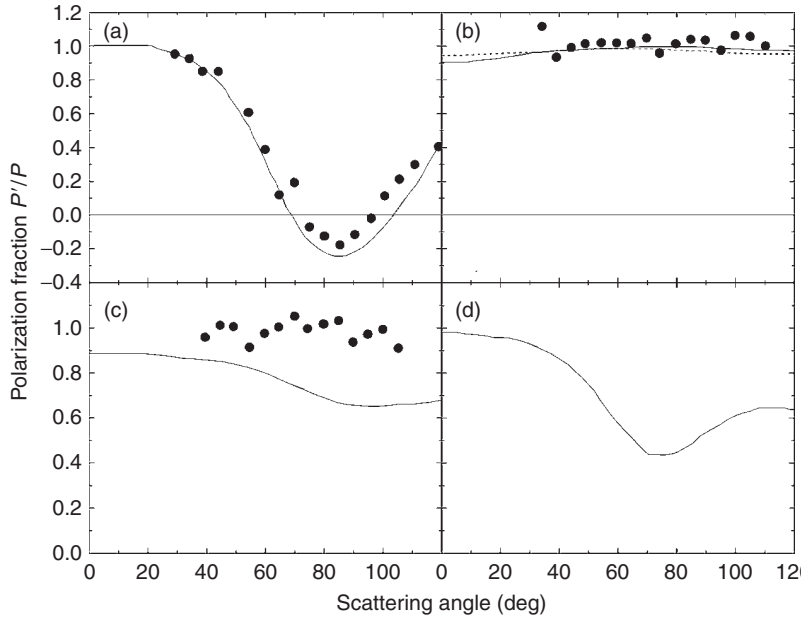


**FIGURE 23** Depolarization fraction $P'/P$ as a function of electron elastic scattering angle (see text). Experimental data of Hegemann et al., (1993). (a) Na, incident electron energy 4 eV, solid line, theory of Bray and McCarthy (1993). (b) $O_2$, 5 eV, dashed line, theory of Fullerton et al. (1994), solid line, theory of Tashiro (2008). (c) NO, 5 eV, solid line, theory of da Paixão et al. (1996). (d) theoretical calculation for 5 eV elastic scattering from the excited $c^3\Pi_u$ state of $H_2$ by Sartori et al. (1997)

problematic for at least two reasons, however. First, it is not clear how summations over the molecular orientation of scattering-angle functions for $P'/P$, which vary between 1 and 0 for the cases presented by da Paixão et al. (1992) (and possibly into negative values for other orientations), can yield an average function which never dips below 0.92—unless the cases with significant depression of $P'/P$ contribute negligibly to the total (differential) scattering cross section. Second, and with the caveat that fundamentally quantum-mechanical processes such as exchange scattering may not be amenable to intuition, it is hard to understand why any open-valence-shell target electron cloud of atomic/molecular dimension would result in radically different ratios of exchange-to-total differential cross sections.

More recently, Nordbeck et al. (1994) have pointed out the validity of the former concern. Using a nine-state $R$-matrix calculation, they also investigated values of $P'/P$ for various molecular orientations of $O_2$ and found results in qualitative agreement with those of da Paixão et al. (1992). However, these orientations were associated with small differential cross sections which contributed little to the orientation-averaged differential cross

sections. The reason for this is clear. For a given incident electron energy, the dependence of the direct and exchange differential cross sections have a qualitatively similar dependence on the molecular target orientation. For certain regions of orientation space where both $f$ and $g$ are small, there will be a specific orientation at which $f$ has a zero. At this point where the total cross section is small, exchange will dominate and the depolarization fractions will approach zero. This result is completely analogous to the production of large electron polarization in the scattering of low-energy unpolarized electrons from heavy atoms (Kessler, 1969). The spin–orbit interaction results in electron diffraction minima that occur at slightly different scattering angles for spin-flip and nonspin-flip amplitudes, leading to restricted angular ranges with low scattering cross section but high polarization. (See Figure 6.)

The question thus persists: why is Na so much more effective at electron depolarization than the molecular targets studied? A clue to the answer may come from some SMC calculations of elastic scattering from the excited state $c^3\Pi_u$ of $H_2$ by Sartori et al. (1997), also shown in Figure 13. The depolarization fraction $P'/P$ is much more similar to that for Na than for the other open-shelled molecular targets. It is also interesting to compare the spin-averaged total scattering cross sections for the three molecular cases and Na. At 5 eV, the total elastic (spin-averaged) scattering cross section is $\sim 300 \times 10^{-16}$ cm$^2$ for Na (McDaniel, 1989), $\sim 8 \times 10^{-16}$ cm$^2$ for $O_2$ (Machado et al., 1999), $\sim 10 \times 10^{-16}$ cm$^2$ for NO (Alle et al., 1996), and $\sim 50 \times 10^{-16}$ cm$^2$ for the $H_2$ $c^3\Pi_u$ state. These low-energy cross sections are dictated to a significant degree by the polarizability of the target, which is in turn related to the proximity of the target electronic state to the next-higher-lying electronic energy levels. The exchange amplitude is proportional to the difference between the two possible spin-scattering amplitudes:

$$g(S) = \frac{1}{(2S+1)}(a^{S-(1/2)} - a^{S+(1/2)}), \tag{14}$$

where $S$ is the spin of the target. Thus we can understand why it would be sensitively dependent on the polarizability. Roughly speaking, an interaction between the incident electron and the target, based on the latter's polarizability, will have more of an effect on the triplet scattering amplitude, in which the active target electron and the incident electron tend to keep their distance during the interaction due to Pauli repulsion forces. Other, shorter range interactions will have a bigger effect on singlet scattering. If the polarization component of the scattering cross section is significant, one could expect large differences between the spin-specific partial cross section, that is, an enhancement in exchange (Fabrikant, 2009;

Sartori et al., 1997). This would explain why large scattering cross sections are correlated with effective depolarization in these experiments.

### 4.1.2. Exchange Effects in Inelastic Scattering

We now consider inelastic collisions in which excited states of the molecular target or its fragments emit polarized light. As we have discussed in the case of atoms, integrated Stokes parameter measurements can provide useful information about how either the orbital or spin angular momentum provided by the incident electron is partitioned in the collision complex. In addition to nuclear and electronic spin, molecular targets also have angular momentum associated with nuclear rotation that complicates the picture (see Figure 6.).

The first measurement of this type was carried out by the Münster group in 1994 (Mette & Hanne, 1994) and, like the Rice experiment discussed above, immediately provided a surprising result. Using a beam of 14.5 eV polarized electrons, they bombarded a target of $N_2$ gas and studied the circular polarization of the $C^3\Pi_u - B^3\Pi_g$ ($v' \rightarrow v'' = 0 \rightarrow 0$) 337 nm light emitted in a direction parallel to the incident electron polarization axis. Because the electrons excite a well-*LS*-coupled triplet state, exchange is ensured, that is, the upper molecular level is guaranteed to be spin polarized. Unlike the excitation of atomic triplet states (Section 3.1.2), however, circular polarization was measured to be equal to zero within the statistical precision of the measurement. The Nebraska group has recently confirmed this result over a broader energy range—from threshold up to 27 eV—in the equivalent $C^3\Pi_u - B^3\Pi_g$ ($v' \rightarrow v'' = 0 \rightarrow 2$) 380 nm transition.

A preliminary analysis of the time scales involved in such collisions suggests a possible cause of this null result. The impulsive excitation of the target takes place in $\sim 10^{-16}$ s, while typical molecular vibration/dissociation time scales are of the order of $10^{-14}$ s, and molecular rotational periods are $\sim 10^{-13}$ s. As in the atomic case, the spin–orbit relaxation times required to convert spin angular momentum into orbital angular momentum are $\sim 10^{-10} - 10^{-9}$ s, while fluorescent decay times are of the order of $10^{-8}$ s. One is, thus, tempted to argue that the spin-polarized electron inserted in the molecule will have a time-averaged value of zero on a time scale associated with the spin–orbit relaxation time, thus providing no net molecular orientation. This is particularly true in the case of $N_2$, a Hund's case (a) molecule (see Figure 24(a)), in which the electron spin is strongly coupled to the internuclear axis.

Time scale considerations also suggest a way to observe the spin transfer. If the molecule is excited to a dissociative state by the electron impact, the spin-polarized atom thus produced will emerge from the collision volume in a time short compared to the molecular rotational period, with no ''tumbling depolarization'' having occurred. This idea led the Nebraska and Perth

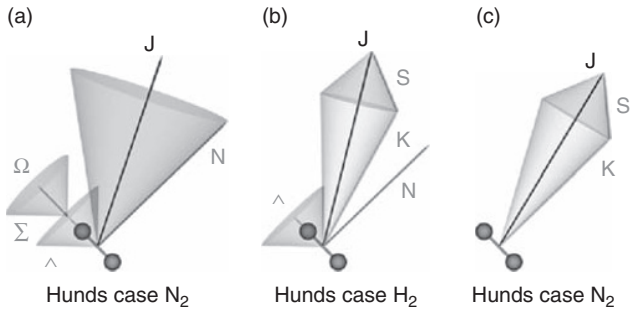


**FIGURE 24** Angular momentum coupling for three Hund's cases: (a) $N_2$ in a $\Pi$ state. (b) $H_2$ in a $\Pi$ state. (c) $N_2$ in a $\Sigma$ state. Electronic and orbital angular momenta projections along the internuclear axis are labeled $\mathbf{\Sigma}$ and $\mathbf{\Lambda}$, respectively. Nuclear rotational angular momentum is **N**, which couples in Hund's case (b) to $\mathbf{\Omega} = \mathbf{\Lambda} + \mathbf{\Sigma}$ to form **K**. The total molecular angular momentum is **J** (nuclear spins are ignored)

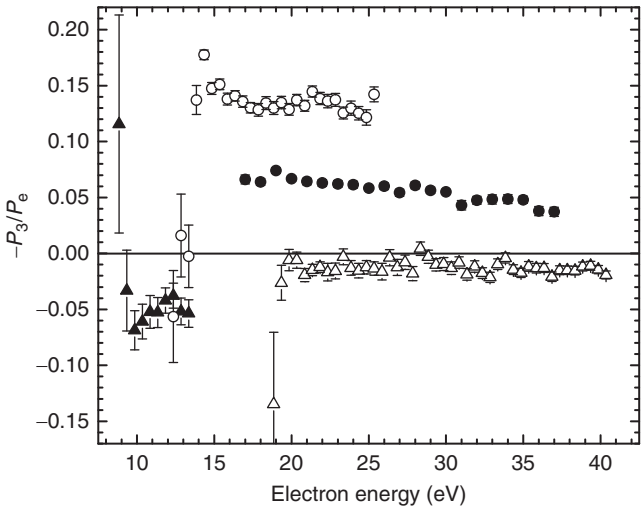


**FIGURE 25** Integrated Stokes parameter $P_3$ versus incident electron energy. Solid circles, Hα light from H atoms following dissociation of $H_2$; open circles: Fulcher band emission from $H_2$* (see text); solid triangles, $N_2$ $B^3\Pi_g \rightarrow A^3\Sigma_u{}^+$ emission with partial rotational resolution; open triangles, $N_2{}^+$ $B^2\Sigma^+{}_u \rightarrow X^2\Sigma^+{}_g$ emission

groups to study the atomic Hα fluorescence resulting from the polarized electron impact dissociation of $H_2$ molecules (Green et al., 2004; Williams & Yu, 2004). The results of the Nebraska measurements are shown in Figure 25 and represent a direct observation of spin transfer from an incident beam into a target in electron collisions with molecules.

It is instructive to compare these polarizations to the atomic case. While no one has studied excitation of H atoms by polarized electrons, the Mainz and Münster groups have studied the alkali metals from Na to Cs (Naß, Eller et al., 1989; Eschen et al., 1989). For direct comparison between the various atomic and molecular targets, we consider the ''polarization transfer'' efficiency, $T$, which is the initial spin polarization of the excited target before any fine or hyperfine depolarization. For alkalis, $T$ is given by $1 - (|f|^2/\sigma_u)$. For excitation of well-$LS$-coupled triplet states, $T$ is 2/3 (Kessler, 1985). For Cs, measurements of the maximum value of $T$, which occurs at energies just above threshold where exchange is most important, vary from ~0.45 (Naß et al., 1989) to ~0.65 (Eschen et al., 1989). The Mainz group has determined a maximum value of $T$ for Na, the lightest atom investigated, to be ~0.22. After we take fine and hyperfine depolarization into account for the H fluorescence, we find in the case of the H dissociation fragments that $T$ varies between ~0.37 and 0.47, depending on whether the H ($n = 3$) -populations immediately after dissociation are taken to be equally populated or the same as those produced by electron impact excitation of H atoms (Green et al., 2004; Kedzierski et al., 2001). This is a remarkable result, because it says that even after an initial transfer of electron spin to the dissociative triplet state of $H_2$ that is only 2/3 efficient (and which must compete with the unpolarized process in which singlet dissociative states produce H$\alpha$ light), dissociated H atoms have an average spin polarization comparable to or greater than direct excitation by polarized electrons. No theoretical understanding of this yet exists.

The naïve ''tumbling depolarization'' idea discussed above is shown to be wrong when we consider *molecular* fluorescence from $H_2$. By isolating a region of the Fulcher-band emission spectrum (corresponding to molecular transitions between states that asymptotically correlate to $n = 3$ and $n = 2$ states of H) between 595 and 605 nm, the Nebraska group found even larger polarizations than were observed in the atomic case (Green et al., 2004; Figure 25). While this spectral region comprises a mix of molecular transitions, the strong ones are almost exclusively from triplet states, allowing circular polarization to be observed. These results immediately raise the question: why are $H_2$ emissions polarized while the $N_2$ emissions are not, even though the latter are guaranteed to be from spin-polarized triplet states?

One chief difference between the emitting $H_2$ and $N_2$ states is that the former are classified as Hund's case (b) states, while the latter correspond to Hund's case (a) (Herzberg, 1950; Figure 24). Thus in $H_2$, the electron is weakly coupled with the internuclear axis, unlike the active $N_2$ electron, which is strongly coupled to the nuclear rotation. In a tumbling depolarization picture, this spin-decoupling for Hund's case (a) molecules would

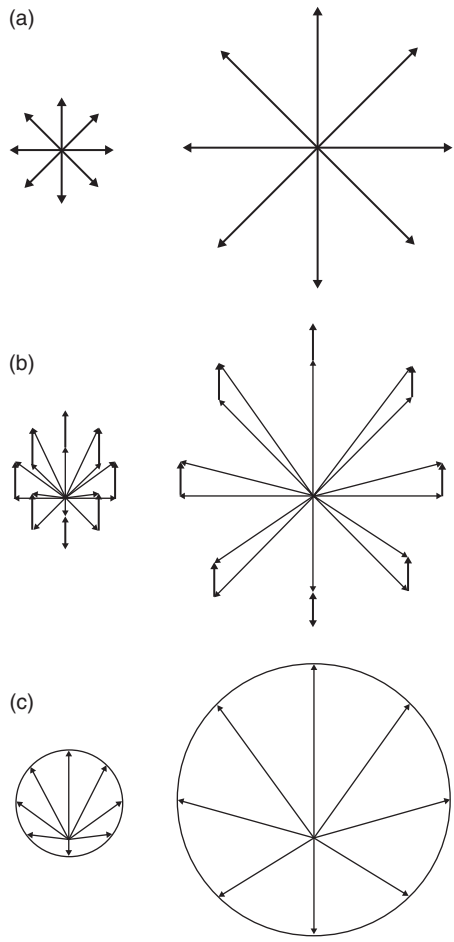


**FIGURE 26** Spin-induced orientation of $H_2$ and $N_2$ *J*-states. (a) Isotropic room temperature nuclear rotational distributions. (b) Spins are added in exchange collisions to form oriented *J*-state distributions. (c) *J*-state distribution is more asymmetric about the zero-angular momentum point in the case of $H_2$

account for the appreciable $H_2$ molecular polarization values. There are two other points to consider in this regard, however. The concept of ''tumbling depolarization'' is inexact and ultimately rather unsatisfactory, since, by conservation of angular momentum, any molecule excited in an exchange collision must be oriented (i.e., have a magnetic dipole moment) and thus be capable of emitting circularly polarized light. However, one might still expect $N_2$ fluorescence to be less polarized, for reasons illustrated in Figure 26. Initially, gas-phase targets will have

isotropic distributions of their rotational orbital angular momenta, **N**. However, the lengths of the **N**-vectors are, on average, significantly greater for a room temperature sample of $N_2$ than for $H_2$. At 292 K, the most likely value of N for $N_2$ is 6; for $H_2$ it is 1. The average values of N are 8.5 and 1.2 for $N_2$ and $H_2$, respectively. If we assume, for simplicity, that the exchange collision produces no excited-state orbital alignment or orientation (i.e., that the initial values of the electronic orbital angular momentum along the internuclear axes, $\Lambda$, are isotropically distributed as well), the rotational quantum number does not change in the collision, and we ignore nuclear spin, then we can consider the orientation of the system produced by **S** alone (Hanne, 2004). The two cases of $N_2$ and $H_2$ are illustrated qualitatively in Figure 26. It is apparent that the total **J** distribution of the two systems is significantly different, with the $N_2$ case being more symmetric about the point corresponding to zero angular momentum. The system's rank-1 multipole moment (or magnetic dipole moment), to which the fluorescence circular polarization $P_3$ is ultimately proportional (Equation (11)), is given by (Blum, 1996)

$$\langle T(J)^{+}_{10} \rangle = \left(\frac{3}{4\pi}\right)^{1/2} \langle \cos\theta_J \rangle, \tag{15}$$

where $\theta_J$ is the angle that a given $J$ makes with the quantization axis. One can show that classically, $\langle T(J)^{+}{}_{10} \rangle \sim 1/N$ for large $N$. Thus, it is apparent that one would expect systems with large initial rotational angular momentum to exhibit lower values of $P_3$. Nonetheless, a residual orientation persists, and one might expect a small, but measurable value of $P_3$ even for $N_2$.

The generally low polarizations observed for molecular emission may also be due in part to the fact that the first measurements by the Nebraska and Münster group were not rotationally resolved. Since $P$ and $R$ branches tend to have opposite polarization while the $Q$-branches are only weakly polarized (Zare, 1988), complete or even partial integration over them will reduce the observed polarization. Recent data from the Nebraska group involving $N_2$ targets with partially resolved rotational structure tend to confirm this. Using a narrow bandpass filter to isolate a few (unknown) rotational transitions in the $v' \rightarrow v'' = 7 \rightarrow 3$ of the first positive band ($B^3\Pi_g \rightarrow A^3\Sigma_u{}^+$), a significant nonzero negative polarization was observed (Figure 25).

Another nonzero result has an interesting physical interpretation (Maseberg & Gay, 2009). In this case, $N_2$ was both excited and ionized by polarized electron impact, leading to fluorescence emitted in the $B^2\Sigma^+_u \rightarrow X^2\Sigma^+_g$ ($v' \rightarrow v'' = 0 \rightarrow 0$) transition at 391.4 nm. An angular momentum coupling diagram for molecules in $\Sigma$ states in shown in Figure 24(c). Ignoring nuclear spin, the only angular momenta that the molecule has is that due to the electronic spin and the rotation of the internuclear axis. In the cases of molecular fluorescence discussed above, the excited states were $\Pi$ states or mixtures of systems dominated by $\Pi$ states. In both Hund's cases (a) and (b) involving $\Pi$ states, the initial molecular electronic spin polarization created by exchange couples primarily with its own orbital angular momentum because of the larger magnetic dipole associated with the electronic as opposed to nuclear orbital angular momentum. Thus, as with atoms, spin orientation is converted to orbital and ultimately $J$-orientation. In the absence of well-defined electronic orbital angular momentum as is the case with $\Sigma$ states, any $J$-orientation resulting in circularly polarized fluorescence must be the result of coupling of the electron spin to the nuclear motion alone (Herzberg, 1950; Van Vleck, 1929), which is much weaker than standard spin–orbit coupling. However, such an effect was observed in the Nebraska data, which provides clear evidence for direct spin torque on nuclear rotational motion in a collisional process. (Such coupling had been observed spectroscopically in the 20s, when it was referred to as ''$\rho$–doubling'' or, later, ''spin-doubling.'') It is likely that this result was observable in the Nebraska experiment because the optical interference they used fortuitously cut out the $R$-branch side of the emission spectrum, yielding some rotational resolution in the experiment.

## 4.2. Chiral Molecular Targets

In our discussion of electron scattering by atoms and molecules so far, the *dynamics* responsible for various spin-dependent effects—exchange scattering, spin–orbit coupling, or combinations of these—could generally be identified, depending on the incident electron energy and $Z$ of the target. We now consider a class of targets that are significantly more complicated: chiral molecules. These targets, because of their symmetry (or lack thereof), allow unique new scattering effects to be observed. The physical mechanisms that actually cause these effects, however, are poorly understood at best.

In addition to these fundamental issues, it is important to note that the interaction of polarized electrons with chiral molecules provides tangential information about the origins of biological homochirality (Compton &

Pagni, 2002; Gidley et al., 1982; Keszthelyi, 1995; Walker, 1979), primarily with regard to the Vester–Ulbricht hypothesis (Vester et al., 1959). This idea states that cosmic beta rays preferentially destroyed one handedness of prebiotic chiral molecules (which were presumably produced in racemic mixtures in electrochemical processes), leaving the opposite handedness to participate in molecular evolution. Any polarization dependence of electron scattering by chiral molecules would thus provide circumstantial evidence for such a picture.

A molecule is chiral if it lacks inversion symmetry, that is, is not superimposable on its mirror image after a proper rotation (Compton & Pagni, 2002). For this to be the case, it must have at least four atoms in a noncoplanar arrangement. Early work by Farago (1980, 1981) and Kessler (1982) laid the groundwork for understanding the symmetry elements relevant for chiral scattering effects. These can be summarized as follows (Gay, 1996). We consider the relationship between the initial- and final-state continuum-electron spin density matrices. For elastic scattering from a spinless chiral target, this is given by

$$\rho_f = M\rho_i M^\dagger, \tag{16}$$

where $M$ can be shown to be

$$M = f\sigma_o + g\,\vec{\sigma}\cdot\hat{n}_2 + h\,\vec{\sigma}\cdot\hat{n}_3, \tag{17}$$

and $\sigma_o$ is the $2 \times 2$ unit matrix, $\vec{\sigma}$ is the Pauli spin matrix, $\hat{n}_2$ is the unit vector perpendicular to the scattering plane, and $\hat{n}_3$ is the unit vector perpendicular to $\hat{n}_2$ and the momentum transfer direction parallel to $\hat{n}_1$. The scattering amplitudes $f$, $g$, and $h$ correspond to nonspin-flip, spin-flip, and parity-violating processes, respectively. The latter amplitude, $h$, will be nonzero only in the presence of chirality in the target, either through the electro-weak interaction (which we neglect) or the stereochemical arrangement of the molecular target's atoms. These considerations lead us to expect three classes of chiral scattering effects:

(1) *Production of in-plane polarization*. In terms of the two in-plane unit vectors $\hat{n}_1$ and $\hat{n}_3$, the polarization vector $\vec{P}$ is given by

$$\vec{P}\cdot\hat{n}_1 = \frac{1}{2I}(|g+ih|^2 - |g-ih|^2) \tag{18a}$$

and

$$\vec{P}\cdot\hat{n}_3 = \frac{1}{2I}(|f+h|^2 - |f-h|^2), \tag{18b}$$

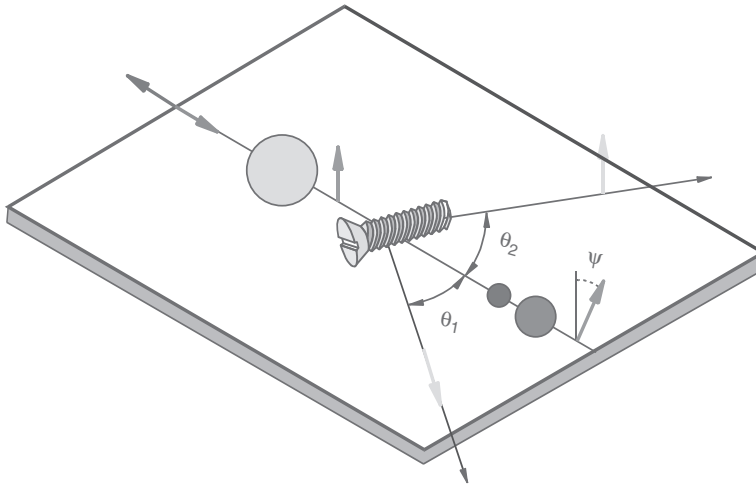


**FIGURE 27** Electron scattering by chiral targets (see text). Spheres represent unpolarized intensities; arrows represent spin-polarized intensity

where $I$ is the scattered electron flux to a given angle in the plane of scattering. This is shown schematically in Figure 27.

(2) *Polarization-dependent beam attenuation*. If the incident electrons are longitudinally polarized, they themselves are chiral, in the sense that their velocity and spin define a pseudoscalar quantity. (Such electrons are sometimes referred to as being ''helicitized'' (Gidley et al., 1982).) Thus one can expect a difference in the differential scattering cross section without spin analysis. Specifically the beam will be attenuated differently by the target depending on its initial spin direction. In analogy with optical circular dichroism, which is related to the helicity dependence of the imaginary part of the index of refraction, one can define a beam attenuation asymmetry

$$A_{L(R)} = \frac{I^{+}_{L(R)} - I^{-}_{L(R)}}{I^{+}_{L(R)} + I^{-}_{L(R)}} = -P_e \frac{4\pi\lambda}{k}(\Delta z)\,\mathrm{Im}(h), \tag{19}$$

where $I^{+(-)}_{L(R)}$ is the transmitted intensity through the left(right)-handed target with spin-forward (+) or backward (−) incident electrons, $\lambda$ is the target's areal density, $k$ is the electron wave number, and $\Delta z$ is the target path length. Note that such ''electron circular dichroism'' (ECD) is essentially the time-reversed equivalent of in-plane polarization production (Figure 27).

(3) *Rotation of incident transverse polarization*. Continuing the analogy to optical effects in a chiral medium, we note that optical activity, the

rotation of linear polarization in the plane perpendicular to the direction of incidence, depends on the real part of the refractive index. Similarly, for forward scattering, the real part of $h$ can be related to a rotation of an incident transverse electron polarization by an angle $\psi$ in the plane perpendicular to the beam direction (Figure 27):

$$\psi = \frac{4\pi\lambda}{k}(\Delta z)\,\mathrm{Re}(h). \tag{20}$$

While collision symmetry permits the quantities in Equations (18), (19), and (20) to be nonzero, their dynamical cause is open to debate, as we shall see.

The first attempts to measure a chiral scattering effect were made by Beerlage et al. (1981). Using camphor as a target, they looked for the production of longitudinal polarization in the elastic scattering of 25 eV unpolarized electrons to angles between 40° and 70°. They measured polarizations consistent with zero for all angles, with a $2\sigma$ upper bound of 0.5%. However, 4 years later, Campbell and Farago (1985, 1987), in a beam attenuation experiment also with a camphor target, found a significant dichroic effect for 5 eV incident electron energy. Their ultimate result, normalized to an incident electron polarization of 28%, was $A = 2.6(4) \times 10^{-2}$. This was an exciting but surprising result. Numerous theoretical calculations (Fandreyer et al., 1990; Gallup, 1994; Hayashi, 1988; Kessler, 1982; Rich et al., 1982), using a variety of qualitatively different physical models (see below), had all predicted values of $A$ to be of the order of $10^{-4}$. Then, in 1995, both the Nebraska (Trantham et al., 1995) and Münster (Mayer & Kessler, 1995; Mayer et al., 1996; Nolting, Mayer, and Kessler, 1997) groups remeasured the transmission asymmetry with camphor, obtaining at 5 eV values of $0(3) \times 10^{-4}$ and $2(2) \times 10^{-5}$ (normalized to incident electron polarization), respectively. The source of the large asymmetry measured by Campbell and Farago (1985, 1987) has not been identified.

However, the Münster group, in addition to measuring a null result with camphor, has succeeded in measuring transmission asymmetries in a variety of chiral molecules having relatively heavy constituents: bromo- and dibromocamphor, bromo- and iodomethylbutane, and $X(hfc)_3$, where X = Pr, Eu, Er, and Yb. With a precision exceeding $10^{-5}$, these targets yield maximum asymmetries of between 1 and $2 \times 10^{-4}$. The Münster data for camphor, bromocamphor and dibromocamphor, are shown in Figure 28. The quasioscillatory structure of these data, particularly in the case of bromocamphor, is striking and is reminiscent of resonance behavior. This would make sense in that a resonant electron–molecule state would allow their constituents to ''sample each other's chirality'' more effectively than would an impulsive collision. In addition to measurement of a

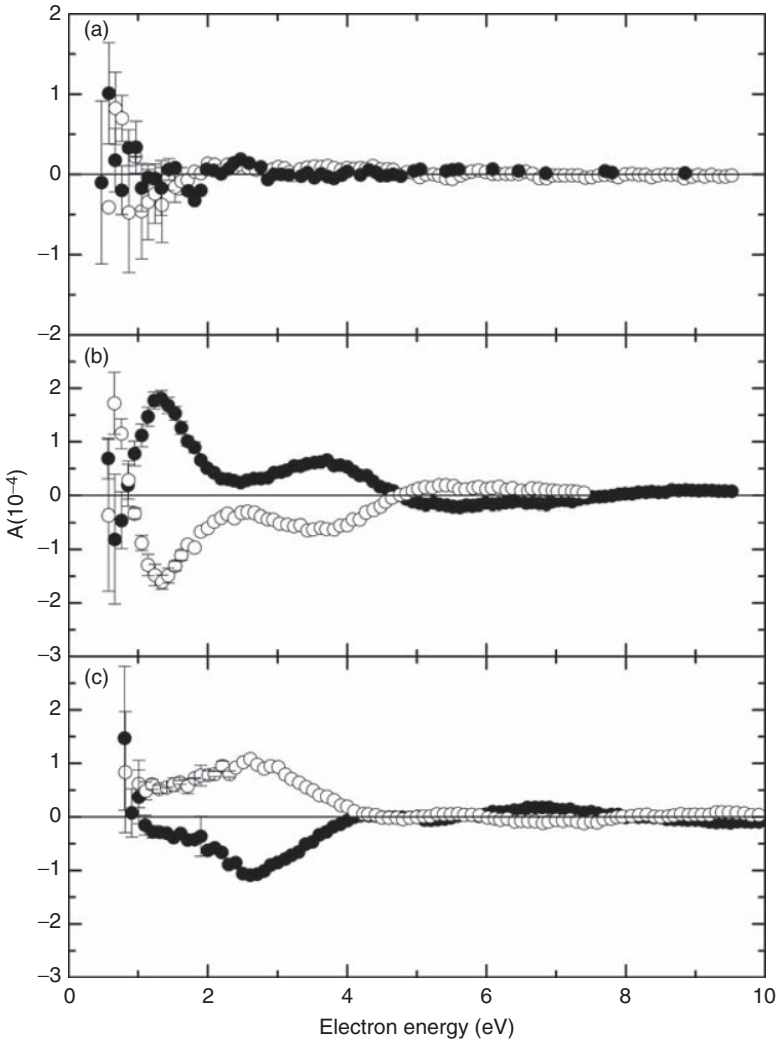


**FIGURE 28** Electron circular dichroism (ECD) asymmetries versus incident electron energy for (a) camphor; (b) bromocamphor; and (c) dibromocamphor. Solid and open circles correspond to different target handedness. Data of Mayer et al. (1996) and Nolting et al. (1997)

transmission asymmetry, the Münster group also measured the production of longitudinal polarization in the forward scattering of unpolarized electrons by bromocamphor. These results were consistent with the time-reversed ECD asymmetry.

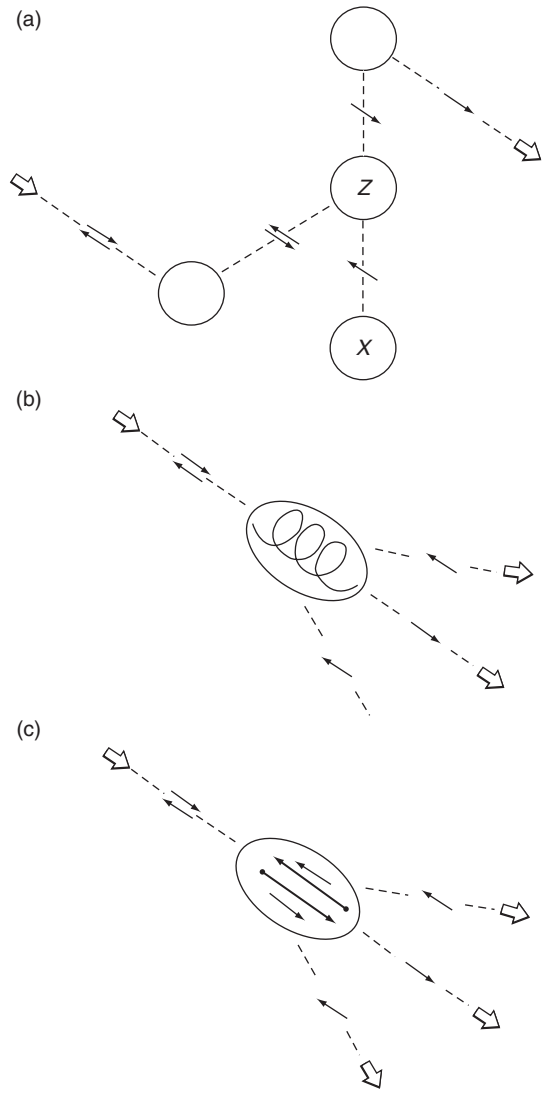


**FIGURE 29** Chiral scattering mechanisms (see text)

The question remains: what dynamical process or processes cause these asymmetries? Three qualitatively different ones have been discussed in the literature. We discuss them in the context of transmission asymmetry measurements of ECD and refer to Figure 29.

(a) *Mott/plural scattering* (Gay, Johnston, et al., 1996; Kessler, 1982;). The incident longitudinally polarized electrons first scatter from a low-$Z$ part of the molecule (Figure 29(a)), which converts longitudinal into transverse polarization through pure Coulomb scattering. Subsequent Mott scattering from a high-$Z$ nucleus is now azimuthally asymmetric due to this transverse polarization, which can result in enhanced forward scattering for electrons of a given incident helicity. In the figure, the chirality of the molecule is such that the lower atom, which could scatter the ''backward'' electron spin, is missing. While such an effect can occur in specific cases with an oriented achiral target, it averages to zero over all molecular orientations. The size of the transmission asymmetry resulting from this mechanism (assuming $P_e = 100\%$) can be expected to be of the order $\eta\ (\alpha Z)^2$, where $\eta$ is a parameter used to gauge the chirality of the target's stereochemical structure, independent of $Z$, the atomic number of the molecule's heaviest nucleus (Gidley et al., 1982; Hegstrom, 1982). Thus a compact chiral structure would have a relatively large $\eta$, whereas a large achiral structure with a small chiral appendage would have a small $\eta$. To set the scale, Hegstrom has estimated that twisted ethylene has an $\eta$ of $10^{-2}$. The Münster ECD asymmetries for bromocamphor and dibromocamphor, being of the order of $10^{-4}$, with $(\alpha Z)^2 \sim 0.1$, yields an $\eta$ of order $10^{-3}$.

(b) ''*Optical*'' *interference between electric and magnetic dipole moments* (Gallup, 1994; Walker, 1982). In a chiral molecule, state-to-state magnetic- and electric-dipole transition amplitudes caused by the electromagnetic pulse of a passing electron can interfere constructively, even after orientational averaging. This results in a transient magnetic moment along the beam axis, independent of the electron polarization (Figure 29(b)). The induced magnetic moment will have a different effect on incident electrons of opposite helicity due to the spin–other orbit interaction, resulting in helicity-dependent scattering. The size of the interference terms (which are also responsible for photon optical activity) should be of the order of $\eta\alpha$; there is no explicit dependence on $Z$ for this effect! The molecular electric and magnetic polarizabilities can depend implicitly on $Z$, but are more strongly correlated with the molecule's atomic weight. If this mechanism is responsible for the Münster results, an $\eta$ value of $10^{-3}$ would dictate asymmetries of the order $10^{-5}$. Alternatively, they would imply values of $\eta$ closer to $10^{-2}$.

(c) *Helicity density dynamics* (Gay, Johnston, et al., 1996a,b; Hegstrom, 1982; Scheer et al., 2006). Due to the spin–orbit interaction between the target electrons and high-$Z$ nuclei, the expectation value of the helicity density operator $\langle \boldsymbol{\sigma} \cdot \mathbf{v} \rangle$, averaged over all electron momenta, is nonzero even though $\langle \boldsymbol{\sigma} \rangle = 0$ and $\langle \mathbf{v} \rangle = 0$. Thus, the chirality of the

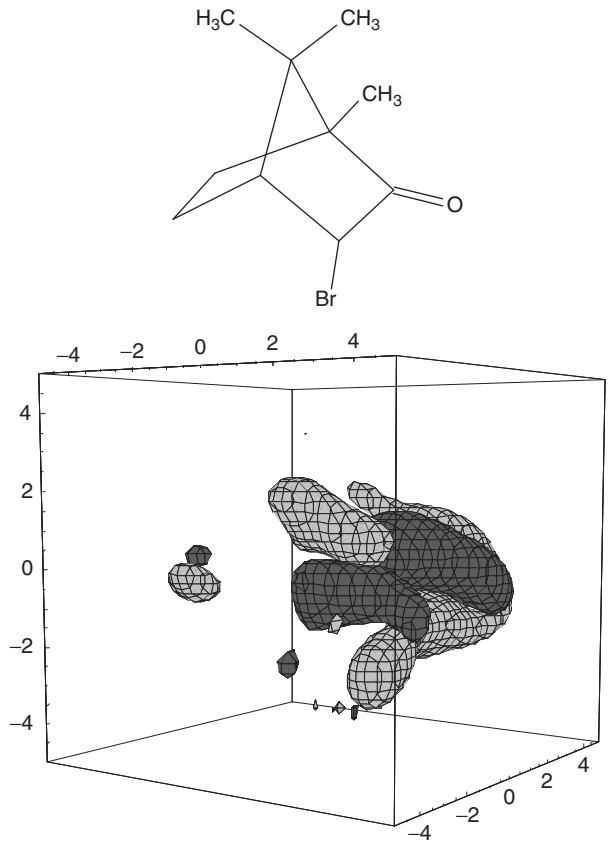


**FIGURE 30** Helicity density plot for bromocamphor (Scheer et al., 2006). Dark and light zones correspond to regions of opposite helicity density. The stereochemical structure indicated is oriented in the same way as the density plot, whose origin is at the molecule's center-of-mass (units in Å)

target's stereochemistry manifests itself in the chirality of the target electrons. Speaking classically, if an electron is headed in a particular direction within the molecular target, its spin will have a nonzero average projection along that direction as well. In an achiral target, regions with local chirality may have an integrated nonzero helicity density, but all of these regions taken together will average to zero. With a chiral molecule, the integral of the helicity density over the entire molecular structure will be nonzero. An example of this, taking the helicity density operator to be a dimensionless $\hbar^{-1}\hat{p} \cdot \vec{\sigma}$ (where $\hat{p}$ is the unit vector in the direction of the electronic momentum), is shown in Figure 30 for bromocamphor (Scheer et al., 2006). It is apparent that

in this case the helicity density is localized near the chiral center of the molecule. The integrated helicity density for the (−) forms of camphor, bromocamphor, and dibromocamphor are, in units of $\alpha^2/2$, −0.58, −15.6, and (surprisingly) −15.4, respectively. Helicity density can affect electron scattering *if* there is a dynamical difference between the scatterings of an incident electron by target electrons which have velocity components of opposite sign along the beam direction (Figure 29(c)). Assume, for example, an extreme case in which only electrons with velocity components antiparallel to the beam direction act to scatter incoming electrons, and that the target handedness is such that these electrons tend to have a component of spin parallel (as opposed to antiparallel) to that direction. There would thus be a different cross section for the scattering of one incident electron helicity over the other because of the differences in the singlet versus the triplet cross sections and (to lower order) spin–spin interactions. Like the Mott/plural scattering mechanism, such effects should scale as $\eta(\alpha Z)^2$ (Onishchuk, 1982).

We now consider the Münster ECD results in light of these three mechanisms. Generally speaking, the experimental data are characterized by quasi-oscillatory structure with peaks separated by several eV over the range of incident electron energies for which data were taken: 0.5–10 eV. The amplitude of the oscillations decreases with increasing energy. In all of these measurements (with the exception of camphor, for which the asymmetry is essentially zero), $A$ is of the order of $10^{-4}$ for all targets, although at the lowest energies it can be as high as 3–4 $\times$ $10^{-4}$. The oscillatory structure is qualitatively similar for the all four of the lanthanoid targets, and is not dissimilar to the structure exhibited in the bromocamphor and dibromocamphor data, albeit with more closely spaced maxima and minima. The iodo- and bromomethylbutane data also suggest oscillatory behavior but with amplitudes less than $5 \times 10^{-5}$.

As mentioned before, the quasi-oscillatory structure suggests that resonant molecular states may be involved in the dichroic transmission. One might expect the second, ''optical'' mechanism to be most sensitive to resonant scattering involving, as it does, the coherent motion of coupled target electrons. The optical picture is bolstered by the fact that most of the data exhibit no strong $Z$-dependence, with the exception of the fact that camphor gives a null result. The brominated camphor targets have $Z^2$ one-quarter to one third that of the lanthanoid targets, but exhibit the largest oscillatory amplitude. We ignore in this discussion the lanthanoid data taken below 1 eV, which may be affected by resonant transmission reduction at low energy (Nolting et al., 1997; Scheer et al., 2008). The exception to this is the iodo- and bromomethylbutane targets, which

exhibit maxima that do scale roughly as $Z^2$. We hasten to add that a high-$Z$ atom would be expected to have little effect if it is not at or near a chiral center of the target molecule. Thus the larger asymmetry exhibited by bromocamphor ($Z = 35$) compared with Yb(hfc)3 may be due solely to the fact that the Yb is not at the chiral center of the molecules, whereas the Br in bromocamphor is.

Scheer et al. (2006, 2008) have attempted to understand the ''resonant'' structure of the lanthanoid sequence of targets, as well as the brominated camphor data, and to evaluate to what extent the helicity density model could be connected with resonant effects. To do this, they measured electron translational spectra (ETS) for these targets to identify the positions of scattering resonances (Sanche & Schulz, 1972). (The Münster group also took ETS data for bromocamphor and $Yb(hfc)_3$.) They also calculated theoretical energy positions of the lowest unoccupied molecular orbitals (LUMOs) for these molecules, as well as the spatial distribution of helicity density for the brominated camphor targets. By comparing the measured resonance energies with the calculated positions of the LUMOs, resonance assignments can be determined with reasonable confidence. This work showed that identifiable ETS scattering resonances do not correlate well with the observed ECD ''resonance'' features for the lanthanoid targets taken as a group. Moreover, the lowest energy resonances have most of their electron density near the high-$Z$ center of the molecule. Since the chiral centers of these molecules are located in the camphorate ligands, the attribution of significant ECD asymmetry to these resonances seems problematic.

In the case of the brominated camphor targets, Scheer et al., (2008) were able to show with some certainty that the ECD asymmetry features in the vicinity of 1.4 eV, an extremum in the case of bromocamphor and a ''shoulder'' in dibromocamphor, could be associated with well-defined resonances in both targets. (The asymmetry maximum in dibromocamphor is not obviously associated with any resonance.) More interestingly, the magnitude of the helicity density–resonant state electron density product predicts the relative magnitude of both asymmetries. This provides some evidence for a helicity density mechanism at work in the production of ECD, at least in this limited instance.

It is apparent from this discussion that much more work with a variety of chiral molecules needs to be carried out to isolate specific dynamical mechanisms responsible ECD. Systematic variation of $Z$ within a given type of molecular structure, as in the lanthanoid series investigated by the Münster group, as well as variation of the stereochemical structure in an incremental, well-defined way will be the key to such studies. This will likely prove to be a challenging task, given the difficulty of synthesizing usable quantities of high-$Z$ chiral compounds with the high vapor

pressures necessary to achieving reasonable apparatus analyzing power without the danger of racemization.

For the purpose of completeness, we note in this context two related experiments done recently with chiral molecules in a solid form. Ray et al. (1999, 2006) have coated Au substrates with ordered chiral films and shined circularly polarized light on them. The films comprise either Langmuir–Blodgett films of (L)- or (D)-stearoyl lysine, or monolayers of double-stranded DNA oligomers. The authors argue that the circularly polarized light produces longitudinally polarized electrons in the Au, which are subsequently emitted through the organic coating. When the helicity of the incident light is flipped, the transmission of the electrons is altered. In the case of the lysine films, this effect reverses when the chirality of coating layers is changed from (L) to (D). Remarkably, the asymmetry in the electron emission with both types of chiral layers is comparable to the polarization of the electrons one would expect to be emitted from atomically clean gold surfaces, about 10–15% (Meier & Pescia, 1981). In the case of the lysine films, long-range chiral order seems to be important as well, given that the transmission asymmetry disappears when L films are contaminated with 1% D molecules.

In a somewhat similar experiment, Rosenberg et al. (2008) used X-rays to photoemit polarized electrons from a magnetized Permalloy substrate coated with randomly oriented chiral (*S*)- or (*R*)-2-butanol. In this case, the rate of C–O bond breakage associated with the chiral carbon atom was monitored. An asymmetry of $5.0(1.3) \times 10^{-2}$, corresponding to the reversal of either the substrate magnetization or the 2-butanol chirality was observed, again, comparable to the expected electron polarization from pristine Permalloy surfaces of 10–15% (Mauri et al. 1989). This latter result is also remarkable, given that it demonstrates a chiral effect in the breakup, or chemistry, of the target, as opposed to a simple transmission asymmetry. It must also be noted that in neither of the experiments just mentioned was the polarization of the photoemitted electrons ever confirmed.

## 5. DEVELOPMENTS IN POLARIZED ELECTRON TECHNOLOGY

In this section, we review the developments in polarized electron technology that have occurred over the last two decades. These improvements have significantly reduced the difficulty of experiments with polarized electrons. We will also discuss new ideas and technologies which hold promise for the next generation of experiments.

## 5.1. Sources of Polarized Electrons

### 5.1.1. Photemission from GaAs and its Variants

Photoemission from negative electron affinity (NEA) optically pumped GaAs was first demonstrated as a source of polarized electrons in the mid-1970s (Pierce et al., 1975). This technique is now the standard one for polarized electron production. The physics and operation of this source has been discussed extensively (Kessler, 1985; Pierce, 1996; Pierce et al., 1980) and will be discussed here only to the extent necessary to explain recent improvements in its capabilities. The canonical Γ-point energy-level diagram for GaAs is shown in Figure 31(a). Direct bandgap transitions from the valence band to the conduction band, driven by circularly polarized light in the electric-dipole approximation, are also indicated in Figure 31(c). In bulk crystalline GaAs, the $^2p_{3/2}$ heavy-hole (hh) and light-hole (lh) bands are degenerate at the Γ point. Given the transition matrix elements (Pierce & Meier, 1976), this means that photons that just

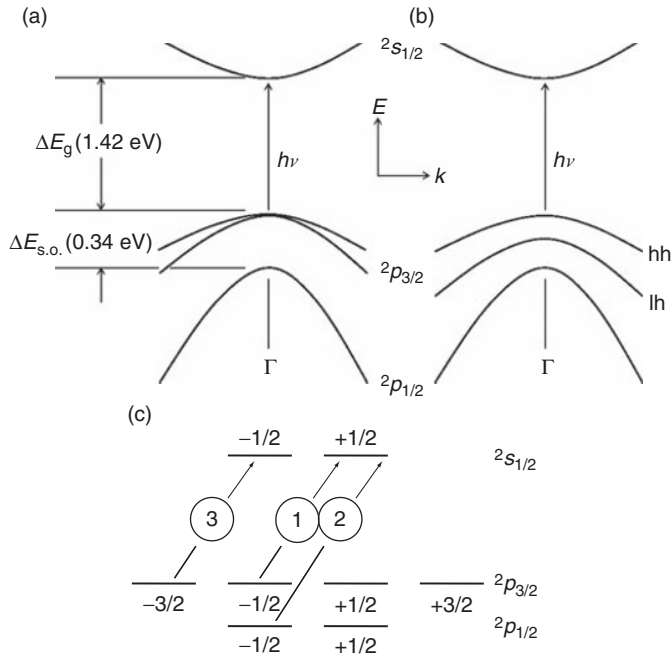


**FIGURE 31** (a) Gamma point energy-level schematic for generic zinc-blende structure, for example, GaAs, showing the band-gap splitting $\Delta E_g$ and the spin-orbit splitting $\Delta E_{s.o.}$. (b) Removal of the Γ-point heavy-hole (hh)–light-hole (lh) degeneracy due to strain (see text). (c) Electric-dipole transition strengths for optical pumping (Pierce & Meier, 1976)

bridge the 1.42 eV bandgap can produce nascent electron polarization in the conduction band of at most 50%. Due to spin-flip scattering processes that occur as the electrons make their way from the bulk to the surface, this is reduced further, typically to values between 25 and 40%. The quantum efficiency (QE; number of emitted electrons per incident photon) for such sources can be as high as a few percent, but for most applications, yields below 0.1% are typical when conditions are less than ideal. The energy spread of the emitted beam is ~0.3 eV, but this can be reduced below 50 meV if the crystal is cooled to 77 K (Feigerle et al., 1984).

In general, the above conditions are sufficient for most tabletop physics experiments, where ''beam time'' is essentially unlimited, and apparatus operating costs in the steady state are low. The need for higher polarizations and quantum yields, however, is a constant driving force in the accelerator-based nuclear physics community, particularly for experiments involving parity violation measurements (Kponou et al., 2008). This push for better source performance has proved to be a benefit for all experiments that need polarized electrons.

In 1991, groups in Japan and the United States (the SLAC/Wisconsin collaboration) succeeded in removing the degeneracy of the heavy-hole and light-hole bands at the GaAs $\Gamma$ point (Figure 31(b)) by using MBE techniques to grow GaAs on substrates with incommensurate crystal spacing. This lattice mismatch strains the GaAs structure, leading to the heavy-hole, light-hole splitting. The splitting must exceed $kT$ and the doping-induced band tailing. Initial polarizations as high as 86% with a QE of 0.02% were observed by the Nagoya group for GaAs(001) grown on a layer of $GaAs_xP_{1-x}$ ($x = 0.17$) (Nakanishi et al., 1991). In the intervening years, increasingly exotic ''superlattice'' photocathodes have been developed, involving, for example, many alternating layers of III–V-based compounds to enhance or maintain uniform uniaxial strain on the photoemitter throughout the sample. One drawback of these highly polarized photoemitters is their uniformly low QE, with an upper bound of 0.8% but more typically 0.1%. This reduced QE is due to the thinness of the epitaxially-grown photoemitting region when compared with bulk GaAs. An interesting attempt to ameliorate this problem has involved the growth of a tuned Bragg reflector, comprising alternating layers of quarter-wave material tuned to the working wavelength of the photoemitter, immediately behind the strained GaAs layers (Groebli et al., 1995). This has provided improvements in the quantum yield by more than an order of magnitude at certain wavelengths. The interested reader is referred to the proceedings of recent International Spin Physics Symposia (e.g., Imai et al., 2007) and the Workshops on Polarized Sources, Targets, and Polarimetry (Kponou et al., 2008) for details of the latest developments. At present, the state of the art for polarization appears to be between 90 and 92%, with a corresponding QE

of 0.5%. These levels can be reached only in sources with exceedingly clean XHV, typically in the $10^{-12}$–$10^{-13}$ range.

It should be noted that the standard ''figure of merit'' for polarized electron sources is

$$F_{\text{source}} = P_{\text{e}}^2 \times \text{QE}, \tag{21}$$

which is inversely proportional to the square of the time required to measure a given experimental asymmetry that depends linearly on the incident electron polarization and intensity (Kessler, 1985; p.242). This parameter for the highest polarization sources is actually significantly less than that of bulk GaAs which, with a well activated sample in a clean environment, can have a polarization of ~0.4, but a QE greater than 10%. In most accelerator-based nuclear physics experiments, where the experimental asymmetries to be measured are extremely small, control of systematic error is what make the GaAs heterostructures with their higher polarization preferable to bulk GaAs.

For reasons related primarily to vacuum cleanliness, polarized electron sources in experiments with proximate atomic and molecular targets generally have much poorer performance with regard to all three important source specifications: polarization, QE, and lifetime. Sources on small systems with solid-state targets and good UHV conditions in the target region typically have performance characteristics somewhere in between these two extremes.

In the case of systems with gas-phase targets with high throughput, effective differential pumping is crucial. The best source performance in these cases is obtained with open structural geometries in the vicinity of the photocathode, and with very high pumping speed provided by ion and/or nonevaporable getter (NEG) pumps. The use of small source chambers and/or turbomolecular pumps to evacuate them should be avoided unless experimental considerations demand it. These setups often require heavy cesiation to produce a NEA activation of the photocathode crystal, and low-level continuous cesiation to maintain a useable QE. Such cesiation can lower the polarization of fancy heterostructure cathodes to that of a typical bulk sample.

Due to chemical degradation of the NEA surface, ambient contaminants such as $CO_2$, $H_2O$, and $O_2$ are usually responsible for the reduction of photoemitter performance due to poor source vacuum. Deleterious effects due to ion bombardment caused by the electron beam ionization of residual gas downstream from the photocathode are also known to reduce lifetimes as well (Sinclair et al., 2007). In this regard, recent work by Mulhollan and Bierman (2008) has shown an improvement in QE and photocathode lifetime by the use of both Cs and Li in the activation process. This bi-alkali

technique is particularly promising when ambient contaminants, particularly $CO_2$, are suspected of degrading source performance.

While some design improvements in the general operation and configuration of GaAs sources have been reported (Al-Khateeb et al., 1999; Hayes et al., 1997; Schedin et al., 1998; Yashin et al., 2000), recent work by the Nagoya group represents what may be regarded as the first fully engineered source for tabletop applications (Jin et al., 2008; Yamamoto et al., 2008). The design, shown in Figure 32, is elegant in its simplicity, sophistication, and performance. It is based on a GaAs–GaAsP heterostructure design, grown on a GaP substrate that is transparent to the photoemission laser wavelength between ~780 and 840 nm. This transparent backing allows the laser beam to be introduced from the upstream side of the crystal, with a short focal length lens mounted immediately behind it. Since the laser beam in this configuration can be focused to a very tiny spot on the photoemitting region of the cathode, a very tight, high-brightness beam can be produced. The performance of this photocathode as a function of laser wavelength is shown in Figure 33. Yamamoto et al., (2008) determined the brightness of beams produced by this source to be $\sim 2 \times 10^7$ A cm$^{-2}$ sr$^{-1}$. Such a source is ideal in UHV and XHV applications with nonvolatile targets. Its use in a typical gas-phase application would presumably result in somewhat poorer polarization and lifetimes.

### 5.1.2. Sources Based on Chemi-Ionization of He*

At present, the best alternative to GaAs technology for the production of polarized electrons is the flowing-afterglow source, invented and developed at Rice University between the mid-1970s and early 1990s (Rutherford et al., 1990 and references therein). In this scheme, the flowing afterglow of a RF helium discharge, rich in metastable He, is optically

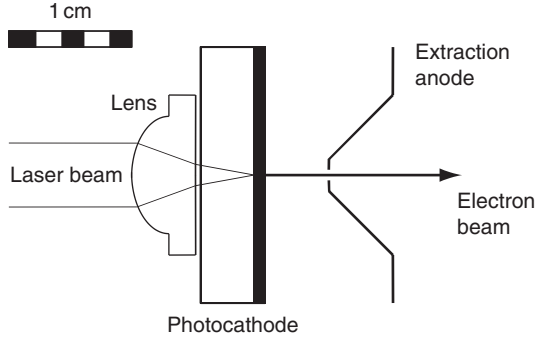


**FIGURE 32** Schematic of the Nagoya polarized electron source (Redrawn with permission from Jin et al., 2008, *Applied Physics Express, 1*, 045002 see text)

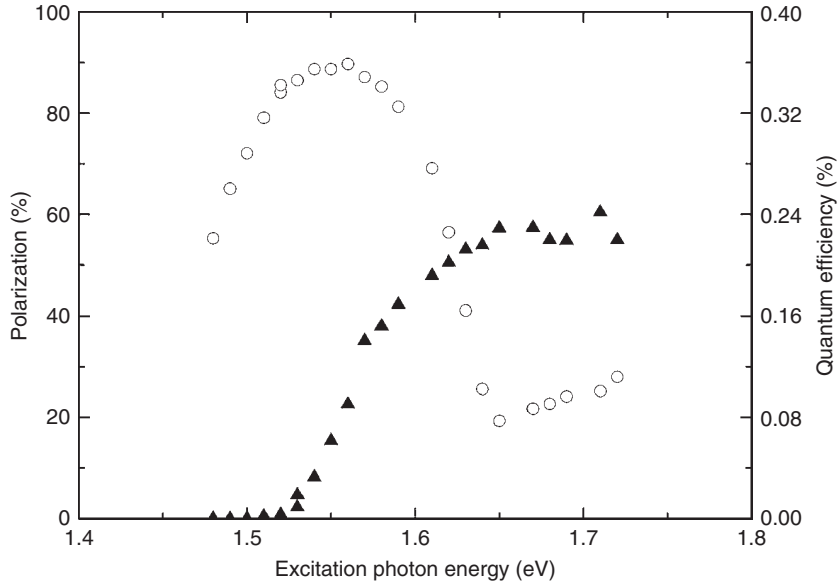


**FIGURE 33** Polarization and quantum efficiency of the Nagoya source as a function of photoemission laser wavelength. Triangles correspond to quantum efficiency, circles to electron polarization. Redrawn with permission from Jin et al. (2008), *Applied Physics Express, 1*, 045002

pumped with 1.08 μm light from a LNA laser. The resultant spin-polarized He($2^3$S) atoms are chemi-ionized with $CO_2$ gas, and the polarized electrons are extracted electrostatically from the chemi-ionization volume. The electron polarization drops monotonically with extracted current. In the most recent versions of this source, developed both at Rice and at Orsay (Arianer et al., 1996), polarizations between 85 and 90% can be achieved if only 100 nA is extracted from the source. However, with extracted currents of 150 μA, the electron polarization is still greater than 50% in the case of the Orsay source. Typical energy spreads of the extracted beam are less than 0.4 eV.

The Orsay source, developed for CW injection at MAMI, was never installed because its performance in terms of polarization and extracted current was surpassed by that of strained GaAs photocathodes. For applications in atomic and molecular scattering and condensed matter studies, however, it remains a viable alternate source. It is reasonably compact and very reliable. The stringent UHV vacuum requirements of GaAs sources are eliminated, but are replaced by the need for large, high speed mechanical pumps to handle the high flow rate of He from the afterglow region. The LNA lasers needed are also somewhat more technically demanding than the simple diodes used for photoemission from GaAs. The biggest

advantage of the flowing afterglow source over GaAs is its lack of a complicated activation procedure necessary to produce a NEA surface.

### 5.1.3. Novel Sources of Polarized Electrons

The last 15 years have seen a variety of new ideas for producing polarized electrons. None of these have yet evolved into robust sources, and many remain at the proposal level. We outline these ideas here to provide the reader with an idea of the broad range of possibilities that exist for future development.

**5.1.3.1. Field emission tips** Field emission sources are attractive because they eliminate the need for activation of a NEA surface, and their small emitting area gives them a very high brightness. Early experiments involved field emission from W tips coated with a magnetic material (see, e.g., Kessler (1985) and references therein). The chief disadvantage of this technique is its lack of optical spin reversibility. The most highly polarized field emission source to date ($P_e \sim 90\%$) used EuS-coated W tips at 10 K and required a high ambient magnetic field in the source region (Kisker et al., 1978). More recent work of this type (Bryl & Altman, 2003) has involved Co-coated W, with the tip operated at room temperature. This scheme produced a few nA of electrons with polarizations between 20 and 35%, but with somewhat unstable spin direction due to the shifting magnetization of the thin Co magnetic layer. We mention in this regard an interesting theoretical proposal to build polarized field emitter tips from magnetic GaN nanotubes (Gao et al., 2004).

A new class of field emitters—bulk GaAs with an etched tip—has the advantage over magnetic tips of optical reversibility (Kuwahara et al., 2006). The Nagoya group has demonstrated such a source with polarizations as high as 38% with an incident laser energy of 1.69 eV. To get a reasonable QE at this energy, however, it was necessary to treat the surface with some Cs and $O_2$ to obtain a slightly positive electron affinity (PEA). Activation to NEA conditions improved the QE by an order of magnitude, but lowered the polarization. Surfaces with PEA were found to be much more robust than NEA surfaces, eliminating to a significant extent the problems associated with NEA activation. A more severe problem occurred when currents greater than 1 μA were extracted; due to local Joule heating of the tips they tended to melt away. The brightness of this source was estimated to be $\sim 2 \times 10^7$ A cm$^{-2}$ sr$^{-1}$, comparable to the Nagoya transparent cathode source (Jin et al., 2008).

In conjunction with these new developments, it is interesting to note the recent demonstration of femtosecond pulses of electrons produced by multiphoton absorption in field emission tips (Barwick et al., 2007; Hommelhoff et al., 2006). Such experiments have not yet been tried with

circularly polarized light, but short pulses of polarized electrons would dramatically broaden the applicability of such sources.

5.1.3.2. Sources involving multiphoton processes Multiphoton production of polarized electrons from both atoms and solids is distinguished from methods involving optical pumping of alkali atoms, to be discussed below. To date, no free beams of polarized electrons have been produced with these methods. With the increasing availability of high-power, short-pulse laser sources, however, techniques of this type show promise. All are based in two- or three-photon resonant or nonresonant ionization of alkalis (Bouchene et al., 2001; Sokell et al., 2000), heavy noble gases (Nakajima & Lambropoulos, 2002), or the alkaline earths (Nakajima et al., 2003, 2008; Yonekura et al., 2004).

The ultrafast method using alkalis (K) is essentially a quantum-beat technique. A circularly polarized laser resonantly and coherently excites the 4p fine-structure doublet from the ground state. This results in an oriented orbital angular momentum which, in the fine-structure relaxation time, orients the atomic spin along the laser axis. At this moment, a second pulse is used to ionize the K*, producing maximally oriented electrons. Using this scheme, Sokell et al. (2000) have demonstrated oscillatory production of $K^+$, but the ionized electron polarization was not analyzed.

The experiments with alkaline earths (Sr) actually involve three laser pulses: one to ablate a Sr disk, one to resonantly excite the specific 5*s*5p $^3P_1$ intermediately coupled fine-structure level, and one to ionize the Sr*. In this case, spin polarization results from the strong spin–orbit coupling of the excited target and the subsequently large fine-structure splitting. In these experiments, the spin polarization of the $Sr^+$ has been measured using laser-induced fluorescence, and polarizations as high as 64% have been observed. Again, the electrons resulting from ionization were not analyzed.

Nakajima and Lambropoulos (2002) have shown that direct, single-color resonant ionization of Xe with circularly polarized light can result in high degrees of spin polarization. This method is essentially an extension of one proposed for the alkalis by Lambropoulos (1973), but has the advantage that Xe targets can be made with higher density. By placing the circularly polarized laser energy between that necessary to excite the $J = 1$ $5p^5 6s$ fine-structure levels, interference between the two should result in almost complete photoelectron polarization. Estimates for a 1 Torr Xe target ionized by a 1 mJ 4.8 eV pulse focused to a diameter of 150 μm are that $\sim 10^{12}$ electrons per pulse should be able to be extracted (T. Nakajima, private communication, 2009).

Finally, the possibility of multiphoton electron emission from bulk GaAs has been suggested (Matsuyama et al., 2001). By using circularly polarized light from a laser with half the photon energy necessary to bridge the bandgap (see Figure 31(c)), only electrons from the $^2p_{3/2}$ level are promoted

to the conduction band level. The absorption of two units of angular momentum along the axis of symmetry guarantees that these excited electrons have 100% initial polarization. Initial experiments with two-photon absorption were performed at 90 K, to match the bandgap of the bulk GaAs (111) crystal (1.504 eV) as closely as possible with the 2-photon energy of the laser. No electrons were extracted from the crystal, but the fluorescence of conduction electron–valance hole recombination was monitored. The polarization of this fluorescence can be related to the electron spin polarization immediately after excitation to the conduction band. The fluorescent polarization doubled when two-photon excitation replaced single-photon excitation with the same total energy. By extrapolating the fluorescent polarization to the instant of electron promotion, a nascent spin polarization of ~95% was inferred for the two-photon process. More recently, similar measurements have been carried out with GaAs (001) surfaces and a variety of other zinc-blende crystals (Bhat et al., 2005).

5.1.3.3. Spin filters Spin filters can act either as sources of polarized electrons or as polarimeters. In essence, a spin filter acts by providing a volume through which electrons of orthogonal polarization have different transmission coefficients. Thus, incident unpolarized electron beams emerge from the filter polarized, and the transmitted intensity of an incident polarized beam depends on that polarization. The mechanisms proposed to date for such polarization discrimination are based on exchange scattering in both gaseous and solid targets, ECD, and the Stern–Gerlach effect. Only the first has resulted in polarized currents with intensity suitable for most atomic or molecular scattering experiments.

In 1999, Batelaan et al. (1999) demonstrated a remarkably simple spin filter based on the optical pumping of Rb (see Figure 34). In this scheme, a target of Rb vapor with a density of $\sim 10^{12}$ cm$^{-3}$ combined with $N_2$ buffer gas at ~1 Torr is optically pumped so that the Rb in its ground state becomes spin polarized. The $N_2$ also acts as the source of unpolarized electrons, in that it is used to maintain an annular cold-cathode discharge in the optical pumping cell. The initially unpolarized electrons migrate through the Rb to the extraction aperture under the action of an axial electric field. As a result of spin-exchange collisions with the Rb, the drifting electrons become spin polarized. Beam currents of the order of several microamperes can be extracted, with $P_e$ of ~20% (Figure 35).

In the apparatus investigated by the Nebraska group, the $N_2$ buffer gas plays several crucial roles simultaneously. As mentioned above, it is the source of the incident electrons, but it also serves to quench excited Rb atoms, and thus reduce the effects of radiation trapping in the optical pumping volume (Wagshul & Chupp, 1994). Since the number density of the $N_2$ ($\sim 10^{16}$) is much greater than that of the Rb, the path length of the electrons through the chamber is much longer, allowing greater chance

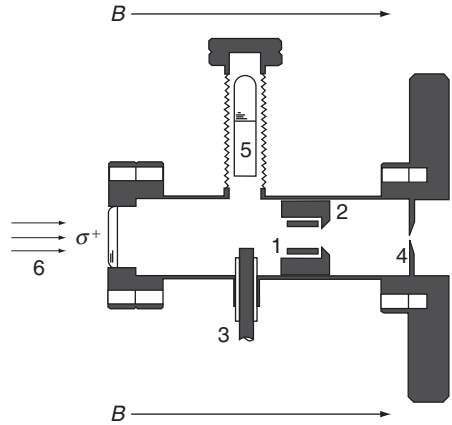


**FIGURE 34** Schematic diagram of an optically pumped Rb spin filter (see text) showing (1) DC-discharge cold cathode; (2) discharge anode; (3) discharge high-voltage feedthrough; (4) electrically-isolated field plate and exit aperture; (5) Rb ampoule; (6) optical pumping radiation. The entire apparatus is immersed in a magnetic field

for interaction with the spin-polarized Rb. Also, the numerous collisions with the $N_2$ serve to thermalize the electrons, so that the cross section for spin exchange is increased significantly (Bahrim et al., 2001). Finally, the relatively high-pressure buffer gas acts to inhibit diffusion of the polarized Rb to the stainless steel walls of the vacuum chamber, thus increasing the depolarization time.

The Rb spin filter was studied in an attempt to develop a ''turnkey'' source of polarized electrons. Unfortunately, the sensitivity of the beam current and polarization to the coupled operating parameters of the electron source and optical pumping volume made this source far from simple to operate. On the other hand, the figure of merit for the source (Equation (21)) makes it comparable to early realizations of the GaAs source.

In this context, we note a recent proposal by A. Zelenski to extract polarized electrons from high-density optically pumped Rb vapor in a high magnetic field (Zelenski, 2007). Earlier work (Zelenskii et al., 1986) had indicated high rates of associative ionization in collisions of excited Rb atoms with densities of the order of $10^{13}$ cm$^{-3}$ produced in the optical pumping process. The high magnetic fields served to prevent radiation trapping depolarization (Tupa & Anderson, 1987). Feasibility studies for this type of source are currently underway at Brookhaven National Laboratory.

Magnetic spin filters, developed at the Ecole Polytechnique and at ETH Zürich, are conceptually similar to the Rb spin filter and are based on the differential transmission of both transversely and longitudinally

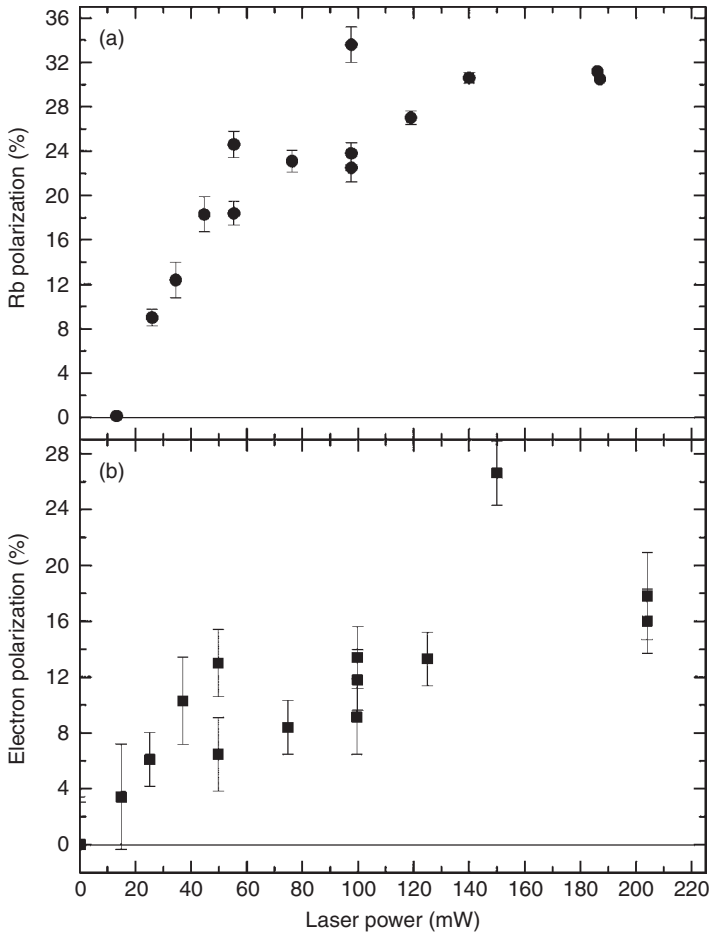


**FIGURE 35** Rb polarization in the spin filter and its corresponding output electron polarization (Batelaan et al., 1999). For these data, the $N_2$ buffer gas pressure is 0.4 Torr and the Rb density is $7 \times 10^{11}$ cm$^{-3}$. Extracted electron current is 2 μA

polarized electrons through thin films of magnetized Co and Fe, sandwiched by Au films (see Cacho et al., 2002; Weber et al., 1999; and references therein). The filtering effect is related to the preferential scattering of incident electrons by minority spin *d*-state holes above the Fermi level. This scattering leads to suppressed transmission of electrons with the corresponding spin and hence the spin filtering effect. Both the French and ETH groups have observed transmission asymmetries greater than 50% with both elastically and inelastically scattered electrons. The drawback to using these devices as sources is that for typical foil

sandwich thicknesses of tens of nm, transmission through the samples is $\sim 10^{-5}$. Moreover, the maximum permissible (unpolarized) current incident on these targets appears to be limited to less than 1 $\mu$A, meaning that only a few pA of maximally polarized electrons are produced.

Similarly, Ray et al. (1999, 2006) have suggested that the Langmuir–Blodgett films of (L)- or (D)-stearoyl lysine, or monolayers of double-stranded DNA oligomers on Au substrates could provide a spin-filtering effect. These films appear to provide almost complete discrimination (i.e., suppression of transmission) against longitudinally polarized electrons of a given handedness, although, again, current handling capability over extended periods might prove to be a concern. Similar results might be expected with iron substrates coated with 2-butanol films (Rosenberg et al., 2008) since the transmission analyzing power in this case is also of the order of unity. We note, however, that while the experiments of Ray et al., (2006) were carried out with laser light sources, making their implementation for source technology possible in a small lab setting, those of Rosenberg et al., (2008) were done at the Advanced Photon Source (APS) with hard ($\sim$1200 eV) X-rays.

Finally, we discuss a controversial suggestion by the Nebraska group to produce polarized electrons by the action of an inhomogeneous longitudinal magnetic field on an unpolarized beam, that is, the Stern–Gerlach effect (Batelaan & Gay, 1998; Batelaan et al., 1997; Gallup et al., 2001; Rutherford & Grobe, 1998). The general Bohr–Pauli edict that macroscopic magnetic fields acting on classical particle trajectories cannot be used to separate electrons by spin has been generally taken to forbid such sources (see, e.g., Kessler, 1985). However, over the years, proposals by Bloch (1953), Brillouin (1928), and Dehmelt (1988,1990) have called this general principle into question for the case of magnetic fields whose inhomogeneities lie along the line of the electron beam whose spin is to be separated. Such proposals seem plausible, in that they circumvent the chief problem with a Stern–Gerlach magnet operating in the orthodox transverse configuration: the blurring of spin separation by Lorentz forces.

Batelaan et al. (1997) showed that Pauli's rejection of the longitudinal scheme was in error. Based on a calculation with quantum-mechanical spin but classical trajectories, they showed complete separation of spins using optimum initial conditions for the beam trajectories. Using more physical initial conditions based on Landau states, they still found a significant separation comparable to the beam spreading itself. However, the degree of separation cannot be made arbitrarily large in the semiclassical case. Moreover, no proposals for a physical source of spin polarized electrons can be rigorously based on semiclassical predictions.

More recently, Gallup et al. (1991) did a rigorous quantum-mechanical calculation of the longitudinal case, incorporating the complete off-axis behavior of the electron Landau wave packets as they moved through an inhomogeneous solenoidal field. They found that arbitrarily large spin separation can be achieved between spin-forward and spin-backward components, to the extent that a pure Landau ground state can be inserted into the magnetic field (see Figure 36). Failure to achieve this does not reduce the spin separation, but does introduce contaminant components into the transmitted beam. The chief drawback to a source of this type is the requirement of extremely low incident electron energy—less than 100 meV for high degrees of electron separation. At this point it is safe to say that even a demonstration of separation at any level would represent a major experimental *tour de force*, so that proposals for an operating source based on these ideas would currently be speculative at best.

## 5.2. Polarimetry

Ultimately, experiments in polarized electron scattering require measurement of either the incident or scattered electron polarization, or both. The gold standard for electron polarimetry is Mott scattering, although methods based on exchange scattering from solid or gaseous targets have been proposed and realized as well. Developed as a technology in the 1950s to investigate beta-ray polarization in studies of weak decay and the electron $g$-factor, Mott polarimetry was a reasonably mature field in the late-1980s. However, experimental imperatives and theoretical questions have spurred significant developments in the field since then which will be outlined below. An alternate technology, optical electron polarimetry, was developed in the 1990s, as were new methods based on magnetic targets. The purpose of this section is to acquaint the reader with the state-of-the-art technology for polarimetric measurements.

### 5.2.1. Mott Polarimetry

Mott polarimetry was reviewed by Gay and Dunning several years ago (Dunning, 1994; Gay, 1996; Gay & Dunning, 1992). (See also Kessler (1985), the proceedings of the most recent International Spin Physics Symposium (Imai et al., 2007), the proceedings of the most recent Workshop on Polarized Sources, Targets, and Polarimetry (Kponou et al., 2008), and references therein.) Essentially, it involves the scattering of transversely polarized electrons by targets made of atoms with a high $Z$ (most often Au or Th) to ensure large spin–orbit coupling between the

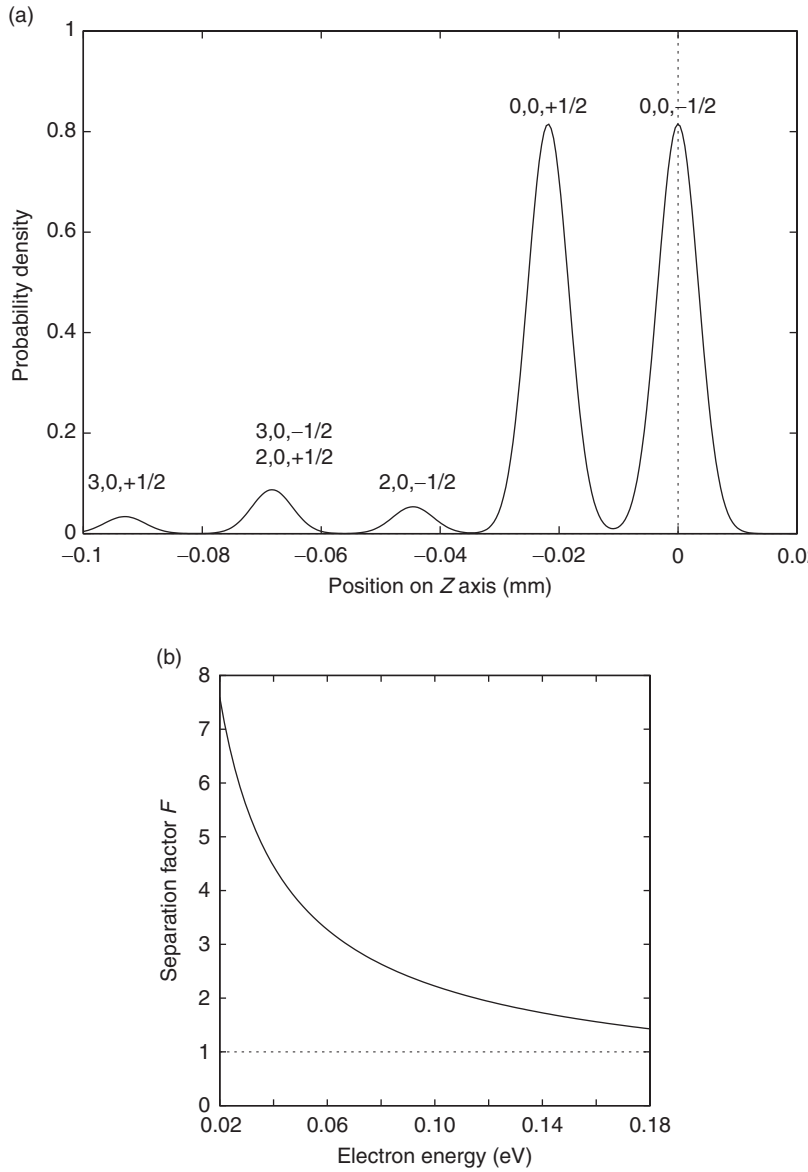


**FIGURE 36** (a) Electron probability density along the axis of a longitudinal Stern–Gerlach magnet for insertion of the lowest Landau-level wave packet under realistic conditions. The two large peaks correspond to the $(n, m_l, m_s) = (0,0,\pm 1/2)$ Landau states and thus the spin-splitting of the beam (Gallup et al., 2001). Secondary peaks are contaminants from higher lying levels. The vertical-dotted line corresponds to no longitudinal acceleration. (b) The separation factor $F =$ (separation of peak centroids/width of peaks) as a function of electron energy for the main peaks shown in (a)

target nuclei and the back-scattered continuum electrons. The electron polarization is then given by the special case of Equation (4):

$$A = \frac{I_R - I_L}{I_R + I_L} = P_e S_{\text{eff}}(E, \Delta E, \theta, \Delta\Omega, t), \tag{22}$$

where $I_{R(L)}$ is the detected intensity of electrons scattered to the right(left) and the ''effective Sherman function'' $S_{\text{eff}}$ is the polarimeter's analyzing power, which depends on the target material, the energy $E$ of the incident electrons, the greatest energy loss, $\Delta E$, that a scattered electron can have suffered and still be detected, the polar scattering angle $\theta$, the solid angle $\Delta\Omega$ subtended by the detector centered on this angle, and the target thickness $t$. In the limit of elastic scattering from a single target atom, $S_{\text{eff}}$ is given by the ''true'' Sherman function $S$. Multiple and plural elastic and inelastic scattering within the bulk or thin film target generally cause $S_{\text{eff}}$ to be smaller than $S$.

The time required to measure electron beam polarization to a given precision is inversely proportional to the square root of the polarimeter figure of merit (analogous to the source figure of merit; Equation (21))

$$F_p = \mathcal{A}^2 \eta, \tag{23}$$

where $\mathcal{A}$ is a generalized analyzing power, equal to $S_{\text{eff}}$ in the case of a Mott polarimeter, and $\eta$ is the analyzer's efficiency, the ratio of the detector count rate to the rate at which electrons enter the device.

Recent Mott polarimeter development has been driven by two issues. Typical Mott analyzers are efficient enough that when they are used to measure the polarization of incident electron beams with currents greater than ~100 nA, most of the beam must be thrown away in order to avoid dead-time issues with the scattered electron detectors, or damage to thin targets. When one wishes to measure the polarization of secondary electrons scattered from a target, however, the efficiency and compactness of the analyzer become paramount (see, e.g., Huang et al., 1993; Barnes et al., 1999). Consequently, the development of Mott polarimeters that maximize $F_p$ and minimize detector volume has been an active area of research.

Retarding-field Mott polarimeters, of the type first proposed by Farago and developed at Rice University, offer the best option for miniaturization. In this design, the incident electrons are first accelerated to the Mott scattering energy, typically between 20 and 120 keV, and upon backscattering they are decelerated by the same field before reaching a detector housed at or near ground potential. Unlike conventional Mott polarimeters, this scheme allows complete energy discrimination of the scattered electrons, that is, $\Delta E$ can be reduced to zero.

Since its first appearance in the late -1980s (Dunning et al., 1987), the Rice ''micro-Mott'' device has set the standard for compact detectors of this type. These instruments are typically operated with a target potential between 20 and 25 kV, which is sufficient to produce a reasonably high Sherman function with good efficiency, without the need for large insulating target standoffs. The most recent version from Rice, the result of several design iterations and improvements, is shown in Figure 37 (Neufeld et al., 2007). With the use of Th targets, which increases both $S_{\text{eff}}$ and $\eta$ relative to Au, small retarding-field Mott polarimeters can now have figures of merit as high as $2 \times 10^{-4}$ (Iori et al., 2006; Neufeld et al., 2007) compared with earlier designs that had values an order of magnitude below this. At 25 kV operating voltage, for example, the Rice polarimeter has an efficiency $\eta$ of $2.5 \times 10^{-3}$ and $S_{eff} = 0.24$ when $\Delta E = 400$ eV. Some designs have used channel- and microsphere plate detectors to enhance timing resolution, the maximum allowable count rates, or the detector solid angle and thus $F_{\text{p}}$ (Iori et al. 2006; Snell et al., 2000).

The Polytechnical group in St. Petersburg has recently developed very compact ''standard'' Mott polarimeters with concentric spherical accelerating electrodes and a target potential of 40 kV (Petrov et al., 2007; Petrov et al., 2003). (''Standard,'' in this context, means that the electrons are not decelerated to ground potential before detection.) Using small

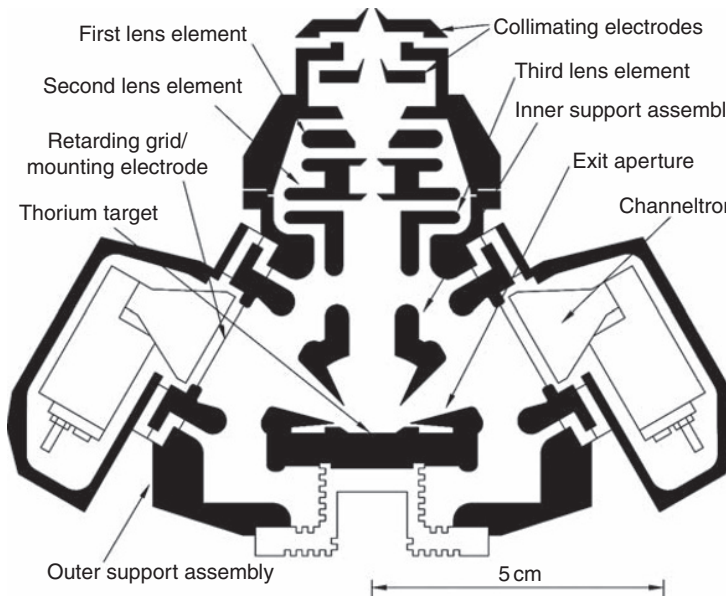


**FIGURE 37** ''Micro-Mott'' polarimeter. Reprinted with permission from Neufeld et al. (2007), *Review of Scientific Instruments, 78*, 025107. Copyright 2007, American Institute of Physics

scintillators and miniaturized photomultiplier tubes, these devices can be mounted on a 6″ Conflat® flange. In addition to their compactness, they have the highest $F_p$ yet reported for a Mott scattering analyzer, $6 \times 10^{-4}$, and have maximum counting rates as high as 2 MHz.

A significant advantage of high-voltage Mott analyzers over low-incident-electron-energy (<1keV) polarimeters based on magnetic exchange scattering, diffraction, or Mott scattering (Gay, 1996) is that $S_{eff}$ is relatively insensitive to target surface conditions, eliminating the need for UHV conditions. Such polarimeters are typically not used in gas-phase experiments. Having said this, low-energy devices have very high figures of merit, often approaching $10^{-2}$. The interested reader is referred to the reviews listed above, as well as papers describing recent developments by Bertacco et al. (2002), Hillebrecht et al. (2002), Klebanoff et al. (1993), Seddon et al. (1999), Winkelmann et al. (2008), and references therein. In this context, we note that all of the methods discussed in Section 5.1.3.3 can, in principle, be used for electron polarimetry. Indeed, iron–gold spin filters were originally proposed and demonstrated as such. Unfortunately, because of their low transmission at energies where $\mathcal{A}$ is significant, these devices are limited to low values of $F_{\mathrm{p}}$. None of the other technologies discussed above seem practicable for polarimetry in the immediate future.

To determine $P_e$, we have assumed in the above discussion that $S_{\mathrm{eff}}$ was a known quantity. Ultimately, since it cannot easily be calculated, $S_{\mathrm{eff}}$ must be measured or determined through a calibration procedure. This can be accomplished in one of several ways.

(1) *Calibration with electrons of known polarization*. Using electrons of known polarization, the measurement of $A$ determines $S_{\mathrm{eff}}$ (Equation (22)). The incident electron polarization can be determined, for example, by chemi-ionization of metastable He whose polarization is known in turn by passage through a transverse Stern–Gerlach magnet (Oro et al., 1991). Other techniques involve the use of optical polarimetry (see below; Fischer & Kessler, 1995; Gay et al., 1996a,b; Humphrey et al., 1992; Trantham et al., 1996), or the use of a ''standard'' photocathode material whose polarization is well known and repeatable (Mulhollan et al., 1996).

(2) *Double scattering experiments*. One can measure directly $S_{\mathrm{eff}}$ by performing a double scattering experiment in which an unpolarized electron beam is first polarized by Mott scattering, and the scattered (polarized) beam is subsequently analyzed by an *equivalent* Mott scattering. Following the first target, the secondary beam's polarization is $P_{\mathrm{scat}} = S_{\mathrm{eff}}(E, \Delta E, \theta, \Delta\Omega)$, and the scattering asymmetry following the second target is given by Equation (22), so that $A = S^2{}_{\mathrm{eff}}$. This is, of course, the method proposed by Mott in the first place to identify

the existence of free electron polarization. The equivalence of both scattering events in principle requires that $E$, $\Delta E$, $\theta$, and $\Delta\Omega$ be the same for both targets. In practice, and especially at high incident energies, these requirements can be relaxed. Such measurements are difficult. They have most recently been made in a series of careful experiments by Gellrich and Kessler (1991) who were able to determine $S_{\text{eff}}$ to 0.3% at $E = 50$ and 120 keV, which represents the best accuracy achieved to date in such a measurement. While the equivalence of $\Delta E$ (and hence $E$) and $\Delta\Omega$ were not ensured in this work, it is unlikely that this provides a systematic uncertainty greater than that quoted.

A similar technique, proposed by Hopster and Abraham (1988), involves the scattering of a transversely polarized primary electron beam from a first target in a plane perpendicular to the polarization direction, followed by a Mott analysis with a second target whose value of $S_{\text{eff}}$ is to be determined. By measuring three Mott asymmetries from the second target with (a) the primary unscattered beam, (b) the scattered beam from the first target with primary beam polarization spin-up, and (c) the same as (b) but with spin-down, one can combine these to yield the $S_{\text{eff}}$ for the second target. Mayer et al. (1993), however, have shown that this method must be used with care to avoid the effects of depolarization of the primary beam in the first target. This can be accomplished by using a thin first target, in which depolarizing processes are negligible, or by measuring the Mott asymmetry from the first target directly, and combining this measurement with the three asymmetries listed above.

(3) *Single-scattering extrapolation procedures*. The values of $S$ and $S_{\text{eff}}$ differ to the extent that single-scattering Mott measurements fail to ensure elastic, single scattering conditions. As one approaches this limit, the Mott asymmetry becomes related directly to $P_e$ by the calculated value of $S$, the most modern values of which are expected to be known to better than 0.5% (Ross & Fink, 1988). Historically, this limit has been approached by extrapolation of $A$ to a scattering foil thickness of zero (Gay & Dunning, 1992). The type of parent function to use for an extrapolation fit has proved controversial, but for sufficiently thin target foils, all physically justifiable forms converge to a simple linear function. With standard Mott polarimeters in which electrons are detected at their scattering energy minus any energy loss they may suffer in the target, elastic scattering conditions are not rigorously ensured, although the use of silicon surface barrier detectors do offer a crude level of energy-loss discrimination.

With the advent of retarding-field polarimeters, however, complete energy discrimination is possible. Setting $\Delta E = 0$ with the retarding field

ensures that only elastic scattering events are detected. This has led some researchers to argue that the true Sherman function can be reached by energy extrapolation alone, even with a thick target. The situation is more complicated than this, however, as is illustrated in Figure 38 (Gay et al., 1992). The loss of analyzing power is seen to be reduced with increasing foil thickness at all values of $\Delta E$, with the ''true'' analyzing power (Corresponding to $S_{\text{eff}} = S$) being reached only by combining both $\Delta E$ and foil-thickness extrapolations. The reason for this is that even when inelastic multiple scattering has been eliminated by energy-loss discrimination, elastic plural scattering, which is much more depolarizing than multiple scattering, occurs with a significant probability (Gay et al., 1992; Mayer et al., 1993). Thus, for the most accurate single-scattering Mott polarimetry, a retarding-field Mott polarimeter operating at target voltages above 100 kV (to minimize the consequences of multiple and plural scattering), with the capability to handle several foils of variable thickness, is

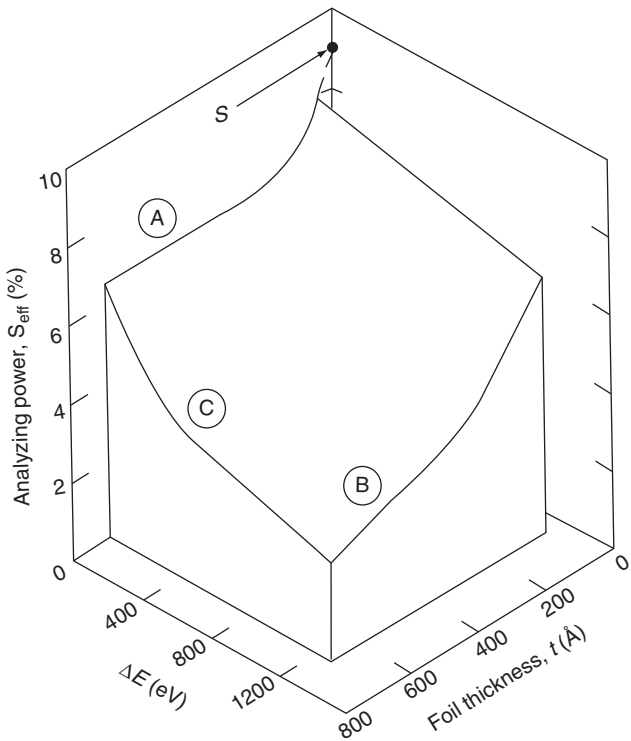


**FIGURE 38** Schematic representation of the effective Sherman function, in the ($\Delta E$,$t$) plane at 20 keV (see text; Gay et al., 1992)

recommended. Using this technique, Gay et al. (1992) were able to measure electron polarization with an extrapolation precision of 0.8%. More recently, Khakoo et al. (2001) and Qiao and Kakizaki (1997) have used Monte Carlo techniques to study in more detail the depolarizing influences on Mott-scattered electrons in foil targets. These studies offer guidance as to the best extrapolation procedures to use and will prove to be invaluable in the design and analysis of the next generation of Mott measurements.

The remaining issue in this case is our knowledge of the Sherman function. In their double-scattering measurements, Gellrich and Kessler (1991) extrapolated their absolutely known effective Sherman functions to zero target thickness. These results thus represent a direct experimental check on the theoretically calculated values of $S$. Their agreement with the most recent calculations—those of Bühring (1984) and Ross and Fink (1988)—is reasonable, but not perfect, indicating the probability of hidden systematic errors in either the experiment or the calculations at a low level.

### 5.2.2. Optical Polarimetry

Optical electron polarimetry involves the measurement of fluorescent polarization in atomic transitions excited by the electrons whose polarization is to be measured. It was first proposed formally by Farago and Wykes (1969) and Wykes (1971), but was not realized experimentally until 1980, with Zn targets (Eminyan & Lampel, 1980). More recently, it was pointed out by Gay and coworkers (Furst et al., 1993; Gay, 1983) that noble gases could be used as polarimetric targets, with a significant reduction in experimental difficulty. In optical polarimetry, polarized electrons excite an atomic target by exchange, and the subsequent atomic electron polarization is converted into electronic orbital orientation by the atom's internal spin–orbit coupling (see Section 3.1.2 above). The fluorescence from the excited state is subsequently circularly polarized. If the fluorescence transition is between two well-$LS$-coupled states, one can ''kinematically'' (i.e., with angular-momentum coupling algebra requiring no dynamical calculation) relate $P_3$ to $P_e$:

$$P_e = \frac{P_3}{\gamma(1+\beta P_1)} = \mathcal{A}^{-1} P_3 \tag{24}$$

where $\gamma$ and $\beta$ are constants depending upon the atomic transition and the detection geometry, and $P_1$ is the linear polarization of the light. We can thus regard the denominator of Equation (24) as the polarimeter's analyzing power.

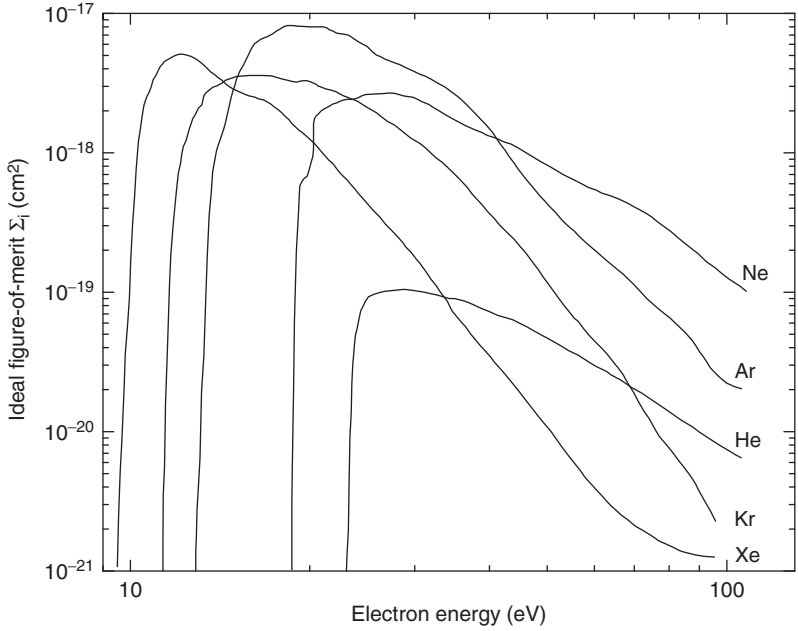


**FIGURE 39** ''Ideal'' figures of merit for the polarimetric transitions in the heavy noble gases, being equal to the transition excitation cross section times the square of the analyzing power (Gay et al., 1996a,b). For each gas, the $np^5(n+1)p\,^3D_3 \rightarrow np^5(n+1)s\,^3P_2$ transition is used for polarimetry

By measuring the complete set of Stokes parameters for the atomic fluorescence, one measures the polarization of the electrons ($P_3$), determines the analyzing power ($P_1$), and determines the validity of the polarimetric equation ($P_2$), because $P_2$ must be zero if $LS$-coupling holds for the transition being monitored. As such, the method is absolute, self-calibrating, and self-checking.

Electron polarimeters are easy to build and do not require high voltages to operate (Gay, Furst, et al., 1996a,b; Humphrey et al., 1992; Trantham et al., 1996). Their analyzing power ($\sim$ 0.5–0.7) is generally much greater than $S_{\text{eff}}$ for Mott polarimeters. They do, however, produce a significant gas load and are much less efficient than Mott polarimeters. This poor efficiency is due primarily to the requirement that for an absolute measurement, the incident electron energy must be kept below the first cascading threshold of the transition in question. For the noble gases, this means that electron energies cannot be more than about 1.1 eV above the excitation threshold (in the best case of Ne), so that the excitation cross sections are quite low. However, one can make an absolute measurement of $P_e$ at an energy just below the first cascading threshold, and then use this measurement to calibrate the polarimeter at a higher

energy where the optical excitation cross section for the polarimetric transition is a maximum. The ''ideal'' figures of merit for the noble gases, being equal to the square of their analyzing power times the relevant optical excitation cross section, are shown in Figure 39.

While the theoretical absolute accuracy of such devices is attractive, the realizable experimental accuracy has not yet been demonstrated to be much better than 5% (Fischer & Kessler, 1995; Gay, Furst, et al., 1996a,b). This may be due, at least in part, to the fact that the analyzing power of optical polarimeters depends on the alignment of the excited target, which in turn depends on the incident electron energy. It is the measurement of the linear polarization fraction $P_1$ that determines the degree of alignment. Thus if the beam of electrons whose polarization is to be determined has an energy spread across which the polarization varies, one would expect that the value of $P_3$ is not related linearly to the ensemble average of the electron beam polarization (Drouhin et al., 1985). It is not expected, however, that heavily cesiated bulk GaAs will exhibit significant variation in the polarization of its photoemitted electrons across its $\sim$0.3 eV energy spread (G. Lampel, private communication). Such issues remain to be studied in detail. Having said this, the statistical precision of optical polarimeters has been demonstrated by Trantham et al. (1996) to be better than 1% for a neon target, which makes optical polarimetry competitive with single-scattering Mott measurements when foil extrapolations must be performed. At present, optical polarimeters are most useful in situations where a reasonably accurate measurement of a primary beam polarization is needed without the necessity of resorting to extensive calibration procedures or double scattering experiments.

## ACKNOWLEDGMENTS

This work was supported by the Atomic, Molecular, Optical, and Plasma Physics Program of the U.S. National Science Foundation. The author would like to thank D. H. Madison, H. Batelaan, P. D. Burrow, I. I. Fabrikant, G. A. Gallup, G. F. Hanne, M. S. Lubell, J. W. Maseberg, W. Moss, and C. K. Sinclair for many useful discussions, and C. C. Lin for his encouragement and support. J. R. Machacek and T. Struble prepared most of the figures; J. Claes provided help with the reference organization.

## REFERENCES

Ait-Tahar, S., Grant, I. P., & Norrington, P. H. (1997). Dirac *R*-matrix modeling of spin-induced asymmetry in the scattering of polarized electrons from polarized cesium atoms. *Physical Review Letters*, *79*, 2955.

Al-Khateeb, H. M., Birdsey, B. G., Bowen, T. C., Green, A. S., Johnston, M. E., & Gay, T. J. (1999). A simple GaAs polarized electron source. *Rev. Sci. Instrum.*, *70*, 3882.

Al-Khateeb, H. M., Birdsey, B. G., & Gay, T. J. (2000). Angular momentum partitioning and hexacontatetrapole moments in impulsively-excited argon ions. *Physical Review Letters*, *85*, 4040.

Al-Khateeb, H. M., Birdsey, B. G., & Gay, T. J. (2005). Angular momentum partitioning and the subshell multipole moments in impulsively excited argon ions. *Physical Review A*, *71*, 032707.

Alle, D. T., Brennan, M. J., & Buckman, S. J. (1996). Low energy total electron scattering cross section and electron affinity for NO. *Journal of Physics B*, *29*, L277.

Anderson, N., & Bartschat, K. (1994). Generalized Stokes parameter approach for analysis of perfect scattering experiments on impact excitation by spin-polarized particles. *Journal of Physics B*, *27*, 3189.

Anderson, N., & Bartschat, K. (2001). *Polarization, alignment, and orientation in atomic collisions*. Berlin: Springer.

Anderson, N., & Bartschat, K. (2002). Search for relativistic effects in electron-impact S → P excitation of heavy alkali atoms: Polarization, alignment and orientation in Cs. *Journal of Physics B*, *35*, 4507.

Andersen, N., Bartschat, K., Broad, J. T., & Hertel, I. V. (1997). Collisional alignment and orientation of atomic outer shells. III. Spin-resolved excitation. *Physics Reports*, *279*, 251.

Arianer, J., Cohen, S., Essabaa, S., Frascaria, R., & Zerhouni, O. (1996). A flowing afterglow as a polarized electron source. *Nuclear Instruments and Methods in Physics Research Section A*, *382*, 371.

Außendorf, G., Jüttemann, F., Muktavat, K., Sharma, L., Srivastava, R., Stauffer, A. D., Bartschat, K., Fursa, D. V., Bray, I., & Hanne, G. F. (2006a). (e, e$\gamma$)-coincidence studies to determine spin-resolved Stokes parameters of the 185 nm emission line in mercury. *Journal of Physics B*, *39*, 2403.

Außendorf, G., Jüttemann, F., Muktavat, K., Sharma, L., Srivastava, R., Stauffer, A. D., Bartschat, K., Fursa, D. V., Bray, I., & Hanne, G. F. (2006b). Total polarization of the 185 nm emission line of mercury excited by electron impact. *Journal of Physics B*, *39*, 4435.

Bahrim, C., Thumm, U., & Fabrikant, I. I. (2001). Negative-ion resonances in cross sections for slow-electron–heavy-alkali-metal-atom scattering. *Physical Review A*, *63*, 042710.

Barnes, J., Mei, L., Lairson, B. M., & Dunning, F. B. (1999). Implementation of scanning electron microscopy with polarization analysis using high-efficiency retarding-potential Mott polarimeters. *The Review of Scientific Instruments*, *70*, 246.

Bartsch, M., Geesmann, H., Hanne, G. F., & Kessler, J. (1992). Asymmetric scattering of polarized electrons from atoms with closed and open shells. *Journal of Physics B*, *25*, 1511.

Bartschat, K. (1993). Low-energy electron scattering from caesium atoms—comparison of a semirelativistic Breit-Pauli and a full relativistic Dirac treatment. *Journal of Physics B*, *26*, 3595.

Bartschat, K. (1995). Electron scattering form laser-excited chromium atoms. *Journal of Physics B*, *28*, 879.

Bartschat, K., & Blum, K. (1982). Theory and physical importance of integrated state multipoles. *Zeitschrift für Physik. A, Atomic Nuclei*, *304*, 85.

Bartschat, K., & Bray, I. (1996). Calculation of electron-Cs scattering at intermediate energies. *Physical Review A*, *54*, 1723.

Barwick, B., Corder, C., Strohaber, J., Chandler-Smith, N., Uiterwaal, C., & Batelaan, H. (2007). Laser-induced ultrafast electron emission from a field emission tip. *New Journal of Physics*, *9*, 142.

Batelaan, H., & Gay, T. J. (1998). A Reply to the Comment by George H. Rutherford and Rainer Grobe. *Physical Review Letters*, *81*, 4773.

Batelaan, H., Gay, T. J., & Schwendiman, J. J. (1997). Stern-Gerlach effect for electron beams. *Physical Review Letters*, *79*, 4517.

Batelaan, H., Green, A. S., Hitt, B. A., & Gay, T. J. (1999). Optically pumped electron spin filter. *Physical Review Letters*, *82*, 4612.

Baum, G., Förster, S., Pavlović, N., Roth, B., Bartschat, K., & Bray, I. (2004). Angle-differential cross sections and spin-asymmetry parameters for spin-polarized electron-impact excitation of spin-polarized cesium atoms. *Physical Review A*, *70*, 012707.

Baum, G., Granitza, B., Grau, L., Leuer, B., Raith, W., Rott, K., Tondera, M., & Witthuhn, B. (1993). Spin asymmetry in electron impact ionization of caesium. *Journal of Physics B*, *26*, 331.

Baum, G., Pavlović, N., Roth, B., Bartschat, K., Fang, Y., & Bray, I. (2002). Detailed experimentation and theoretical study of elastic scattering at intermediate energies in the electron–cesium system. *Physical Review A*, *66*, 022705.

Baum, G., Raith, W., Roth, B., Tondera, M., Bartschat, K., Bray, I., Ait-Tahar, S., Grant, I. P., & Norrington, P. H. (1999). Spin asymmetries in low-energy electron scattering from cesium atoms. *Physical Review Letters*, *82*, 1128.

Beerlage, M. J. M., Farago, P. S., & Van der Wiel, M. J. (1981). A search for spin effects in low-energy electron scattering from optically active camphor. *Journal of Physics B*, *14*, 3245.

Bellm, S., Lower, J., McEachran, R. P., Wiegold, E., Ryan-Anderson, C., & Madison, D. H. (2008a). Spin- and fine-structure-resolved ionization of krypton. *Physical Review A*, *78*, 062707.

Bellm, S., Lower, J., Stegen, Z., Madison, D. H., & Saha, H. P. (2008b). Investigating many-electron exchange effects in electron–heavy-atom scattering. *Physical Review A*, *77*, 032722.

Bertacco, R., Marcon, M., Duò, L., & Ciccacci, F. (2002). Spin and energy analysis of electron beams: Coupling a polarimeter based on exchange scattering to a hemispherical analyzer. *The Review of Scientific Instruments*, *73*, 1.

Besch, K. H., Sauter, M., & Nakel, W. (1998). Fine-structure effect in the relativistic (*e*, 2*e*) process. *Physical Review A*, *58*, R2638.

Bhat, R. D. R., Nemec, P., Kerachian, Y., van Driel, H. M., Sipe, J. E., & Smirl, A. L. (2005). Two-photon spin injection in semiconductors. *Physical Review B*, *71*, 035209.

Birdsey, B. G. (2003). *Ph.D. thesis*. University of Nebraska Available from T. J. Gay, Angular momentum partitioning in the impulsive excitation of the intermediately-coupled $4p^5 5p$ manifold of krypton.

Birdsey, B. G., Al-Khateeb, H. M., Johnston, M. E., Bowen, T. C., Gay, T. J., Zeman, V., & Bartschat, K. (1999). Near-threshold measurement of integrated Stokes parameters for Kr excited by polarized electrons. *Physical Review A*, *60*, 1046.

Bloch, F. (1953). Experiments on the g-factor of the electron. *Physica*, *19*, 821.

Blum, K. (1996). Chiral effects in elastic electron–molecule collisions. *Density matrix theory and applications*. New York: Plenum.

Blum, K., & Thompson, D. G. (1997). Chiral effects in electron scattering by molecules. *Advances in Atomic, Molecular and Optical Physics*, *38*, 39.

Bouchene, M. A., Zamith, S., & Girard, B. (2001). Spin-polarized electrons produced by a sequence of two femtosecond pulses. Calculation of differential and global polarization rates. *Journal of Physics B*, *34*, 1497.

Bray, I., Beck, J., & Plottke, C. (1999). Spin-resolved electron-impact ionization of lithium. *Journal of Physics B*, *32*, 4309.

Bray, I., & McCarthy, I. E. (1993). Spin-dependent observables in electron–sodium scattering calculated using the coupled-channel optical method. *Physical Review A*, *47*, 317.

Brillouin, L. (1928). Is it possible to test by a direct experiment the hypothesis of the spinning electron? *Proceedings of the National Academy of Sciences of the United States of America*, *14*, 755.

Bryl, R., & Altman, M. S. (2003). Spin-polarized vacuum tunneling in field emission from Co-coated W(111) tips. *Journal of Applied Physics*, *94*, 4670.

Bühring, W. (1984). An approximate phase shift formula applied to elastic scattering of electrons by mercury atoms. *Zeitschrift für Physik. A, Atomic nuclei*, *317*, 241.

Bukhari, M. A. H., Beyer, H. J., Chaudhry, M. A., Campbell, D. M., Duncan, A. J., & Kleinpoppen, H. (1995). Excitation of spin-polarized sodium and potassium atoms by electron impact. *Journal of Physics B*, *28*, 1889 and references therein.

Burke, P. G., & Joachain, C. J. (Eds.), (1997). *Photon and electron collisions with atoms and molecules*. New York: Plenum.

Burke, P. G., & Mitchell, J. F. B. (1974). Spin-polarization in the elastic scattering of electrons by one-electron atoms. *Journal of Physics B*, *7*, 214.

Cacho, C., Lassailly, Y., Drouhin, H. J., Lampel, G., & Peretti, J. (2002). Spin filtering of free electrons by magnetic multilayers: towards an efficient self-calibrated spin polarimeter. *Physical Review Letters*, *88*, 066601.

Campbell, D. M., & Farago, P. S. (1985). Spin-dependent electron scattering from optically active molecules. *Nature*, *258*, 419.

Campbell, D. M., & Farago, P. S. (1987). Electron optic dichroism in camphor. *Journal of Physics B*, *20*, 5133.

Campbell, D. M., & Kleinpoppen, H. (Eds.), (1996). *Selected topics on electron physics*. New York: Plenum.

Compton, R. N., & Pagni, R. M. (2002). The chirality of biomolecules. *Advances in Atomic, Molecular and Optical Physics*, *48*, 219.

da Paixão, F. J., Lima, M. A. P., & McKoy, V. (1992). Spin exchange in elastic $e$–$O_2$ collisions. *Physical Review Letters*, *68*, 1698.

da Paixão, F. J., Lima, M. A. P., & McKoy, V. (1996). Elastic $e$-NO collisions. *Physical Review A*, *53*, 1400.

Dehmelt, H. (1988). New continuous Stern-Gerlach effect and a hint of ''the'' elementary particle. *Z Phys. D*, *10*, 127.

Dehmelt, H. (1990). Experiments on the structure of an individual elementary particle. *Science*, *247*, 539.

Dorn, A., Elliott, A., Guo, X., Hurn, J., Lower, J., Mazevet, S., McCarthy, I. E., Shen, Y., & Wiegold, E. (1997). ($e$, 2$e$) collisons on xenon with spin-polarized electrons. *Journal of Physics B*, *30*, 4097.

Drouhin, H. J., Hermann, C., & Lampel, G. (1985). Photoemission from activated gallium arsenide II: Spin polarization versus kinetic energy analysis. *Physical Review B*, *31*, 3872.

Dümmler, M., Bartsch, M., Geesmann, H., Hanne, G. F., & Kessler, J. (1992). Low-energy data of the Sherman function of Hg, Tl and Pb. *J. Phys. B*, *25*, 4281.

Dümmler, M., Hanne, G. F., & Kessler, J. (1995). Left–right asymmetries in elastic and inelastic scattering of polarized electrons from argon, krypton and xenon atoms. *Journal of Physics B*, *28*, 2985.

Dunning, F. B. (1994). Mott electron polarimetry. *Nuclear Instruments and Methods in Physics Research Section A*, *347*, 152.

Dunning, F. B., Gray, L. G., Ratliff, J. M., Tang, F. C., Zhang, X., & Walters, G. K. (1987). Simple and compact low-energy Mott polarization analyzer. *The Review of Scientific Instruments*, *58*, 1706.

Dunning, F. B., & Hulet, R. G. (Eds.), (1996). *Experimental methods in the physical sciences—Atomic, molecular, and optical physics: Atoms and molecules*, *V*. *29A and 29B*. San Diego: Academic Press.

Eminyan, M., & Lampel, G. (1980). Optical measurement of free-electron polarization. *Physical Review Letters*, *45*, 1171.

Eschen, F., Hanne, G. F., Jost, K., & Kessler, J. (1989). Determination of the light polarisation for the optical transitions $8^2S_{1/2}$–$6^2P_{1/2,3/2}$ and $6^2P_{3/2}$–$6^2S_{1/2}$ in caesium after impact excitation by polarised electrons. *Journal of Physics B*, *22*, L455.

Fabrikant, I. I. (2009). *Private communication*.

Fandreyer, R., Thompson, D., & Blum, K. (1990). Attenuation of longitudinally polarized electron beams by chiral molecules. *J. Phys. B*, *23*, 3031.

Farago, P. S. (1980). Spin-dependent features of electron scattering from optically active molecules. *Journal of Physics B*, *13*, L567.

Farago, P. S. (1981). Electron optic dichroism and electron optic activity. *Journal of Physics B*, *14*, L743.

Farago, P. S., & Wykes, J. S. (1969). Optical detection of electron polarization. *Journal of Physics B*, *2*, 747.

Feder, R. (Ed.), (1985). *Polarized electrons in surface physics*. Singapore: World Scientific.
Feigerle, C. S., Pierce, D. T., Seiler, A., & Celotta, R. J. (1984). An intense source of monochromatic electrons: photoemission from GaAs. *Applied Physics Letters*, *44*, 866.
Fischer, T., & Kessler, J. (1995). Experimental comparison of a helium electron polarimeter with a calibrated high-precision Mott detector. *The Review of Scientific Instruments*, *66*, 4885.
Fisher, G. P. (1971). The electric dipole moment of a moving magnetic dipole. *American Journal of Physics*, *39*, 1528.
Fullerton, C. M., Wöste, G., Thompson, D. G., Blum, K., & Noble, C. J. (1994). Exchange processes in the scattering of polarized electrons by oxygen molecules. *J. Phys. B*, *27*, 185.
Furst, J. E., Gay, T. J., Wijayaratna, W. M. K. P., Bartschat, K., Geesmann, H., Khakoo, M. A., & Madison, D. H. (1992). An attempt to observe Mott scattering optically. *Journal of Physics B*, *25*, 1089.
Furst, J. E., Wijayaratna, W. M. K. P., Madison, D. H., & Gay, T. J. (1993). Investigation of spin-orbit effects in the excitation of noble gases by spin-polarized electrons. *Physical Review A*, *47*, 3775.
Gallup, G. A. (1994). In H. Erhardt & L. A. Morgan (Eds.), *Electron collisions with molecules, clusters, and surfaces*. New York: Plenum.
Gallup, G. A., Batelaan, H., & Gay, T. J. (2001). Quantum-mechanical analysis of a longitudinal Stern-Gerlach effect. *Physical Review Letters*, *86*, 4508.
Gao, S., Zhou, G., Wu, J., Duan, W., & Gu, B. L. (2004). Spin-polarized electron emitter: Mn-doped GaN nanotubes and their arrays. *Physical Review B*, *69*, 113403.
Gay, T. J. (1983). A simple optical electron polarimeter. *Journal of Physics B*, *16*, L533.
Gay, T. J. (1996). In F. B. Dunning & R. G. Hulet (Eds.), *Atomic, molecular, and optical physics: Atoms and molecules—Experimental methods in the physical sciences, 29A*. San Diego: Academic Press.
Gay, T. J., Khakoo, M. A., Brand, J. A., Furst, J. E., Meyer, W. V., Wijayaratna, W. M. K. P., & Dunning, F. B. (1992). Extrapolation procedures in Mott scattering electron polarimetry. *Rev. Sci. Instrum.*, *63*, 114.
Gay, T. J., & Dunning, F. B. (1992). Mott electron polarimetry. *The Review of Scientific Instruments*, *63*, 1635.
Gay, T. J., Furst, J. E., Trantham, K. W., & Wijayaratna, W. M. K. P. (1996a). Optical electron polarimetry with heavy noble gases. *Physical Review A*, *53*, 1623.
Gay, T. J., Johnston, M. E., Trantham, K. W., & Gallup, G. A. (1996b). In D. M. Campbell & H. Kleinpoppen (Eds.), *Selected topics in electron physics*. New York: Plenum.
Gehenn, W., & Reichert, E. (1977). Scattering of electrons by Cs atoms at low energies. *Journal of Physics B*, *10*, 3105.
Gellrich, A., & Kessler, J. (1991). Precision measurement of the Sherman asymmetry function for electron scattering from gold. *Physical Review A*, *43*, 204.
Gidley, D. W., Rich, A., Van House, J., & Zitzewitz, P. W. (1982). $\beta$-decay and the origins of biological chirality: experimental results. *Nature*, *297*, 639.
Guinea, W. E., Hanne, G. F., Went, M. R., Daniell, M. L., Stevenson, M. A., Bartschat, K., Payne, D., MacGillivray, W. R., & Lohmann, B. (2005). Spin asymmetries in elastic and inelastic scattering from rubidium. *Journal of Physics B*, *38*, 3359.
Green, A. S., Gallup, G. A., Rosenberry, M. A., & Gay, T. J. (2004). Spin-exchange-induced circularly polarized molecular fluorescence. *Physical Review Letters*, *92*, 093201.
Groebli, J. C., Oberli, D., Meier, F., Dommann, A., Mamaev, Yu. A., Subashiev, A., & Yashin, Y. u. (1995). Polarization resonances of optically spin-oriented photoelectrons emitted from strained semiconductor photocathodes. *Physical Review Letters*, *74*, 2106.
Guo, X., Hurn, J. M., Lower, J., Mazevet, S., Shen, Y., Wiegold, E., Granitza, B., & McCarthy, I. E. (1996). Fine structure effect in electron impact ionization. *Physical Review Letters*, *76*, 1228.
Guo, X. Q., & Lubell, M. S. (1993). Energy dependence of the spin asymmetry for electron impact ionization of atomic hydrogen and its implication for the Wannier theory of double escape. *Journal of Physics B*, *26*, 1221.

Hanne, G. F. (1983). Spin effects in inelastic electron–atom collisions. *Physics Reports*, *95*, 95.
Hanne, G. F. (1997). In P. G. Burke & C. J. Joachain (Eds.), *Photon and electron collisions with atoms and molecules*. New York: Plenum.
Hanne, G. F. (1998). In K. Becker (Ed.), *Novel aspects of electron-molecule collisions*. Singapore: World Scientific.
Hanne, G. F. (2004). Private communication. This discussion benefits from early suggestions and analysis made by Prof. Hanne along these lines.
Hanne, G. F., McClelland, J. J., Scholten, R. E., & Celotta, R. J. (1993). Spin-resolved superelastic electron scattering from laser-excited chromium atoms. *Journal of Physics B*, *26*, L753.
Hayashi, S. (1988). Asymmetry in elastic scattering of polarized electrons by optically active molecules. *J. Phys. B*, *21*, 1037.
Hayes, P. A., Yu, D. H., Furst, J. E., Donath, M., & Williams, J. F. (1996). Excitation of He $3^3$P and Ne 3p states by polarized electrons. *Journal of Physics B*, *29*, 3989.
Hayes, P. A., Yu, D. H., & Williams, J. F. (1997). Computer stabilized spin polarized electron source. *Rev. Sci. Instrum.*, *68*, 1708.
Hayes, P. A., Yu, D. H., & Williams, J. F. (1998). Electron correlation and spin dependence in simultaneous ionization and excitation collision. *Journal of Physics B*, *31*, L193.
Hegemann, T., Oberste-Vorth, M., Vogts, R., & Hanne, G. F. (1991). Study of exchange in collisions of polarized electrons with atoms and molecules. *Physical Review Letters*, *66*, 2968.
Hegemann, T., Schroll, S., & Hanne, G. F. (1993). Observation of exchange in collisions of polarized electrons with atoms and molecules. *Journal of Physics B*, *26*, 4607.
Hegstrom, R. A. (1982). $\beta$-decay and the origins of biological chirality: Theoretical results. *Nature*, *297*, 643.
Herting, C., Hanne, G. F., Bartschat, K., Grum-Grzhimailo, A. N., Muktavat, K., Srivastava, R., & Stauffer, A. D. (2002). Orientation propensities in spin-resolved electron impact excitation of mercury. *Journal of Physics B*, *35*, 4439.
Herting, C., Hanne, G. F., Bartschat, K., Muktavat, K., Srivastava, R., & Stauffer, A. D. (2003). Validation of orientation propensities in electron-impact excitation of lead. *Journal of Physics B*, *36*, 3877.
Herzberg, G. (1950). *Spectra of diatomic molecules*. Princeton: Van Nostrand.
Hilgner, W., & Kessler, J. (1969). Zur Spinpolarisation langsamer Elektronen nach der Streuung an Molekülen. *Zeitschrift für Physik*, *221*, 305.
Hilgner, W., Kessler, J., & Streeb, E. (1969). Zur Spinpolarisation langsamer Elektronen nach der Streuung an Molekülen. *Zeitschrift für Physik*, *221*, 324.
Hillebrecht, F. U., Jungblut, R. M., Wiebusch, L., Roth, C. H., Rose, H. B., Knabben, D., Bethke, C., Weber, N. B., Manderia, S. t., Rosowski, U., & Kisker, E. (2002). High-efficiency spin polarimetry by very-low-energy electron scattering from Fe(100) for spin-resolved photoemission. *The Review of Scientific Instruments*, *73*, 1229.
Hommelhoff, P., Sortais, Y., Aghajani-Talesh, A., & Kasevich, M. A. (2006). Field emission tip as a nanometer source of free electron femtosecond pulses. *Physical Review Letters*, *96*, 077401.
Hopster, H., & Abraham, D. L. (1988). New method for accurate calibration of electron-spin polarimeters. *The Review of Scientific Instruments*, *64*, 957.
Huang, D. J., Lee, J. Y., Suen, J. S., Mulhollan, G. A., Andrews, A. B., & Erskine, J. L. (1993). Adapting a compact Mott spin polarimeter to a large commercial electron energy analyzer for spin-polarized electron spectroscopy. *The Review of Scientific Instruments*, *64*, 3474.
Humphrey, I., Ranganathaiah, C., Robins, J. L., Williams, J. F., Anderson, R. A., & Macklin, W. C. (1992). Mott and helium polarimetry of a spin-polarized electron source. *Measurement Science & Technology*, *3*, 884.
Imai, K., Murakami, T., Saito, N., & Tanida, K. (Eds.), (2007). *Proceedings of the 17th international spin physics symposium. AIP conference proceedings,* Vol. 915. New York: AIP.
Iori, K., Miyamoto, K., Narita, H., Sakamoto, K., Kimura, A., Qiao, S., Shimada, K., Namatame, H., & Taniguchi, M. (2006). The self-calibration of a retarding-type Mott

spin polarimeter with a large collection angle; electron spin detector for spin-resolved x-ray photoelectron spectroscopy. *The Review of Scientific Instruments*, *77*, 013101.

Jin, X., Yamamoto, N., Nakagawa, Y., Mano, A., Kato, T., Tanioku, M., Ujihara, T., Takeda, Y., Okumi, S., Yamamoto, M., Nakanishi, T., Saka, T., Horinaka, H., Kato, T., Yasue, T., and Koshikawa, T. (2008). Super-high brightness and high-spin-polarization photocathode. *Applied Physics Express, 1*, 045002; see also Yamamoto, N., Nakanishi, T., Mano, A., Nakagawa, Y., Okumi, S., Yamamoto, M., Konomi, T., Jin, X., Ujihara, T., Takeda, Y., Ohshima, T., Saka, T., Kato, T., Horinaka, H., Yasue, T., Koshikawa, T., and Kuwahara, M. (2008). High brightness and high polarization electron source using transmission photocathode with GaAs-GaAsP superlattice layer. *Journal of Applied Physics, 103*, 064905; Jin, X. G., Maeda, Y., Saka, T., Tanioku, M., Fuchi, S., Ujihara, T., Takeda, Y., Yamamoto, M., Nakanishi, T., Horinaka, H., Kato, T., Yasue, T., and Koshikawa, T. (2008). Highly spin-polarized electron photocathode based on GaAs-GaAsP superlattice grown on mosaic-structured buffer layer. *Journal of Crystal Growth, 310*, 5039.

Jones, S., Madison, D. H., & Hanne, G. F. (1994). Spin-resolved (*e*, 2*e*) coincidences for heavy rare-gas targets. *Physical Review Letters*, *72*, 2554.

Kedzierski, W., Abdellatif, A., McConkey, J. W., Bartschat, K., Fursa, D. V., & Bray, I. (2001). Polarization of Balmer-alpha radiation following electron impact on atomic hydrogen. *Journal of Physics B*, *34*, 3367.

Keller, S., Dreizler, R. M., Ancarani, L. U., Ast, H., Walters, H. R. J., & Whelan, C. T. (1999). Interpretation of relativistic (*e*, 2*e*) experiments in coplanar asymmetric geometry: Atomic-number-dependent effects. *Physical Review A*, *59*, 1284.

Kennedy, J. V., Myerscough, V. P., & McDowell, M. R. C. (1977). Electron impact excitation of the resonance transitions of Li, Na and K. *Journal of Physics B*, *10*, 3759.

Kessler, J. (1969). Electron spin polarization by low-energy scattering from unpolarized targets. *Reviews of Modern Physics*, *41*, 3.

Kessler, J. (1982). Polarization components violating reflection symmetry in electron scattering from optically active molecules. *Journal of Physics B*, *15*, L101.

Kessler, J. (1985). *Polarized electrons* (2nd ed.). Berlin: Springer.

Kessler, J. (1991). Electron-polarization phenomena in electron–atom collisions. *Advances in Atomic, Molecular and Optical Physics*, *27*, 81.

Kessler, J., Lorenz, J., Rempp, H., & Bühring, W. (1971). Differentielle Wirkungsquerschnitte und Spinpolarisation für elastische Streuung langsamer Elektronen an $Sb_4$-Molekülen. *Zeitschrift für Physik*, *246*, 348.

Keszthelyi, L. (1995). Origin of the homochirality of biomolecules. *Quarterly Reviews of Biophysics*, *28*, 473.

Khakoo, M. A., Roundy, D., Hicks, C., Margolis, N., Yeung, E., Ross, A. W., & Gay, T. J. (2001). Monte Carlo studies of Mott scattering asymmetries from gold foils. *Physical Review A*, *64*, 052713.

Kirschner, J. (1985). *Polarized electrons at surfaces*. Berlin: Springer.

Kisker, E., Baum, G., Mahan, A. H., Raith, W., & Reihl, B. (1978). Electron field emission from ferromagnetic europium sulfide on tungsten. *Physical Review B*, 2256.

Klebanoff, L. E., Van Campen, D. G., & Pouliot, R. J. (1993). Electron spin detector for spin-resolved x-ray photoelectron spectroscopy. *The Review of Scientific Instruments*, *64*, 2863.

Kleinpoppen, H., & Newell, W. R. (Eds.), (1995). *Polarized electron/polarized photon physics*. New York: Plenum.

Kponou, A., Makdisi, Y., & Zelenski, A. (Eds.), (2008). *Polarized ion sources, targets, and polarimetry—PSTP 2007. AIP conference proceedings,* Vol. 980. New York: AIP.

Kuwahara, M., Nakanishi, T., Okumi, S., Yamamoto, M., Miyamoto, M., Yamamoto, N., Yasui, K., Morino, T., Sakai, R., Tamagaki, N., & Yamaguchi, K. (2006). Field emission of spin-polarized electrons extracted from photoexcited GaAs tip. *Japan Journal of Applied Physics*, *45*, 2645.

Lambropoulos, P. (1973). Spin-orbit coupling and photoelectron polarization in multiple ionization of atoms. *Physical Review Letters*, *30*, 413.

Leuer, B., Baum, G., Grau, L., Niemeyer, R., Raith, W., & Tondera, M. (1995). Measurement of exchange and spin-orbit effects and their interference in elastic e-Cs scattering at 7eV. *Zeitschrift für Physik D*, *33*, 39.

Lorentz, S. R., Scholten, R. E., McClelland, J. J., Kelley, M. H., & Celotta, R. J. (1993). Spin-resolved elastic scattering of electrons from sodium. *Physical Review A*, *47*, 3000.

Louisell, W. H., Pidd, R. W., & Crane, H. R. (1954). An experimental measurement of the gyromagnetic ratio of the free electron. *Physical Review*, *94*, 7.

Lower, J., Wiegold, E., Berakdar, J., & Mazevet, S. (2001a). Magnetic and orbital dichroism in (*e*, 2*e*) ionization of sodium. *Physical Review Letters*, *86*, 624.

Lower, J., Wiegold, E., Berakdar, J., & Mazevet, S. (2001b). Orbital and spin-polarization transfer in ionizing electron–atom collisions. *Physical Review A*, *64*, 042701.

Lubell, M. (1993). Comparative analysis of the threshold behavior of two-electron escape in electron-impact ionization of valence-1 atoms. *Physical Review A*, *47*, R2450.

Luke, T. M. (1986). A correction method for fine-structure calculations. II. Application to neon 3s and 3p excited levels. *Journal of Physics B*, *19*, 843.

Machado, L. E., Ribeiro, E. M. S., Lee, M. T., Fujimoto, M. M., & Brescansin, L. M. (1999). Cross sections and polarization fractions for elastic $e^-$–$O_2$ collisions. *Physical Review A*, *60*, 1199.

Madison, D. H., Kravtsov, V. D., & Mazevet, S. (1998). Role of exchange scattering in spin-dependent (*e*, 2*e*) collisions. *Journal of Physics B*, *31*, L17.

Maseberg, J. W., & Gay, T. J. (2006). Fluorescence polarization of helium negative-ion resonances excited by polarized electron impact. *Journal of Physics B*, *39*, 4861.

Maseberg, J. W., & Gay, T. J. (2009). Spin torque on molecular rotation induced by polarized electrons. *Physical Review A*, *79*, 022705.

Matsuyama, T., Horinaka, H., Wada, K., Kondo, T., Hangyo, M., Nakanishi, T., Okumi, S., & Togawa, K. (2001). Spin-dependent luminescence of highly polarized electrons generated by two-photon absorption in semiconductors. *Japan Journal of Applied Physics*, *40*, L555.

Mauri, D., Scholl, D., Siegmann, H. C., & Kay, E. (1989). Magnetism in very thin films of permalloy measured by spin polarized cascade electrons. *Applied Physics A*, *49*, 439.

Mayer, S., Fischer, T., Blaschke, W., & Kessler, J. (1993). Calibration of a Mott electron polarimeter: Comparison of different methods. *The Review of Scientific Instruments*, *64*, 952.

Mayer, S., & Kessler, J. (1995). Experimental verification of electron optical dichroism. *Physical Review Letters*, *74*, 4803.

Mayer, S., Nolting, C., & Kessler, J. (1996). Electron scattering from chiral molecules. *Journal of Physics B*, *29*, 3497.

McClelland, J. J., Kelley, M. H., & Celotta, R. J. (1989). Superelastic scattering of spin-polarized electrons from sodium. *Physical Review A*, *40*, 2321.

McDaniel, E. W. (1989). In *Atomic collisions—Electron and photon projectiles*. (p. 184). New York: Wiley.

Meier, F., & Pescia, D. (1981). Band structure investigation of gold by spin-polarized photo-emission. *Physical Review Letters*, *47*, 374.

Meintrup, R., Hanne, G. F., & Bartschat, K. (2000). Spin exchange in elastic collision of polarized electrons with manganese atoms. *Journal of Physics B*, *33*, L289.

Mergl, E., Prinz, H. Th., Schroter, C. D., & Nakel, W. (1992). Photon emission asymmetry in the elementary process of bremsstrahlung from transversely polarized electrons. *Physical Review Letters*, *69*, 901.

Mette, C., & Hanne, G. F. (1994). Spin effects in electron-molecule collisons. *Verhandlungen Der Deutschen Physikalischen Gesellschaft (VI)*, 29, 462.

Mette, C., Simon, T., Herting, C., Hanne, G. F., & Madison, D. H. (1998). Spin-resolved triple differential cross sections of xenon. *Journal of Physics B*, *31*, 4689.

Mott, N. F. (1929). The scattering of fast electrons by atomic nuclei. *Proceedings of the Royal Society of London. Series A*, *124*, 425.

Mulhollan, G. A., & Bierman, J. C. (2008). Enhanced chemical immunity for negative electron affinity GaAs photoemitters. *Journal of Vacuum Science & Technology. A*, *26*, 1195.

Mulhollan, G. A., Clendenin, J., Sáez, P., Schulz, D., Tang, H., Hopster, H., Trantham, K., Gay, T. J., Johnson, B., Magugumela, M., Dunning, F. B., Walters, G. K., & Hanne, G. F.

(1996). A derivative standard for polarimeter calibration. In *Particle accelerator conference 95 proceedings* Vol. 2. (p. 1043). New Jersy: IEEE Press.

Müller, H., & Kessler, J. (1994). Cross-check of Sherman-function measurements for xenon using two independent methods. *Journal of Physics B*, *27*, 5893.

Nakajima, T., & Lambropoulos, P. (2002). Electron spin-polarization in single-, two- and three-photon ionization of xenon. *Europhysics Letters*, *57*, 25.

Nakajima, T., Matsuo, Y., & Kobayashi, T. (2008). All-optical control and direct detection of ultrafast spin polarization in a multi-valence-electron system. *Physical Review A*, *77*, 063404.

Nakajima, T., Yonekura, N., Matsuo, Y., Kobayashi, T., & Fukuyama, Y. (2003). Simultaneous production of spin-polarized ions/electrons based on two-photon ionization of laser-ablated metallic atoms. *Applied Physics Letters*, *83*, 2103.

Nakanishi, T., Aoyagi, H., Horinaka, H., Kamiya, Y., Kato, T., Nakamura, S., Saka, T., & Tsubata, M. (1991). Large enhancement of spin polarization observed by photoelectrons from a strained GaAs layer. *Physics Letters A*, *158*, 345.

Naß, C. P., Eller, M., Ludwig, N., Reichert, E., & Webersinke, M. (1989). Polarization transfer in the $n^2P$-excitation of alkali atoms by longitudinally polarized electrons. *Zeitschrift für Physik D*, *11*, 71.

Neufeld, D. D., Aliabadi, H., & Dunning, F. B. (2007). Compact retarding-potential Mott polarimeter. *The Review of Scientific Instruments*, *78*, 025107.

Nickich, V., Hegemann, T., Bartsch, M., & Hanne, G. F. (1990). Left–right asymmetry in superelastic collisions of polarized electrons with unpolarized laser-excited sodium atoms. *Zeitschrift für Physik D*, *16*, 261.

Nolting, C., Mayer, S., & Kessler, J. (1997). Electron dichroism—New data and an experimental cross-check. *Journal of Physics B*, *30*, 5491.

Nordbeck, R. P., Fullerton, C. M., Wöste, G., Thompson, D. G., & Blum, K. (1994). The scattering of spin-polarized electrons from oriented and rotating oxygen molecules. *Journal of Physics B*, *27*, 5375.

Onishchuk, V. A. (1982). Spin polarization in the Coulomb ionization of optically active molecules. *Soviet Physics JETP*, *55*, 412.

Oro, D. M., Butler, W. H., Tang, F. C., Walters, G. K., & Dunning, F. B. (1991). Absolute calibration of a retarding-potential Mott polarimeter. *The Review of Scientific Instruments*, *62*, 667.

Panajotovic, R., Lower, J., Wiegold, E., Prideaux, A., & Madison, D. H. (2006). (*e*, 2*e*) measurements on xenon: reexamination of the fine-structure effect. *Physical Review A*, *73*, 052701.

Payne, D., Krueger, B., & Bartschat, K. (2005). Channel coupling and relativistic effects in electron-impact excitation of rubidium. *Journal of Physics B.*, *38*, 3349.

Petrov, V. N., Grebenshikov, V. V., Andronov, A. N., Gabdullin, P. G., & Maslevtcov, A. V. (2007). Ultrafast compact classical Mott Polarimeter. *The Review of Scientific Instruments*, *78*, 025102.

Petrov, V. N., Grebenshikov, V. V., Grachev, B. D., & Kamochkin, A. S. (2003). New classical 40 kV Mott polarimeter. *The Review of Scientific Instruments*, *74*, 1278.

Pierce, D. T. (1996). In F. B. Dunning & R. G. Hulet (Eds.), *Atomic, molecular, and optical physics: Atoms and molecules—Experimental methods in the physical sciences,* Vol. 29A. San Diego: Academic Press.

Pierce, D. T., Celotta, R. J., Wang, G. C., Unertl, W. N., Galejs, A., Kuyatt, C. E., & Mielczarek, S. R. (1980). GaAs spin polarized electron source. *The Review of Scientific Instruments*, *51*, 478.

Pierce, D. T., & Meier, F. (1976). Photoemission of spin-polarized electrons from GaAs. *Physical Review B*, *13*, 5484.

Pierce, D. T., Meier, F., & Zürcher, P. (1975). Negative electron affinity GaAs: A new source of spin-polarized electrons. *Applied Physics Letters*, *26*, 670.

Pravica, L., Cvejanović, D., Williams, J. F., & Napier, S. A. (2007a). Angular momentum effects in the ionization-with-excitation process of open and closed 3*d*-shell states of zinc atoms. *Physical Review A*, *75*, 030701.

Pravica, L., Cvejanović, D., Williams, J. F., & Napier, S. A. (2007b). Angular-momentum-dependent Fano profiles in excited zinc atoms. *Journal of Physics: Conference Series*, *88*, 012067.

Pravica, L., Williams, J. F., Cvejanović, D., & Napier, S. A. (2007c). Spin-resolved negative ion resonances in zinc near 11eV. *Physical Review A*, *75*, 012721.

Prideaux, A., & Madison, D. H. (2004). Doubly differential cross sections for ionization of xenon by spin-polarized electrons. *Journal of Physics B*, *37*, 4423.

Prinz, H. Th., Besch, K. H., & Nakel, W. (1995). Spin-orbit interaction for the continuum electrons in relativistic (*e*, 2*e*) measurements. *Physical Review Letters*, *74*, 243.

Qiao, S., & Kakizaki, A. (1997). Monte Carlo calculations for the design of Mott scattering spin polarimeters. *The Review of Scientific Instruments*, *68*, 4017.

Raeker, A., Blum, K., & Bartschat, K. (1993). Charge cloud distribution of heavy atoms after excitation by polarized electrons. *Journal of Physics B*, *26*, 1491.

Ratliff, J. M., Rutherford, G. H., Dunning, F. B., & Walters, G. K. (1989). Electron exchange in collisions with $O_2$ and NO. *Physical Review A*, *39*, 5584.

Ray, S. G., Daube, S. S., Leitus, G., Vager, Z., & Naaman, R. (2006). Chirality-induced spin-selective properties of self-assembled monolayers of DNA on gold. *Phys. Rev. Lett.*, *96*, 036101.

Ray, K., Ananthavel, S. P., Waldeck, D. H., & Naaman, R. (1999). Asymmetric scattering of polarized electrons by organized organic films of chiral molecules. *Science*, *283*, 814.

Rich, A., Van House, J., & Hegstrom, R. A. (1982). Calculation of a mirror asymmetric effect in electron scattering from chiral targets. *Phys. Rev. Lett.*, *48*, 1341.

Rosenberg, R. A., Abu Haija, M., & Ryan, P. J. (2008). Chiral-selective chemistry induced by spin-polarized secondary electrons from a magnetic substrate. *Physical Review Letters*, *101*, 178301.

Ross, A. W., & Fink, M. (1988). Atomic scattering factor and spin-polarization calculations. *Physical Review A*, *38*, 6055.

Rutherford, G. H., & Grobe, R. (1998). Comment on ''Stern-Gerlach effect for electron beams'' *Physical Review Letters*, *81*, 4772.

Rutherford, G. H., Ratliff, J. M., Lynn, J. G., Dunning, F. B., & Walters, G. K. (1990). Improved source of polarized electrons based on a flowing helium afterglow. *The Review of Scientific Instruments*, *61*, 1460.

Sanche, L., & Schultz, G. (1972). Electron transmission spectroscopy: Rare gases. *Physical Review A*, *5*, 1672.

Sartori, C. S., da Paixão, F. J., & Lima, M. A. P. (1997). Superelastic cross sections in $e^-$–$H_2$ scattering. *Physical Review A*, *55*, 3243.

Sauter, M., Ott, H., & Nakel, W. (1998). Spin asymmetry in relativistic (*e*, 2*e*) processes: Atomic-number dependence. *Journal of Physics B*, *31*, L967.

Schedin, F., Warburton, R., & Thornton, G. (1998). Bolt-on source of spin-polarized electrons for inverse photoemission. *Rev. Sci. Instrum.*, *69*, 2297.

Scheer, A. M., Gallup, G. A., & Gay, T. J. (2006). An investigation of electron helicity density in bromocamphor and dibromocamphor as a source of electron circular dichroism. *Journal of Physics B*, *39*, 2169.

Scheer, A. M., Gallup, G. A., & Gay, T. J. (2008). Assignment of normally unoccupied orbitals to the temporary negative ion states of several lanthanide NMR shift reagents and comments on the resonance involvement in electron circular dichoism. *The Journal of Physical Chemistry A*, *112*, 4029.

Schull, C. G., Chase, C. T., & Myers, F. E. (1943). Electron polarization. *Physical Review*, *63*, 29.

Seddon, E. A., Malins, A. E. R., Petty, M., Crapper, M. D., Wardell, I. R. M., Hide, A. K., Hardiman, M., Xu, Y. B., Hucknall, P., Greig, D., Clones, S., & McCash, E. M. (1999). Amorphous alloys as secondary standards for electron spin polarimetry. *Measurement Science & Technology*, *10*, 269.

Sherman, N. (1956). Coulomb scattering of relativistic electrons by point nuclei. *Physical Review*, *103*, 1601.

Sinclair, C. K., Adderley, P. A., Dunham, B. M., Hansknecht, J. C., Hartmann, P., Poelker, M., Price, J. S., Rutt, P. M., Schneider, W. J., & Steigerwald, M. (2007). Development of a high average current polarized electron source with long cathode operational lifetime. *Physical Review Special Topics: Accelerators and Beams*, *10*, 023501.

Smith, F. J. (1966). Hydrogen atom spin change collisions. *Planet. Space. Sci.*, *14*, 929.

Snell, G., Viefhaus, J., Dunning, F. B., & Berrah, N. (2000). Microsphere plate detectors used with a compact Mott polarimeter for time-of-flight studies. *The Review of Scientific Instruments*, *71*, 2608.

Sohn, M., & Hanne, G. F. (1992). Charge-cloud distribution of $Hg^*(6^3P_1)$ in e-e$\gamma$ experiments with polarized electrons. *Journal of Physics B*, *25*, 4627.

Sokell, E., Zamith, S., Bouchene, M. A., & Girard, B. (2000). Polarization-dependent pump-probe studies in atomic fine-structure levels: Towards the production of spin-polarized electrons. *Journal of Physics B*, *33*, 2005.

Srivastava, R., Blum, K., McEachran, R. P., & Stauffer, A. D. (1996). Excitation of the lowest $^3P_1$ and $^1P_1$ states in argon and xenon by polarized electrons. *Journal of Physics B*, *29*, 5947.

Srivastava, R., McEachran, R. P., & Stauffer, A. D. (1995). Relativistic distorted-wave calculation of the excitation of the $^3D_3$ state of heavy noble gases. *Journal of Physics B*, *28*, 869.

Streun, M., Baum, G., Blask, W., Rasch, J., Bray, I., Fursa, D. V., Jones, S., Madison, D. H., Walters, H. R. J., & Whelan, C. T. (1998). Spin dependence of (*e*, 2*e*) collisions on lithium at 54.4 eV. *Journal of Physics B*, *31*, 4401.

Tashiro, M. (2008). Exchange effects in elastic collisions of spin-polarized electrons with open-shell molecules with $^3\sum_g^-$ symmetry. *Physical Review A*, *77*, 012723.

Thumm, U., Bartschat, K., & Norcross, D. W. (1993). Relativistic effects in spin-polarization parameters for low-energy electron-Cs scattering. *Journal of Physics B*, *26*, 1587.

Trantham, K. W., Gay, T. J., & Vandiver, R. J. (1996). An inline optical electron polarimeter. *The Review of Scientific Instruments*, *67*, 4103.

Trantham, K. W., Johnston, M. E., & Gay, T. J. (1995). Failure to observe electron circular dichroism in camphor. *Journal of Physics B*, *28*, L543.

Tseng, H. K. (2002). Relativistic calculation of the unpolarized triple-differential cross section and the polarization correlation of the electron bremsstrahlung from atoms. *Journal of Physics B*, *35*, 1129.

Tupa, D., & Anderson, L. W. (1987). Effect of radiation trapping on the polarization of an optically pumped alkali-metal vapor in a weak magnetic field. *Physical Review A*, *36*, 2142.

Uhrig, M., Hanne, G. F., & Kessler, J. (1994). Electron–photon coincidence experiment after polarized-electron impact on xenon. *Journal of Physics B*, *27*, 4009.

Van Vleck, J. H. (1929). On σ-type doubling and electron spin in the spectra of diatomic molecules. *Physical Review*, *33*, 467.

Vester, F., Ulbricht, T. L. V., & Krauch, H. (1959). Optical activity and parity violation in $\beta$-decay. *Die Naturwissenschaften*, *46*, 68.

Wagshul, M. E., & Chupp, T. E. (1994). Laser optical pumping of high-density Rb in polarized $^3$He targets. *Physical Review A*, *49*, 3854.

Walker, D. C. (Ed.). (1979). *Origins of optical activity in nature*. Amsterdam: Elsevier.

Walker, D. W. (1982). Electron scattering from optically active molecules. *Journal of Physics B*, *15*, L289.

Weber, W., Oberli, D., Riesen, S., & Siegmann, H. C. (1999). The ferromagnetic spin filter. *IEEE Transactions on Magnetics*, *35*, 2907.

Went, M. R., McEachran, R. P., Lohmann, B., & MacGillivray, W. R. (2002). Spin asymmetries for elastic scattering in krypton at intermediate energies. *Journal of Physics B*, *35*, 4885.

Williams, J. F., & Yu, D. H. (2004). Electron exchange in dissociative excitation of molecular hydrogen using polarized electrons. *Physical Review Letters*, *93*, 073201.

Winkelmann, A., Hartung, D., Engelhard, H., Chiang, C. T., & Kirschner, J. (2008). High efficiency electron spin polarization analyzer based on exchange scattering at Fe/W(001). *The Review of Scientific Instruments*, *79*, 0833031.

Wykes, J. S. (1971). A general optical detector of the polarization of low energy electrons. *Journal of Physics B*, *4*, L91.

Yashin, Yu.P., Ambrajei, A. N., & Mamaev, Yu.A. (2000). A computer-controlled setup for studying spin-polarized electron photoemission. *Inst. Exp. Tech.*, *43*, 245.

Yonekura, N., Nakajima, T., Matsuo, Y., Kobayashi, T., & Fukuyama, Y. (2004). Electron-spin polarization of photoions produced through photoionization from the laser-excited triplet state of Sr. *The Journal of Chemical Physics*, *120*, 1806.

Yu, D. H., Hayes, P. A., & Williams, J. F. (1997a). Stokes parameters form neon 3p($J = 2$) states excited by polarized electrons. *Journal of Physics B*, *30*, L487.

Yu, D. H., Hayes, P. A., Williams, J. F., & Locke, C. (1997b). Resonance formation in the excitation of the Ne 3p[½]$_1$ state by polarized electrons. *Journal of Physics B*, *30*, L461.

Yu, D. H., Hayes, P. A., Williams, J. F., Zeman, V., & Bartschat, K. (2000). Internal spin-orbit coupling and electron exchange in the excitation of $np^5(n + 1)$p states of neon, krypton and xenon atoms by polarized electrons. *Journal of Physics B*, *33*, 1881.

Yu, D. H., Pravica, L., Williams, J. F., & Hayes, P. A. (2001). Polarized electron inner-shell ionization-with-excitation of zinc atoms. *Journal of Physics B*, *34*, 3899.

Yuan, J. (1995). Intra-atomic relativistic effects on the spin polarization in low-energy electron scattering from Ca, Sr, Ba, and Yb atoms. *Physical Review A*, *52*, 4647.

Zare, R. N. (1988). *Angular momentum*. New York: Wiley.

Zelenski, A. (2007). Optically-pumped polarized electron, $H^-$ (proton), deuteron and $^3He^{++}$ion source development at BNL. In K. Imai, T. Murakami, N. Saito & K. Tanida (Eds.), *Proceedings of the 17th international spin physics symposium. AIP conference proceedings*, Vol. 915. New York: AIP.

Zelenskii, A. N., Kokhanovsky, V. G., Polushkin, V. G., & Vishnevsky, K. N. (1986). Anomalous ionization effects in charge-exchange of a proton beam in a high-density optically-pumped sodium cell. *Soviet Physics JETP Letters*, *44*, 24.

Zeman, V., Bartschat, K., Gay, T. J., & Trantham, K. W. (1997). Electron-collision-induced alignment of rare gases near threshold. *Physical Review Letters*, *79*, 1825.

Zeman, V., McEachran, R. P., & Stauffer, A. D. (1994). Relativistic distorted-wave calculation of electron impact excitation of caesium. *Journal of Physics B*, *27*, 3175.

Zeman, V., McEachran, R. P., & Stauffer, A. D. (1995). A test of the LS approximation for electron-impact excitation of caesium. *Journal of Physics B*, *28*, 3063.

Zhou, H. L., Whitten, B. L., Trail, W. K., Morison, M. A., MacAdam, K. B., Bartschat, K., & Norcross, D. W. (1995). Low-energy electron collisions with sodium: Scattering of spin-polarized electrons. *Physical Review A*, *52*, 1152.

Žutić, I., Fabian, J., & Das Sarma, S. (2004). Spintronics: Fundamentals and applications. *Reviews of Modern Physics*, *76*, 323.